Sustainable Mobility

Selective Photocatalytic Reduction of NO_x with Fe-doped TiO_2: A New Approach Towards Photocatalyst Design

Qingping WU

Dit proefschrift is goedgekeurd door promotor:
Prof. dr. B. Dam

Copromotor: Dr. ir. R. van de Krol

Samenstelling promotiecomissie:

Rector Magnificus,	Voorzitter
Prof. dr. B. Dam,	Technische Universiteit Delft, promotor
Dr. ir. R. van de Krol,	Technische Universiteit Delft, copromotor
Dr. P.E. de Jongh,	Universiteit Utrecht
Prof. dr. ir. H.J.H. Brouwers,	Technische Universiteit Eindhoven
Prof. dr. A. Mills,	Queen's University Belfast (UK)
Prof. dr. S.J. Picken,	Technische Universiteit Delft
Prof. dr. J.J.C. Geerlings	Technische Universiteit Delft

The research described in this thesis was carried out in the section Materials for Energy Conversion and Storage (MECS), Department of Chemical Engineering, Faculty of Applied Sciences, at Delft University of Technology

The research described in this thesis was financially supported by the Shell/TU Delft Sustainable Mobility Program.

ISBN: 978-94-6191-368-5

Art direction & lay-out: Esther Beekman (www.estherontwerpt.nl)
Printed by: Ipskamp drukkers BV, Enschede

Selective photocatalytic reduction of NO_x with Fe-doped TiO_2: A new approach towards photocatalyst design

Proefschrift

ter verkrijging van de graad van doctor
aan de Technische Universiteit Delft;
op gezag van de Rector Magnificus
prof. ir. K.C.A.M. Luyben;
voorzitter van het College voor Promoties
in het openbaar te verdedigen op
dinsdag 4 september 2012 om 15:00 uur

door

Qingping WU

Master of Science in Physical Chemistry, Fuzhou University

Geboren te Putian, China

Contents

Chapter 1

General introduction

Photocatalysis, catalytic reactions based on light absorbance, has been intensively investigated for sustainable energy production and environmental protection by utilizing solar light (Fig. 1). In general, photocatalytic reactions include traditional photo-oxidation (e.g. mineralizing organic pollutants to CO_2 and H_2O) and the less-common photo-reduction route (e.g. photo-conversion from CO_2 and H_2O to fuels; from NO_x to N_2 and O_2). Photocatalytic material properties determine the catalytic selectivity. In this chapter, the basic concept of photocatalysis and several approaches for designing new photocatalytic materials will be discussed. The focus of this thesis is to outline a new approach for changing the photocatalytic selectivity of common photocatalysts such as TiO_2 from oxidation to reduction and to improve its use for air purification (photo-decomposing NO_x to N_2 and O_2).

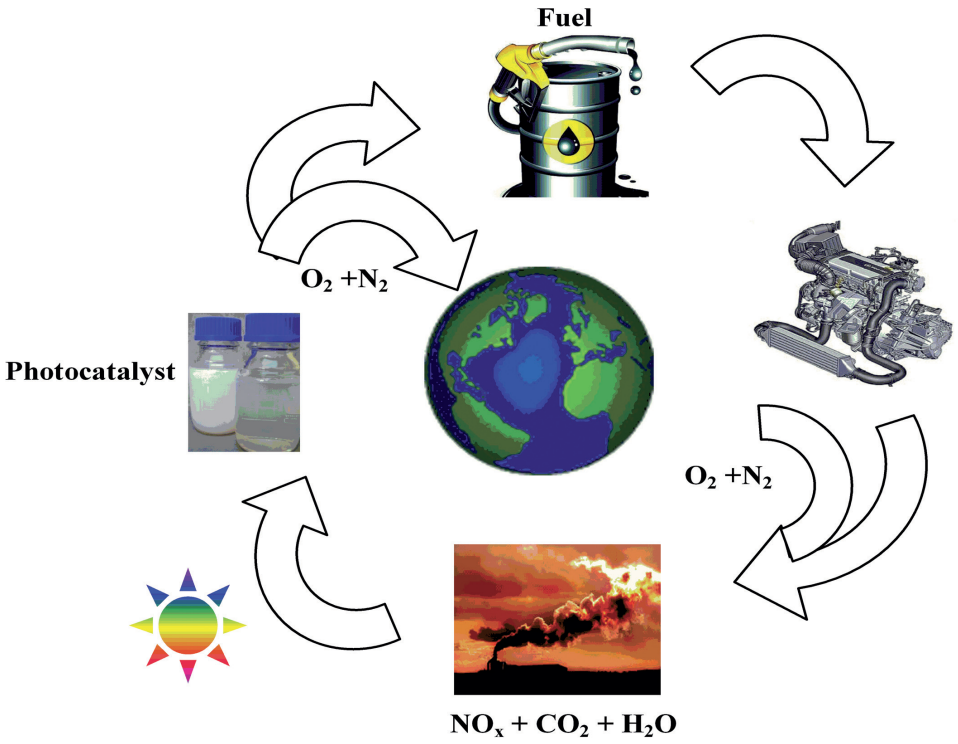

Figure 1: Energy and environmental sustainability.

1.1 Photocatalytic background

In recent decades, on a global scale there are still serious environmental problems related to harmful pollutants (e.g. benzene, phenol, SO_2 and NO_x) caused by industrial development.[1-3] One of the most harmful environmental pollutants in air is nitrogen oxide (NO_x).[4] The emission of NO_x, generally a mixture of nitric oxide (NO) and nitrogen dioxide (NO_2),[5] is mainly produced by automotive engines and industrial combustion systems that operate at high temperatures.[6] Highly concentrated NO_x, especially NO_2, causes damage to the lung tissue of human beings and contributes to the formation of yellow smog and acid rain. As indicated by the satellite image in Fig. 1.1, most NO_2 emissions in the world originates from European Union countries and China. European Union regulations have become increasingly strict ($NO_2 \leq 40$ μg/m^3, ~ 20 ppb), and call for urgent efforts to remove NO_x from air. In addition, NO_x is an indirect greenhouse gas, which can deplete the stratospheric ozone layer. Therefore, it is very urgent to remove NO_x from air.

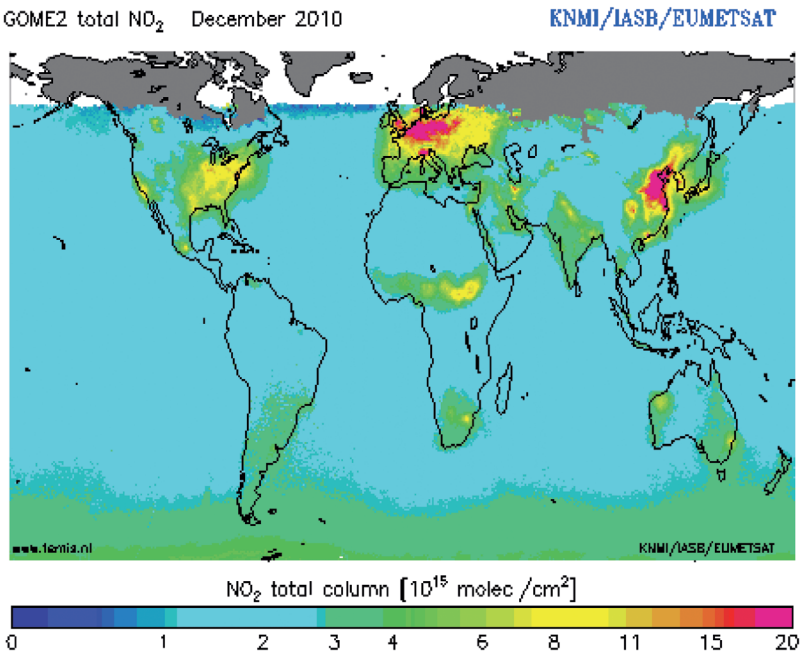

Figure 1.1: NO_2 emission sources in the world (www.temis.nl).

One of the most promising technologies for removing NO_x from air is photocatalysis, which can operate at ambient pressure and room temperature by utilizing solar energy. Until today, photocatalysis is mainly based on semiconductors. Semiconductor photocatalysis (chemical reactions occurring at the surface of irradiated semiconducting materials) offers a potential solution for the complete elimination of harmful pollutants.[7] Titanium dioxide (TiO_2), one of best-known semiconductor photocatalysts, has been widely studied for use in air purification, deodorants, sterilization, anti-fouling, demisters and many other areas.[8] Commonly, two crystal forms of TiO_2 can be used for photocatalytic reactions: anatase (E_g = 3.2 eV, a = b = 0.3785 nm, c = 0.9514 nm) and rutile (E_g = 3.0 eV, a = b = 0.4593 nm, c = 0.2959 nm),[9,10] as shown in Fig. 1.2.

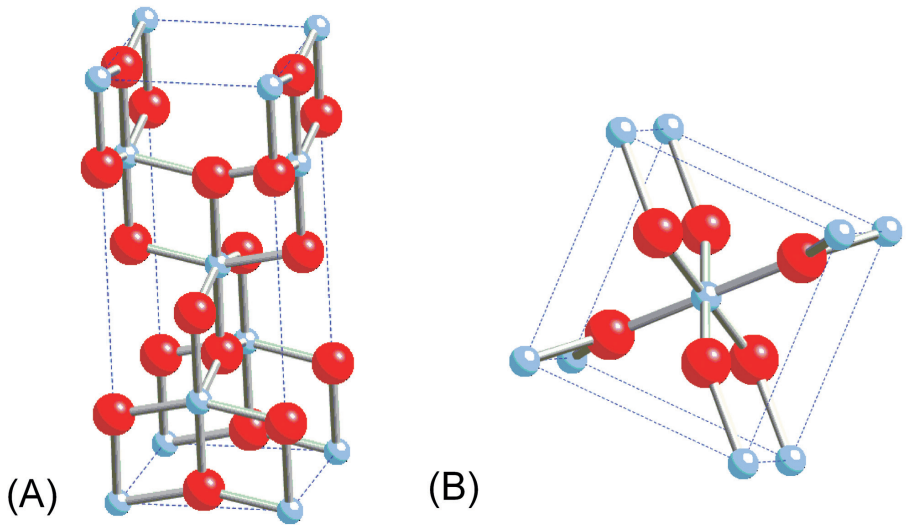

Figure 1.2: Crystal structure of TiO_2 (A) Anatase; (B) Rutile :O : Ti

One of the photocatalytic applications of TiO_2 is its ability to decompose the NO_x present in air.[11] However, the current application of TiO_2 in photocatalytic decomposition of NO_x is confronted with three main disadvantages:

1. TiO_2 photo-oxidizes NO_x to NO_3^- ions, which do not spontaneously desorb and therefore de-activate the surface[12] (Fig. 1.3).

2. When the nitrate (NO_3^-) is washed away by rain, nitric acid is formed. This product is corrosive and pollutes the soil when the concentration becomes too high.

3. TiO_2 is only active under UV light irradiation due to its wide band gap (~3.2 eV).[13] It precludes the use of visible light, which has a much higher intensity and which could be much more effective.

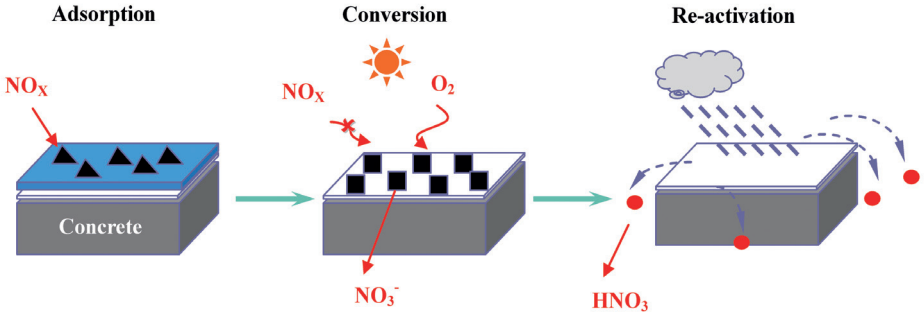

Figure 1.3: NO_x removal using TiO_2 under solar light irradiation.

The deactivation and corrosion, caused by the formation of nitric acid, can be avoided if we can change the reaction mechanism from photo-oxidation to photo-reduction. This means the decomposition products will be N_2 and O_2 instead of nitric acid. It was reported by Anpo et al. that the selectivity for photo-reduction was greatly improved by reducing the coordination number of Ti^{4+} from its usual value of 6 (TiO_6, octahedra) to 4 (TiO_4 tetrahedra).[15] For catalysts prepared by depositing isolated titanium oxide clusters (TiO_4, tetrahedra) inside the cavities of zeolite-Y (Fig. 1.4), a high activity for photo-reducing NO_x to N_2 and O_2 with UV light irradiation has been observed.[16] The visible light photo-activity of TiO_2 / zeolite catalysts can be achieved by doping with nitrogen or various transition metals, e.g. Cr or V with ion beam implantation method. However, large scale application of zeolites and ion beam implantation techniques are economically unattractive.

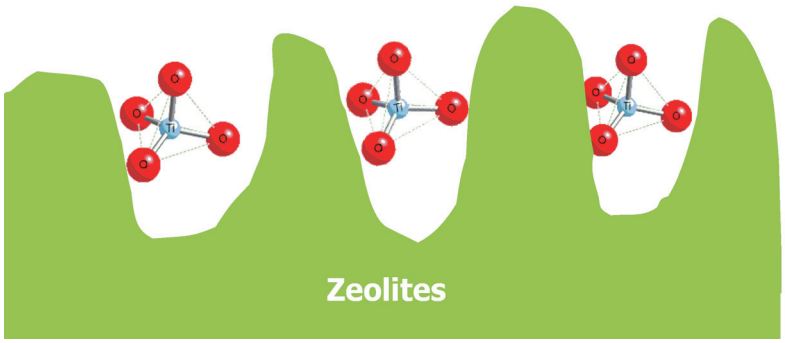

Fig. 1.4 Isolated TiO_4 (tetrahedra) in zeolite cavities.

As a second line of investigation, to overcome the large band gap of TiO_2, much attention has been focused on modifying TiO_2. For achieving visible light absorption, the general approach is to dope TiO_2 with metal ions (e.g. Fe^{3+}, Mo^{5+}, Re^{5+}, Ru^{3+}, V^{4+}, Rh^{3+}) [9] or non-metal ions (e.g. B, C, N or S).[14]

1.2 Theoretical background

1.2.1 Semiconductor photocatalysts

As their name implies, semiconductors (e. g. TiO_2, ZnO, Fe_2O_3, $SrTiO_3$) conduct more electricity than insulators, but less than metals. This results from the electronic structure of the different materials. In semiconductors and insulators, electrons are restricted in a number of energy bands. The "band gap" refers to the energy difference between the top of the highest energy band occupied with electrons (valence band) and the bottom of the lowest unoccupied band (conduction band). Electric conduction is only available if there is net crystal momentum. This means completely empty or filled bands don't conduct electricity. The band gap of an insulator is so large that electrons can not be excited from valence band (VB) to conduction band (CB), which suggests completely filled VB and completely empty CB. Therefore, insulators can not conduct electricity. Whereas the VB and CB of a metal overlaps with each other, which means partially filled bands. Usually, semiconductors are characterized by a band gap (E_g) roughly less than 4 eV.[17] The different band gap diagrams of an insulator, a semiconductor and a metal are illustrated in Fig. 2.1.

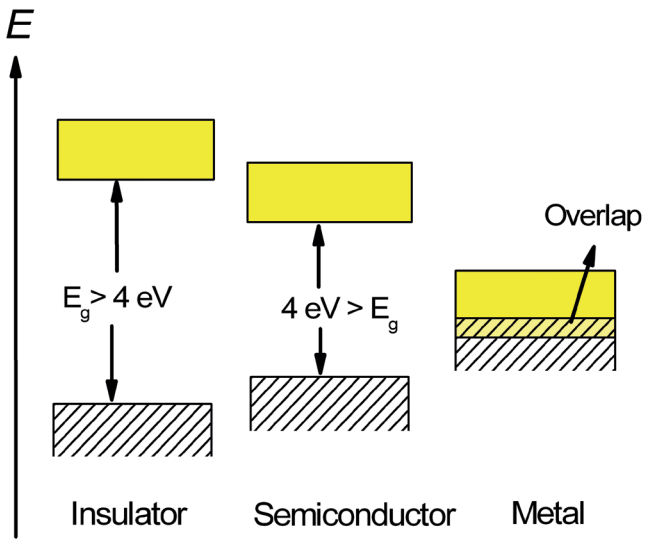

Figure 2.1: Band diagrams for insulator, semiconductor and metal.

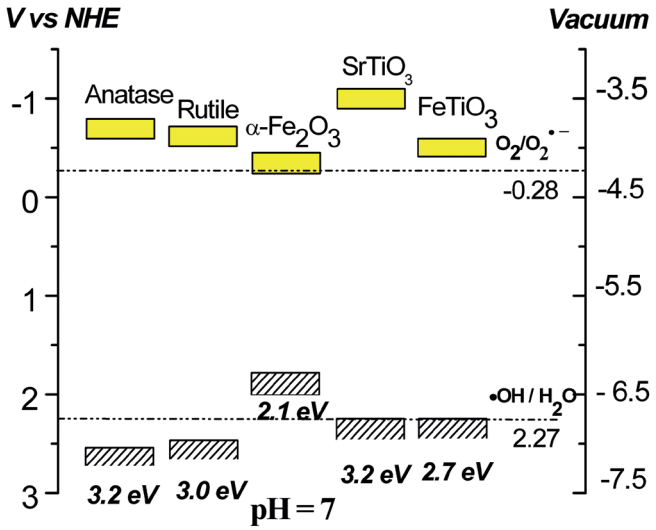

Figure 2.2: Bandgap energies, conduction and valence band energy levels of various semiconductors (pH = 7).[25,26]

The electrochemical potential of a semiconductor is given by the so-called Fermi level, which is defined as the energy level for which the chance of occupation by an electron is ½. The Fermi level of an intrinsic (i.e., undoped) semiconductor or insulator is approximately at the middle of VB and CB.[18] The Fermi level of p-type and n-type semiconductors shifts towards VB and CB, respectively, due to excess charge carriers. Mainly, there are three factors related to the band structure of semiconductors that play an important role in photocatalytic reactions.

1. The width of the band gap
2. The energy of the bottom of the conduction band, E_{CB}
3. The energy of the top of the valence band, E_{VB}

The band gap energies and band positions of some semiconducting materials at pH = 7 are shown in Fig. 2.2.

The band diagram of semiconductor titanium dioxide (TiO_2) is shown in Fig. 2.3. The VB of TiO_2 is comprised mainly of the 2p orbitals of oxygen (O), whereas the CB is made up of the 3d orbitals of titanium (Ti). When TiO_2 is irradiated with light of an energy exceeding the band gap (E_g), electrons are excited from the VB to the CB, creating electron - hole pairs (e^- - h^+). Some of the photo-generated e^- and h^+ pairs recombine, thereby producing heat. The other e^- and h^+ pairs are transferred to the surface of the semiconductor and are trapped by surface adsorbed groups (e.g. OH^-, O_2), forming intermediate species. These intermediate species will decompose the target pollutant via photo-oxidative or photo-reductive reactions. Unfortunately, the explicit mechanism for photocatalytic process of both photo-oxidation and photo-reduction of NO_x is still not clear.[19,20]

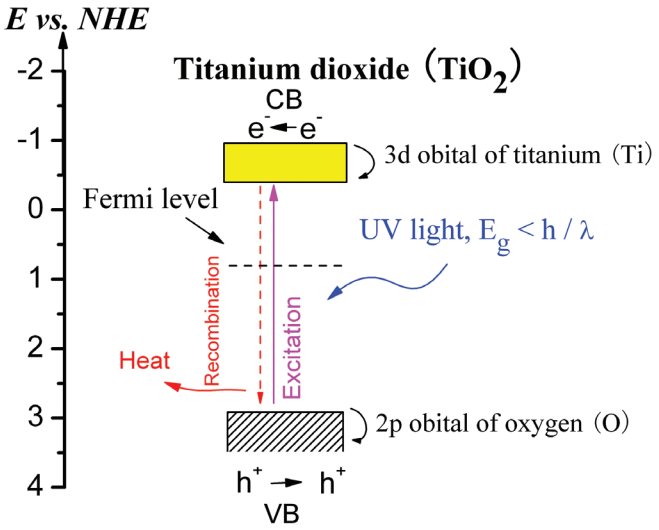

Fig. 2.3 Band diagram of semiconductor TiO_2 under UV irradiation.

1.2.2 Reaction mechanisms for photo-oxidation

Although there is still no explicit mechanism about photooxidation and photoreduction of pollutants, here some possible explanations are presented for a better understanding of photocatalytic decomposing mechanisms. One of the notable features of TiO_2 is the strong oxidative activity. Two possible ways for photo-degradation via oxidation have been reported, and will be outlined below.

1.2.2.1 Mechanism involving $^{\bullet}OH$ radicals

One of the possible photocatalytic mechanisms published in many papers is to assume $^{\bullet}OH$ radicals play a key role in the photocatalytic process as the main oxidizing species. It is known that the surface of TiO_2 contains adsorbed water and surface OH groups (Ti-OH_s).[21, 22] There are two possible ways of producing $^{\bullet}OH$ radicals. First, it can be formed by interaction of photogenerated holes with adsorbed water or Ti-OH_s.[23]

$$h^+ + H_2O_{ads} \rightarrow {}^{\bullet}OH_{ads} + H^+_{ads} \quad (1)$$

Second, the photo-generated electrons can reduce gaseous oxygen with the formation of superoxide anions ($O_2^{\bullet-}$) and H_2O_2.[24,25]

$$O_2 + e^- \rightarrow O_2^{\bullet-} \quad (2)$$

$$2O_2^{\bullet-} + 2H^+ \rightarrow H_2O_2 + O_2 \quad (3)$$

$$e^- + H_2O_2 \rightarrow {}^\bullet OH + OH^- \quad (4)$$

The combination of e^- and H_2O_2 will also lead to the production of $^\bullet$OH radicals in the solution. The high oxidative $^\bullet$OH radicals are responsible for decomposing organic pollutants with formation of CO_2 and H_2O as the final products. For photocatalytic oxidation of NO using TiO_2 catalyst, it is reported that $^\bullet$OH radicals will react with adsorbed NO to form two major products: NO_2 and HNO_3.[13]

$$NO + 2{}^\bullet OH \rightarrow NO_2 + H_2O \quad (5)$$

$$NO_2 + {}^\bullet OH \rightarrow HNO_3 \quad (6)$$

1.2.2.2 Mechanism involving Ti-O$^\bullet$ radicals

Based on ESR experiments, Howe et al. first reported that photoinduced holes were trapped at lattice oxygen of TiO_2 without producing any $^\bullet$OH radical at low temperature (77 K).[27] The conclusion has been confirmed later by Micic et al. by direct observation of Ti-O$^\bullet$ radicals.[28] It has been proposed that a nucleophilic attack of an H_2O molecule by a surface trapped hole at a lattice O site will result in bond breaking and subsequent generation of Ti-O$^\bullet$ radicals (see Fig. 2.4 below).[29]

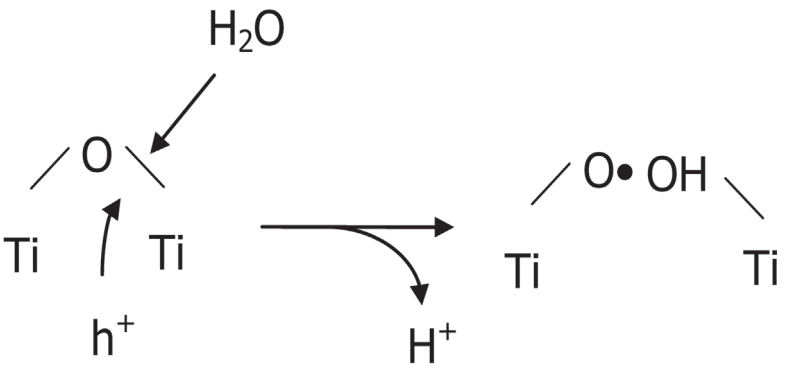

Figure 2.4: Proposed mechanism for Ti-O$^\bullet$ radical formation.[29]

Possible photocatalytic mechanisms for water splitting based on Ti-O$^\bullet$ radicals are listed below:[29]

$$2[Ti\text{-}O\bullet HO\text{-}Ti]_s \rightarrow [Ti\text{-}O\text{-}O\text{-}Ti]_s + [Ti\text{-}O\text{-}Ti]_s + H_2O$$

$$[Ti\text{-}O\text{-}O\text{-}Ti]_s + h^+ + H_2O \rightarrow [Ti\text{-}O\text{-}O\bullet HO\text{-}Ti]_s + H^+$$

$$[Ti\text{-}O\text{-}O\bullet HO\text{-}Ti]_s + h^+ \rightarrow [Ti\text{-}O\text{-}Ti]_s + O_2 + H^+$$

The detailed photocatalytic mechanism for decomposing NO_x and subsequent reactions of Ti-O$^{\bullet}$ intermediate radicals are still unknown. A possible reaction mechanism is:

$$2[Ti\text{-}O\bullet HO\text{-}Ti]_s \rightarrow [Ti\text{-}O\text{-}O\text{-}Ti]_s + [Ti\text{-}O\text{-}Ti]_s + H_2O$$

$$[Ti\text{-}O\text{-}O\text{-}Ti]_s + NO \rightarrow [Ti\text{-}O\text{-}Ti] + NO_2$$

$$[Ti\text{-}O\text{-}O\bullet HO\text{-}Ti]_s + NO \rightarrow [Ti\text{-}O\text{-}Ti]_s + HNO_3$$

1.2.2.3 Modifying TiO_2 photocatalysts

Another application of TiO_2 is its ability to photoreduce certain species. One approach to change the reaction mechanism from photooxidation to photoreduction is by reducing the coordination number of Ti from 6 to 4.[15] One may be able to artificially lower the coordination number by creating oxygen vacancies ($V_O^{\bullet\bullet}$). The creation of $V_O^{\bullet\bullet}$ in a metal oxide (TiO_2) can be expressed by using Kröger-Vink defect notation:[22]

$$O_O^X \overset{TiO_2}{\rightleftharpoons} V_O^{\bullet\bullet} + 2e' + \frac{1}{2}O_2(g) \quad (7)$$

The oxygen vacancies can be formed by annealing pure TiO_2 in a vacuum or argon atmosphere. However, since reaction (7) is reversible, the oxygen vacancies will slowly disappear when the photocatalyst is exposed to air. In order to stabilize $V_O^{\bullet\bullet}$, some metal and nonmetal ions (e.g. Fe^{3+} and N^{3-}) can be introduced into the lattice of TiO_2. For Fe^{3+} doping, there are two different compensation mechanisms.

$$Fe_2O_3 \xrightarrow{TiO_2} 2Fe'_{Ti} + 3O_O^X + V_O^{\bullet\bullet}$$ (Ionic compensation) (8)

$$Fe_2O_3 + \frac{1}{2}O_2(g) + 2e' \xrightarrow{TiO_2} 2Fe'_{Ti} + 4O_O^X$$

(Electronic compensation) (9)

The electronic compensation reaction is obtained when subtracting reaction (7) from reaction (8). For the ionic compensation reaction, $V_O^{\bullet\bullet}$ is generated without producing any electrons, which means that reaction (7) cannot occur in the reverse direction, Hence, doping TiO_2 with Fe gives a stable concentration of $V_O^{\bullet\bullet}$ through the incorporation of acceptor dopants as charge-compensating species.
Another method for stabilizing $V_O^{\bullet\bullet}$ is to replace some oxygen (O^{2-}) of the TiO_2 lattice with N^{3-} ions. Two different compensation mechanisms are possible, depending on the fate of the hydrogen atoms:

$$NH_3 \xrightarrow{TiO_2} N_O' + V_O^{\bullet\bullet} + 3H_i^{\bullet} + V_{Ti}^{////} \quad (10)$$

$$3e' + NH_3 \xrightarrow{TiO_2} N_O' + V_O^{\bullet\bullet} + V_{Ti}^{////} + \frac{3}{2}H_2(g) \quad (11)$$

Again, in both cases negatively charged ionic defects are formed which stabilize the oxygen vacancies.

The role of oxygen vacancies for changing photocatalytic selectivity from oxidation to reduction and possible explanation will be revealed later in this thesis.

1.2.2.4 Improving photocatalytic activity

Many efforts have been spent on improving the photocatalytic activity of TiO_2 (e.g. controlling particle size, making heterojunctions, doping with metal and non-metal ions).[29,30]

One of the most simple and popular approaches is to control the particle size. The particle size may affect photocatalytic activity in several ways: (1) surface area of the catalysts; (2) band gap; (3) carrier diffusion distance.[31] Small particle size (e.g. nanoparticles) can enlarge the surface area and reduce carrier transfer times from bulk to surface. In this way, the photocatalytic activity may be improved. However, a small particle size also increases the band gap through the quantum size effect, and would require light with a lower wavelength. For metal oxide photocatalysts, however, the quantum size effect is usually negligible due to the large effective mass of the charge carriers.

Another popular technology is to use other semiconductors (e.g. porous Si, CdS, CuO) and couple these with TiO_2 for making so-called "type II" heterojunctions. Those semiconductors should have appropriate band levels, as indicated in Fig. 2.5. In this way, photo-induced electrons from the other semiconductor can be transferred to the conduction band of TiO_2, due to the energy difference between two bands. With the same principle, holes from the valence band of TiO_2 can also be transferred to the valence band of the other semiconductor. In this way, charge separation is greatly enhanced which reduces the possibility of recombination. This could improve the photocatalytic activity, since more electrons and holes are available for initiating photocatalytic reactions.

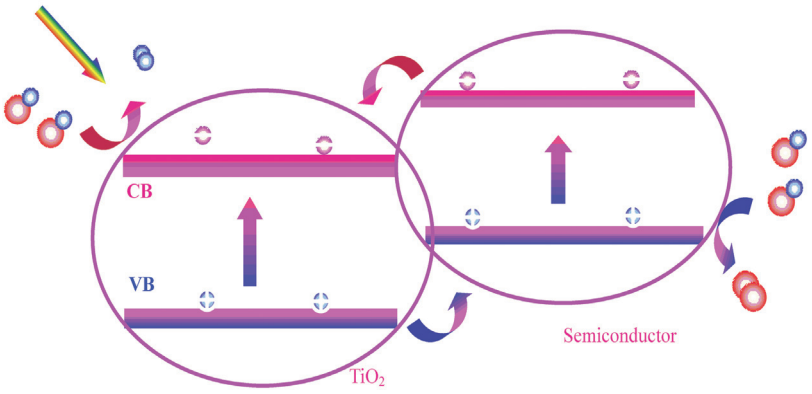

Figure 2.5: Proposed mechanism for improving the photocatalytic activity using a type II heterojunction.

1.3 Material synthesis

Many methods have been investigated for synthesizing new and highly efficient photocatalysts (e.g. sol-gel method, hydrothermal method, solvothermal method, and chemical spray pyrolysis).[32-34] The sol-gel method, a wet-chemical technique, has been widely used for nano-material synthesis, since it can be operated at room temperature and ambient pressure. Sols are homogeneous dispersions of colloidal particles (Diameter: 1-100 nm) in a liquid solution.[35] Gels can be obtained from a sol by evaporating a certain amount of solvent, which results in cross-linking of the particles. Normally, sol-gel method consists of two main steps: hydrolysis of a metal alkoxide, followed by poly-condensation. The chemical reaction using water as solvent is usually written as below:[36]

1. Hydrolysis

$$M(OR)_n + H_2O \rightarrow M(OR)_{n-1}(OH) + ROH$$

2. Condensation

$$M(OR)_n + M(OR)_{n-1}(OH) \rightarrow M_2O(OR)_{2n-2} + ROH$$

$$2M(OR)_{n-1}(OH) \rightarrow M_2O(OR)_{2n-2} + H_2O$$

The hydrolysis and condensation processes are mainly influenced by several factors:

1. pH value; acidified solvent may accelerate hydrolysis process,[37] and adsorption of positively charged proton (H^+) on the surface of the nanoparticles stabilizes the colloidal solution by repulsive forces between the particles, as indicated in Fig. 3.1.

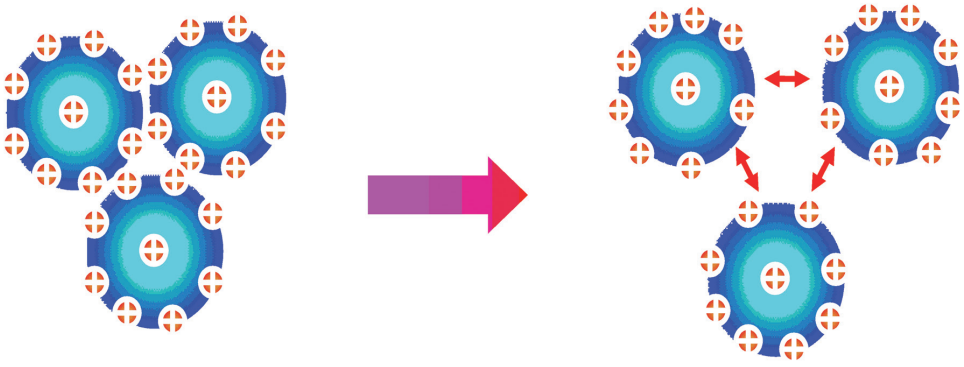

Figure 3.1: Preventing particle agglomeration by protons in colloidal solution (Blue ball: Colloidal particle; Orange ball: proton).

2. Temperature, Heating the solution accelerates the hydrolysis and condensation processes, due to evaporation of reaction products.
3. Solvent, Different solvents can accelerate or slow down the hydrolysis process.

1.4 Outline of this thesis

Within this PhD project, our main objective is to develop new, low cost and chemically stable photocatalysts for air purification with the following properties:

1. The ability to selectively reduce NO_x to N_2 and O_2
($NO \rightarrow \frac{1}{2} N_2 + \frac{1}{2} O_2$; ΔH = -86.6 KJ/mol)[38] instead of oxidizing it to nitrate groups;

2. Relative high activity under UV light irradiation.

In order to achieve this main objective, we aim to create a large number of oxygen vacancies in order to 'artificially' create Ti sites that are coordinated by 4 instead of 6 oxygen ions. Since the coordination geometry is still octahedral (4 oxygen ions + 2 oxygen vacancies, Fig. 4A), the big challenge is whether this strategy will indeed favor the reduction pathway. It is also possible that a sufficiently large concentration of oxygen vacancies leads to a true tetrahedral coordination geometry at the surface. Distinguishing between these possibilities is one of the challenges that this thesis aims to address. A secondary objective is to develop a better understanding of the way in which the particle size and overall dopant concentrations affect the distribution of surface defects. A better understanding of these fundamental aspects is essential for the further development of novel photo-catalyst materials.

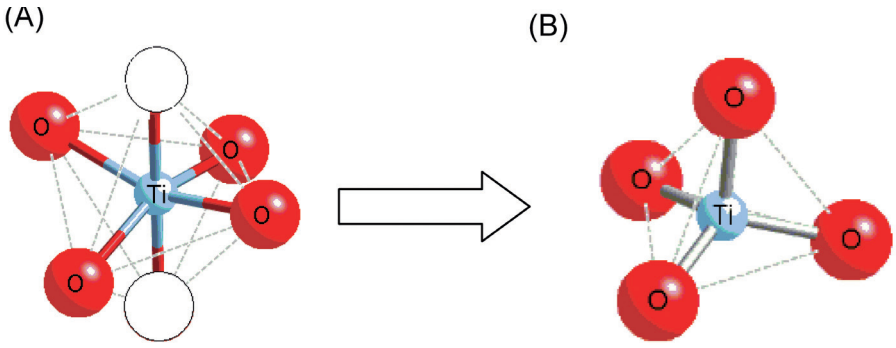

Figure 4: (A) Octahedrally coordinated Ti with 2 oxygen vacancies; (B) Tetrahedrally coordinated Ti. : O; : Ti; : oxygen vacancy

With this Ph.D programme, Fe-doped TiO_2 nanoparticles with controllable oxygen vacancy concentrations are proposed as promising photocatalysts for NO_x reduction. Several steps are taken for understanding material structure, surface adsorption species and possible photocatalytic reaction mechanisms.

1. The incorporation of Fe as a dopant in (anatase) TiO_2 lattice and possible creation of oxygen vacancies were systematically investigated by a combination of XRD, Raman and TEM-EDX techniques. Due to very similar radii of Ti^{4+} and Fe^{3+}, a high solubility of Fe^{3+} in the TiO_2 lattice is possible. Therefore, the creation and stabilization of high concentration of oxygen vacancies are expected. For high concentrations of oxygen vacancies, a change in coordination geometry of Ti^{4+} from octahedra (TiO_6) to tetrahedra (TiO_4) is expected, which we measured by EXAFS/XANES spectra (Chapter 2).

2. The very first step of photocatalytic process, NO adsorption and release (in dark) at Fe^{3+} sites of Fe-doped TiO_2 nanoparticle surface, was measured by in-situ Diffuse Reflectance Infrared Fourier Transformed spectroscopy. As the photocatalytic material is exposed to air in real-life applications, the influence of H_2O to NO adsorption have also been investigated and are described in Chapter 3.

3. The contribution of oxygen vacancies to the photocatalytic selectivity of NO degradation has been studied using an on-line NO_x analyzer in combination with gas chromatography. The Fe^{3+} dopant can be stabilized by Fe^{2+} and can be photo-reduced to Fe^{2+}. This provides a recombination pathway that suppress the formation of NO_2 and thus change the selectivity of Fe-doped TiO_2 for NO decomposition from photo-oxidation to photo-reduction The outcome of this study is described in Chapter 4.

4. The confirmation of photocatalytic mechanism from Chapter 4, including photon-assisted NO adsorption-desorption and its influence on the photocatalytic selectivity of Fe-doped TiO_2 nanoparticles, was measured by a combination of in-situ Diffuse Reflectance Infrared Fourier Transformed spectroscopy and on-line NO_x analyzer. The results of this study are described in Chapter 5.

In this thesis, oxygen vacancies are successfully created by doping Fe into TiO_2 lattice. The EXAFS/XANES measurements show that the coordination of Ti^{4+} was partially changed from 6 to 4 at high oxygen vacancy concentrations. The activity of photo-reduction reactions can be greatly improved by doping the TiO_2 nanoparticles with Fe^{3+}. The stoichiometric formation of N_2 an O_2 are confirmed by gas chromatography. Moreover, the reduction of Fe^{3+} to Fe^{2+} provides a recombination pathway that almost completely suppresses the formation of NO_2, thus enhances the selectivity for N_2 and O_2 formation. The influence of oxygen vacancies to catalytic selectivity provides a new approach for designing highly selective photocatalytic materials.

References

[1] M. Signoretto, E. Ghedini, V. Trevisan, C. L. Bianchi, M. Ongaro and G. Cruciani, *Appl. Catal. B*, 2010, 95, 130.

[2] M. R. Hoffmann, S. T. Martin, W. Choi, and D. W. Bahnemann, *Chem. Rev.,* 1995, **95**, 69.

[3] T. D. Bui, A. Kimura, S. Higashida, S. Ikeda, M. Matsumura, *Appl. Catal. B*, 2011, **107**, 119.

[4] L. Ma, J. Li, R. Ke and L. Fu, *J. Phys. Chem. C*, 2011, **115**, 7603.

[5] S. Devahasdin, C. Fan, J. K. Li and D. H. Chen, *J. Photochem. Photobiol. A: Chem.*, 2003, **156**, 161.

[6] J. A. Rodriguez, T. Jirsak, G. Liu, J. Hrbek, J. Dvorak and A. Maiti, *J. Am. Chem. Soc.*, 2001,**123**, 9597.

[7] A. Yuksel, M. Sasaki, M. Goto, *J. Hazard. Mater.*, 2011, **190**, 1058.

[8] A. Fujishima, T. N. Rao and D. A. Tryk, *J. Photochem. Photobiol., C: Photochem. Rev., 2000,* **1**,1.

[9] U. Diebold, *Surf. Sci. Rep.*, 2003, **48**, 53.

[10] Y. R. Park and K. J. Kim, *Thin Solid Films*, 2005, **484**, 34.

[11] Y. OhKo, Y. Nakamura, A. Fukuda, S. Matsuzawa and K. Takeuchi, *J. Phys. Chem. C*, 2008, **112**, 10502.

[12] H. Wang, Z. Wu, W. Zhao and B. Guan, *Chemosphere*, 2007, **66**,185.

[13] L. Ge, *J. Mol. Catal. A: Chem.*, 2008, **282**, 62.

[14] S. Chu, S. Inoue, K. Wada, D. Li and J. Suzuki, *Langmuir*, 2005, **21**, 8035.

[15] M. Anpo, M. Takeuchi, K. Ikeue and S. Dohshi, *Curr. Opin. Solid State Mater. Sci.*, 2002, **6**, 381.

[16] H. Yamashita, Y. Ichihashi, S. G. Zhang, Y. Matsumura, Y. Souma, T. Tatsumi and M. Anpo, *Appl. Surf. Sci.,* 1997, **121**, 305.

[17] http://en.wikipedia.org/wiki/Semiconductor

[18] M. Fox, *Optical properties of solids*, Oxford University Press, New York (2001).

[19] Y. Li, Z. Liu, L. Liu, and W. Gao, *J. Am. Chem. Soc.*, 2010, **132**, 13008.

[20] J. Yang, C. Chen, H. Ji, W. Ma and J. Zhao, *J. Phys. Chem. B*, 2005, **109**, 21900.

[21] M. Takeuchi, G. Martra, S. Coluccia and M. Anpo, *J. Phys. Chem. B*, 2005, **109**, 7387.

[22] O. Carp, C. L. Huisman and A. Reller, *Prog. solid state chem.*, 2004, **32**, 33.

[23] Y. Du and J. Rabani, *J. Phys. Chem. B*, 2003, **107**, 11970.

[24] T. Hirakwa and Y. Nosaka, *Langmuir*, 2002, **18**, 3247.

[25] M. Grätzel, *Nature*, 2001, **414**, 338.

[26] L. A. Harris and R. H. Wilson, *Ann. Rev. Mater. Sci.,* 1978, **8**, 99.

[27] R. F. Howe and M. Grätzel, *J. Phys. Chem.,* 1987, **91**, 3906.

[28] O. I. Micic, Y. Zhang, K. R. Cromack, A. D. Trifunac and M. C. Thurnauer, *J. Phys. Chem.,* 1993, **97**,13284.

[29] R. Nakamura and Y. Nakato, *J. Am. Chem. Soc.,* 2004, **126**, 1290.

[30] N. Saton, T. Nakashima, K. Kamikura and K. Yamamoto, *Nature nanotech.*, 2008, **3**,106.

[31] M. Kaneko and I. Okura, (Eds) *Photocatalysis: Science and Technology*, Springer, 2002.

[32] X. Chen and S. S. Mao, *Chem. Rev.*, 2007, **107**, 2891.

[33] A. Kafizas, C. W. Dunnill and I. P. Parkin, *Phys. Chem. Chem. Phys.*, 2011, **13**, 13827.

[34] X. Chen, S. Shen, L. Guo and S. S. Mal, *Chem. Rev.*, 2010, **110**, 6503.

[35] J. T. Davis and E. K. Rideal, *Interfacial Phenomena*; Academic Press: New York, 1963.

[36] C. Su, B.-Y. Hong and C.-M. Tseng, *Catal. Today*, 2004, **96**, 119.

[37] L. L. Hench and J. K. West, *Chem. Rev.*, 1990, **90**, 33.

[38] S. Roy and A. Baiker, *Chem. Rev*., 2009, **109**, 4054.

Chapter 2

Creating oxygen vacancies as a novel strategy to form tetrahedrally coordinated Ti^{4+} in Fe/TiO_2 nanoparticles

Abstract

The incorporation of Fe as a dopant in anatase TiO_2 nanoparticles has been systematically investigated with the aim of changing the coordination geometry of Ti via the formation of oxygen vacancies. Although Fe^{3+} ions are present in the solution during growth of the nanoparticles, a high temperature heat treatment is found to be necessary to incorporate Fe^{3+} as a substituent for Ti^{4+} in the bulk of the TiO_2 nanoparticles. The Fe^{3+} acceptors are found to be charge-compensated by oxygen vacancies, up to dopant concentrations as high as 10%. The surprisingly high solubility of Fe is attributed to the very similar radii of Ti^{4+} and Fe^{3+}, and to the energetically favorable Coulomb attraction between the negatively charged Fe acceptor and the positively charged oxygen vacancies. A combined EXAFS/XANES study reveals that part of the Ti^{4+} ions changes their coordination number from 6 to 4 at high oxygen vacancy concentrations. The deliberate use of oxygen vacancies to modify the coordination geometry of metal ions represents a new strategy that offers exciting possibilities to tune the selectivity of photo-catalytically active metal oxide nanoparticles.

2.1 Introduction

Titanium dioxide (TiO_2), one of best-known semiconductor photocatalysts, has been intensely investigated for applications in air cleaning, water purification, water splitting, and artificial photo-synthesis.[1-5] Although TiO_2 generally shows high activities for the photocatalytic oxidation of organic pollutants,[6] the photocatalytic activity and selectivity towards reduction reactions (e.g. NO_x to N_2, or CO_2 and H_2O to fuels) are still very low.[7] A well known method in catalysis to change the selectivity of a reaction is to change the coordination number of the metal ion. In the case of TiO_2, changing the Ti coordination number from its usual value of 6 (octahedra, TiO_6) to 4 (tetrahedra, TiO_4) was indeed found to change the reaction mechanism of NO_x degradation from photo-oxidation (forming nitrates) to photo-reduction (forming N_2 and O_2).[8] This has been achieved by depositing isolated titanium oxide clusters inside the cavities of zeolite-Y with ion beam implantation techniques.[8,9] However, large scale application of zeolites modified by ion beam implantation is economically unattractive. In this paper, we explore an alternative strategy to reduce the coordination number of Ti^{4+} by creating a high concentration of oxygen vacancies in the TiO_2 lattice.

Oxygen vacancies can be created by annealing pure TiO_2 at elevated temperatures (generally >400°C) in an oxygen-poor environment, such as a pure He, N_2 or Ar gas atmosphere.[10] This process is described by reaction (7) in chapter 1.
However, the oxygen vacancies ($V_O^{\bullet\bullet}$) formed will slowly disappear while the material is exposed to air, even at room temperature, since this reaction is reversible. To stabilize the oxygen vacancies one can introduce acceptor-type dopants, such as Fe^{3+}, as ionic charge-compensating species (reaction (8), chapter 1).
This dissolution reaction is irreversible. Alternatively, the effective negative charge of the Fe^{3+} acceptor can be compensated by a decrease in the concentration of free electrons in the TiO_2 (reaction (9), chapter 1).

This electronic compensation reaction also helps to stabilize the oxygen vacancies (albeit indirectly), since decreasing the concentration of free electrons in TiO_2 will shift the equilibrium of reaction (7) in Chapter 1 to the right.

In addition to tuning the desired *selectivity*, oxygen vacancies located at the surface are also known to enhance the *activity* of the (photo)catalyst in certain cases.[12-14] Another, more common method to enhance the catalytic activity is by decreasing the particle size in order to increase the effective surface area. For mesoporous TiO_2 films consisting of 15 nm particles, effective surface area enhancements by a factor of ~800 are possible.[15] Combining these strategies by synthesizing TiO_2 nanoparticles with a large concentration of oxygen vacancies would therefore seem a promising route towards highly active and selective (photo)catalysts. The main challenge for achieving this goal is to control the incorporation of dopants inside the nano-particles. This is far from trivial due to the well known "self-purification" effect, in which impurities tend to segregate towards the surface of the nanoparticle.[16]

In this paper, we show that for high oxygen vacancy concentrations, the coordination of part of the titanium ions can be changed from an octahedral to a tetrahedral geometry. Moreover, we show that the required high concentration of oxygen vacancies can be achieved and stabilized by doping TiO_2 nanoparticles with Fe^{3+} ions.

2.2 Experimental section

Synthesis of Fe-doped TiO_2. Both pure TiO_2 and Fe-doped TiO_2 colloidal nano-particles were synthesized by a simple, template-free sol-gel method.[17] Briefly, titanium isopropoxide (TTIP) is dropwise added to a slightly acidified solution of ultrapure water under vigorous stirring. For Fe-doped samples, $Fe(NO_3)_3 \cdot 9H_2O$ was dissolved in the aqueous solution before adding the TTIP. After 2 hours of stirring, an opaque suspension is obtained which contains TiO_2 and propanol as the main reaction products. A homogeneous colloidal TiO_2 (~ 0.13 g/ml) solution was produced after evaporating the propanol at 333 K in a rotary evaporator. A part of the colloidal solution was dried at 373 K for producing a nano-particulate powder with dopant concentrations ranging between 0% (undoped) and 10% Fe. For each dopant concentration, part of the powder was investigated as dried (at 373 K), and part was further annealed at high temperature (>720 K) in air for 3 hours. The remaining colloidal solution was used for making thin films on glass substrates (Schott Borofloat 33) by a tape casting method for Raman characterization.

Characterization. The crystal structure of Fe-doped TiO_2 nanoparticles was investigated by a high resolution Transmission Electron Microscope (TEM) equipped with a 200 kV FEI TECNAI TF20 field emission gun (FEG) and an energy dispersive X-ray (EDX) system for determining the Fe concentration. Samples were mounted on Quantifoil® grid (carbon polymer supported copper grid) by placing a few droplets of a suspension of the material in ethanol and drying at ambient conditions. To identify crystalline phases and to estimate crystallite sizes, X-ray diffraction (XRD) was performed using a Bruker D8 Advance diffractometer with either a Cu-Kα source in

combination with a Si point detector, or a Co-Kα source with a LynxEye linear detector. In both cases, the sources were operated at 35 kV, 40 mA. The crystallite sizes were calculated from the XRD peak widths using the Scherrer equation, after correcting for the instrumental resolution. High resolution X-ray photoelectron spectroscopy (XPS, Thermo Escalab 250 with a monochromatic Al Kα X-ray source) was used to identify the Fe valence state of various Fe/TiO_2 samples. The total spectrum acquisition time was 3.5 minutes. Adventitious carbon (C_{1s} peak at 284.6 eV) was used to calibrate the Fe-related binding energies. UV-Vis-NIR Diffuse Reflectance Spectra (DRS) were recorded on a Perkin-Elmer Lambda 900 spectrometer (scanning step: 1 nm) with an integrating sphere assembly. A $BaSO_4$ standard was used as a reference sample for baseline correction. Raman spectra were measured on a Renishaw Raman imaging microscope, system 2000. A 514.5 nm argon-ion laser beam (20 mW) was used for excitation. A Leica DMLM optical microscope with a Leica PL floutar L500/5 objective lens was used to focus the beam on the sample. The wavelength of the Raman spectra was calibrated using the 520 cm^{-1} peak of a silicon wafer as a reference.

XAFS analysis. X-ray absorption fine atructure (XAFS) experiments were performed on the DUBBLE beamline (BM26A) at the European Synchrotron Radiation Facility (ESRF, Grenoble, France), operating at 6 GeV with beam currents ranging from 160 to 200 mA. About 5 mg of the samples mixed with 50 mg boron nitride (99.5%) were pressed into a pellet. Measurements were performed at room temperature in air in transmission mode for the Ti K-edge at 4966 eV and in fluorescence mode for the Fe K-edge at 7112 eV. The beamline was equipped with a Si (111) double-crystal monochromator, which was detuned to 60% of the Bragg peak intensity to suppress higher harmonics. For the fluorescence mode, a 9-element Ge solid state detector was used. Extended X-ray absorption fine structure (EXAFS) data were extracted from the measured absorption spectra with XDAP software.[18] Three scans for each sample were averaged together to improve the signal-to-noise ratio. The edge-energy was determined from the first maximum of the first derivative of main edge-jump and calibrated with Fe and Ti reference foils. A smooth atomic background function, represented by a cubic spline, was used to extract the EXAFS oscillation from the absorption spectrum. The obtained data was normalized by the background height 50 eV after the edge. Experimental data were fitted in R-space. The quality of the fit was verified by comparing the k^1 and k^3 weighted spectra.[19]

2.3 Results and discussion

UV-Vis-NIR diffuse reflection spectra have been recorded to investigate the nature of the Fe species within the material. Figure 1a shows the optical absorption spectra for undoped and Fe-doped TiO_2 powder after drying at 373 K (i.e., before annealing). A steep increase of the absorption at ~400 nm for pure TiO_2 and Fe/TiO_2 is assigned to the indirect band gap of anatase TiO_2.[20] Some agglomerated Fe_2O_3 is also present at the surface of Fe-doped TiO_2, as evidenced by the broad peak between 740 and 1100 nm which is also observed for a pure commercial α-Fe_2O_3 reference powder.

For the Fe-doped powders, a pronounced narrow peak at ~480 nm is observed. This peak is not observed for undoped TiO_2, and appears to be related to the presence of Fe^{3+} species. To verify this, a control experiment was performed in which a small amount of $Fe(NO_3)_3$ was added to a colloidal solution of undoped TiO_2 nanoparticles. The UV/Vis spectrum of this solution also showed a clear peak at 480 nm (Figure 1c). No peak at 480 nm was found either for an aqueous solution of $Fe(NO_3)_3$ or a pure TiO_2 colloid. We therefore assign the 480 nm peak to the presence of Fe^{3+} species adsorbed at the surface of TiO_2. Although the peak at 480 nm partially obscures the band–to–band transition, the pronounced red-shift of the absorption edge that is often reported for Fe-doped TiO_2[21] is not clearly observed in Figure 1a. Apparently, the presence of Fe^{3+} ions in the solution during the formation and growth of the TiO_2 nanoparticles does not result in the actual incorporation of Fe^{3+} in the TiO_2 lattice.

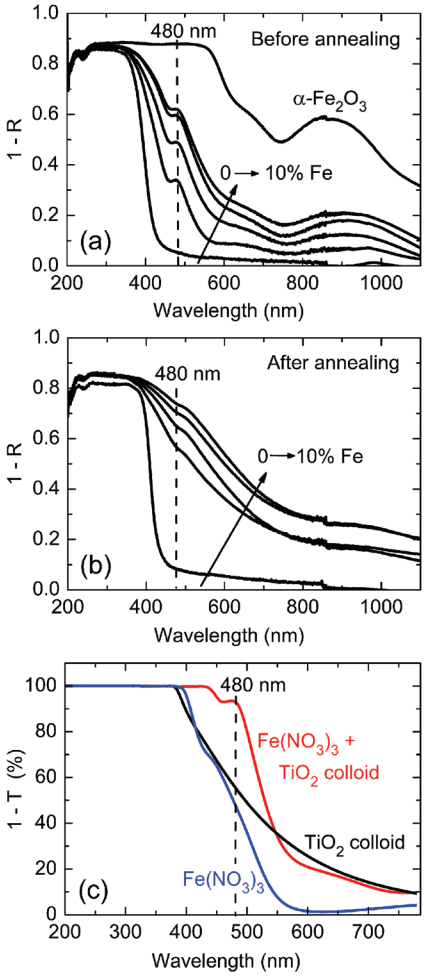

Figure 1: (a) UV-Vis-NIR diffuse reflection spectra of undoped and Fe-doped TiO_2 nanopowders before annealing. The dopant concentrations are 2%, 5%, 8% and 10% of Fe. A diffuse reflectance spectrum for commercial α-Fe_2O_3 powder is shown for comparison. (b) Similar spectra after annealing in air at 773 K. (c) UV-Vis-NIR transmission spectra of a TiO_2 colloidal solution, a $Fe(NO_3)_3$ solution and a mixture of both solutions.

In an attempt to let the Fe^{3+} ions diffuse from the surface into the bulk of the TiO_2 nanoparticles, the samples were annealed in air for 3 hours at 773 K. Figure 1b shows the absorption spectra after this treatment. The absorption peak at 480 nm (adsorbed Fe^{3+} ions) and the broad peak between 740 – 1100 nm (Fe_2O_3) have virtually disappeared, even for 10% Fe/TiO_2. In addition, the optical absorption edge of Fe/TiO_2 shifts to the visible region, in accordance with the observed color change of the samples from yellow to dark brown with increasing Fe concentrations. The absorption edge shift has been observed many times for Fe-doped TiO_2.[21] It cannot be attributed to the presence of oxygen vacancies, since the corresponding energy levels are ~ 1.7 eV below the conduction band of TiO_2, i.e., too far away from the band edge.[22] The shift is instead caused by the presence of the Fe^{3+} dopant, which has an energy level located 0.06 – 0.1 eV above the valence band (Figure 2).[22-25] These observations clearly indicate that the Fe^{3+} ions at the surface of the TiO_2 – either as adsorbed ions or in the form of an adjacent α-Fe_2O_3 phase – diffuse into the bulk of the nanoparticles during the high temperature treatment.

The 3+ oxidation state of the Fe dopant ions in TiO_2 is confirmed by XPS analysis of the Fe/TiO_2 samples after firing at high temperature in air (Figure 3). The peaks at 711.2 eV and 724.8 eV correspond to the Fe $2p_{3/2}$ and Fe $2p_{1/2}$ binding energies of Fe^{3+}, while the absence of a peak at 709.3 eV reveals that no Fe^{2+} is present in any of the Fe/TiO_2 samples.[26,27]

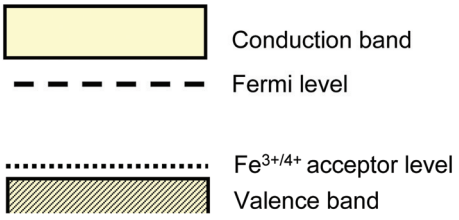

Figure 2: Band diagram of Fe-doped TiO_2.[22,23]

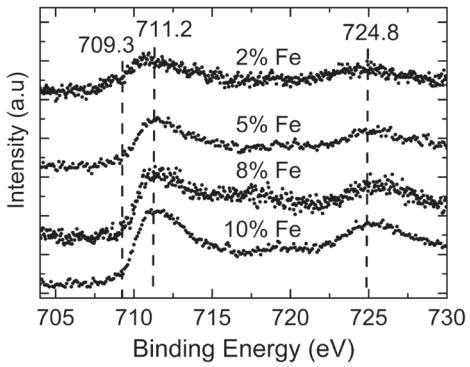

Figure 3: XPS Fe-2p spectra of Fe-doped TiO_2 after annealing in air at 773 K. The peaks at 711.2 and 724.8 eV provide conclusive evidence for the presence of Fe^{3+}.

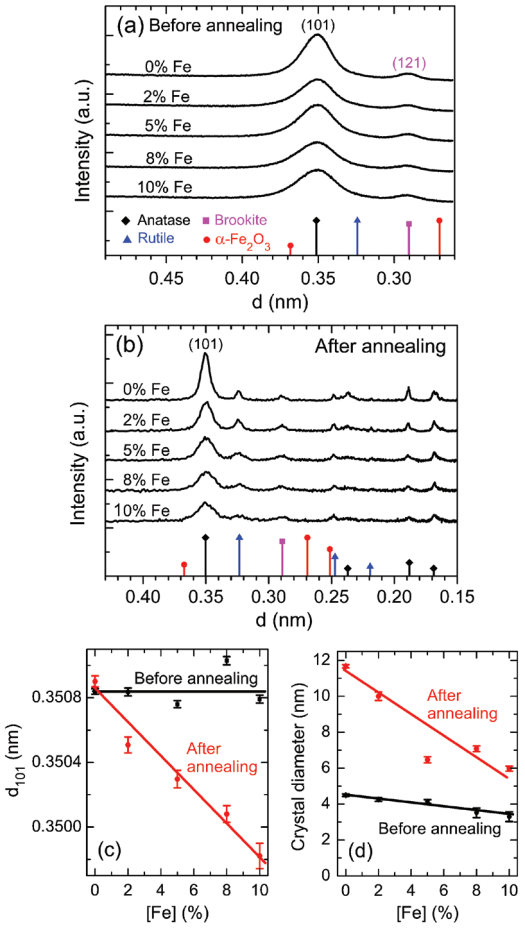

Figure 4: (a) XRD patterns of pure TiO_2 and Fe/TiO_2 powders before annealing. (b) Similar patterns after annealing in air. The vertical lines represent the powder diffraction patterns of anatase (PDF No. 01-073-1764), rutile (PDF No. 00-021-1276), α-Fe_2O_3 (PDF No. 01-079-1741), and brookite (PDF No. 01-076-1935). (c) d_{101} lattice spacing of pure TiO_2 and Fe/TiO_2 before and after annealing in air. (d) Crystal sizes for pure TiO_2 and Fe/TiO_2 before and after annealing in air, determined from the anatase (101) peak.

We now turn our attention to the crystal structure of the Fe/TiO_2 nanoparticles. Before annealing, the pure TiO_2 and Fe/TiO_2 samples are mainly composed of the anatase crystal phase, as evidenced by the main anatase (101) peak shown in the XRD patterns in Figure 4a. A small amount of brookite is also present, as indicated by the small peak at d_{121} = 0.29 nm. No crystalline phases related to α-Fe_2O_3 (main peak at d_{104} = 0.27 nm) or any other iron oxides are found, even for the highest Fe concentration of 10%. This suggests that the iron oxide is present as an amorphous phase, or that it is very finely dispersed over the surface of the particles. After annealing in air at 773 K, a small amount of rutile is present for all samples. No Fe- or Fe_2O_3-related phases can be identified from the XRD patterns, even for 10% Fe/TiO_2 (Figure 4b), and the anatase phase remains the dominant phase for all concentrations.

To investigate if Fe is actually incorporated in the TiO_2 structure, the change in lattice parameters is determined from the position of the anatase (101) peak. The peak is fitted with a pseudo-Voigt function, and plotted as a function of the Fe concentration in Figure 4c. Before annealing, no significant change in lattice spacing is observed with increasing Fe concentration. This indicates that the Fe ions do not enter the TiO_2 lattice, and remain on the surface of the nanoparticles. However, after annealing in air, the anatase (101) peak position shifts towards smaller *d* values with increasing Fe concentration. The observed shift is linear with the amount of Fe, which proves that Fe ions are indeed incorporated into the TiO_2 lattice.

The decrease in lattice constant is, however, contrary to what one might initially expect, since the radius of Fe^{3+} ions (0.65 Å) is slightly larger than Ti^{4+} radius (0.61 Å) for six-fold coordinated ions.[28] This can be explained by the formation of oxygen vacancies as charge-compensating defects for the acceptor-type Fe dopants, according to the ionic compensation reaction given by Eq. (2). One would expect the formation of vacant oxygen sites to cause a significant decrease in the lattice parameter, and the negative slope in Figure 4c suggests that it in fact fully negates the lattice expansion caused by the Fe^{3+} ions. The preference of the system for ionic compensation instead of electronic compensation (Eq. (3)) is simply due to the fact that there are few free electrons available; the donor density in undoped TiO_2 is usually in the order of 10^{17} cm^{-3},[29] whereas a concentration of ~10^{20} cm^{-3} would be required to fully compensate 1% of Fe donors. Moreover, electronic compensation of the Fe acceptor by free holes (transition to p-type conductivity) is very unlikely, since the valence band of TiO_2 is mainly composed of O-2p orbitals and therefore not very receptive to holes.[30]

The high temperature treatment in air significantly reduces the anatase peak widths (Figures 4a vs. 4b), which indicates a growth in average crystallite size due to sintering. The crystallite sizes are calculated by the Scherrer equation and plotted in Figure 4d. This figure shows a linear decrease in crystallite size with increasing Fe concentrations, both before and after annealing. The fairly modest decrease in particle size before annealing has been tentatively attributed to the presence of adsorbed Fe^{3+} ions at the surface of the TiO_2 particles while they are formed in solution.[17] The presence of Fe^{3+} is likely to affect the number of available adsorption sites and/or the surface free energy of the particle, and can therefore slow down the growth kinetics of the sol-gel process.

For the annealed samples, a much stronger decrease in particle size with increasing Fe content is observed (red line in Figure 4d). This implies that the kinetics of particle growth during high-temperature annealing slow down with increasing Fe concentration (the difference between the red and black lines decreases with increasing Fe concentration in Figure 4d). This may seem counter-intuitive at first, since a higher Fe concentration implies a higher oxygen vacancy concentration, and therefore a higher mobility of ions and faster sintering in the TiO_2 bulk. It should be realized, however, that the growth of such small nano-particles is likely to be dominated by *surface* processes instead of bulk ion transport. We speculate that the presence of Fe^{3+} at the surface of the TiO_2 nanoparticles decreases the surface free energy, and thereby reduces the thermodynamic driving force for particle growth.

High resolution TEM images have been recorded to further support the evidence for the presence of oxygen vacancies in the Fe-doped TiO_2 nanoparticles. Figure 5

shows the results for undoped and Fe-doped samples after annealing at 773 K in air. Well-ordered anatase fringes (d_{101} = 0.35 nm) are observed for undoped TiO_2 samples (Figure 5a). However, for 10% Fe/TiO_2, the anatase fringes at d_{101} have a somewhat fuzzy appearance, indicating extensive disorder—or even some amorphicity—in the lattice (large circle in Figure 5b). Such a large amount of disorder would indeed be expected for an oxygen vacancy concentration in the order of ~5% (one oxygen vacancy compensates two Fe^{3+} ions, see Eq. (2)). To determine the Fe concentration in the sample, the electron beam was focused on a single nanoparticle of 10% Fe-doped TiO_2 (small circle in Figure 5b) and an EDX spectrum was recorded. The result shown in Figure 5c indicates a Ti : Fe ratio of approximately 10 : 1, which suggests that all Fe is indeed incorporated into the TiO_2 lattice. Figure 5d illustrates the average nanoparticle size for the 10% Fe/TiO_2 samples, which is consistent with the 6 nm found from the XRD data as shown in Figure 4d.

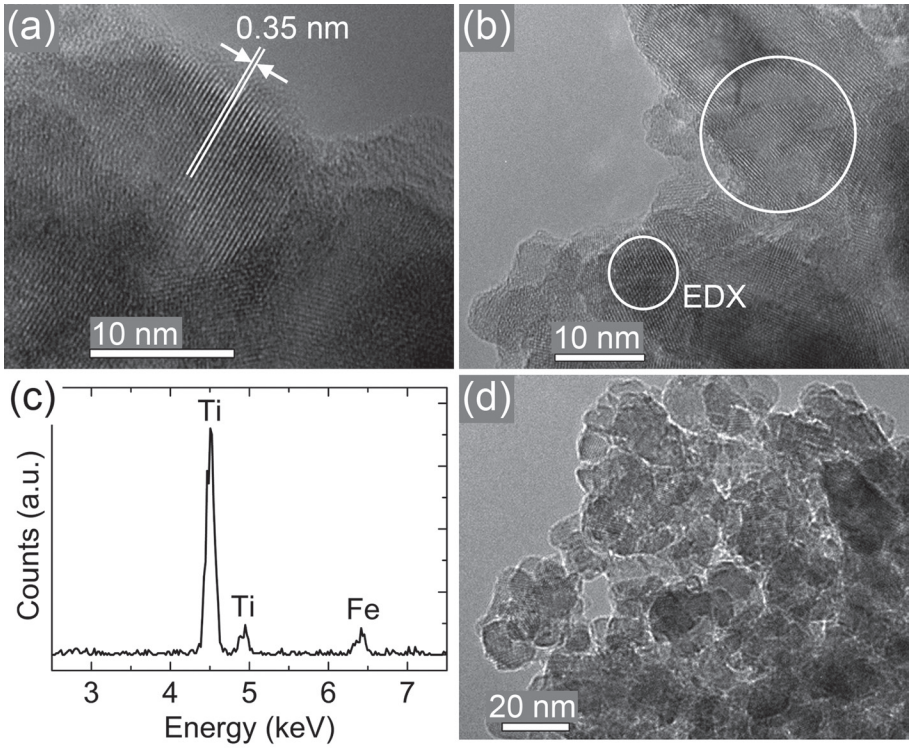

Figure 5: (a) High resolution TEM image of pure TiO_2 after annealing in air; (b) High resolution TEM image of 10% Fe/TiO_2 after annealing in air; (c) EDX spectrum of 10% Fe/TiO_2 when focusing the electron beam on the "EDX" area shown in (b); (d) TEM image of 10% Fe/TiO_2 after annealing in air.

To further elucidate the presence of oxygen vacancies in Fe/TiO_2, a Raman spectroscopy study was carried out. Four Raman active modes at ~143 cm^{-1} (E_g), 399 cm^{-1} (B_{1g}), 519 cm^{-1} (B_{1g}) and 639 cm^{-1} (E_g) are observed for both pure TiO_2 and Fe-doped TiO_2 after annealing in air (Figure 6a).[31] This suggests that all samples are mainly composed of anatase, which is consistent with our XRD and TEM observations. Closer inspection of Figure 6a shows that the peak position of the strongest anatase E_g mode at ~143 cm^{-1} shifts toward higher wavenumbers with increasing Fe concentration. A similar shift of the E_g vibrational mode has been observed by Parker et al. for strongly reduced TiO_{2-x}.[32] They observed a linear relationship between the E_g peak position and the O/Ti ratio, which is related to the concentration of oxygen vacancies via $[O/Ti] = 2 - x = 2 - [V_O^{\bullet\bullet}]$. We can now compare the peak shift of our Fe-doped TiO_2 with that of Parker's reduced TiO_{2-x} by plotting both datasets as a function of $[V_O^{\bullet\bullet}]$. To convert the Fe concentration to an oxygen vacancy concentration, we use the electroneutrality equation $[Fe_{Ti}^{/}] = 2[V_O^{\bullet\bullet}]$. As shown in Figure 6b, the datasets overlap almost perfectly. This strongly suggests that all Fe^{3+} ions are compensated by oxygen vacancies, even up to Fe doping levels as high as 10%, and is consistent with the absence of iron oxide phases in the XRD patterns.

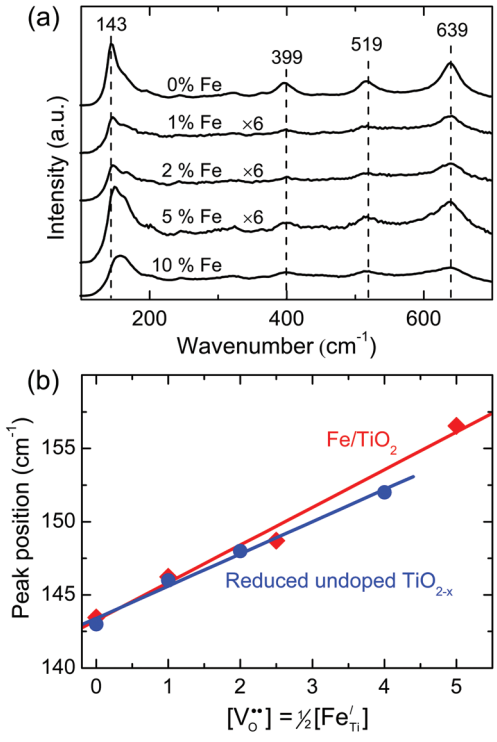

Figure 6: (a) Raman spectra of Fe/TiO_2 after annealing in air. (b) Peak positions of the strongest anatase E_g vibrational mode for Fe-doped TiO_2 prepared in this study, and for reduced undoped TiO_2 as reported by Parker et al.[32]

At first glance, the absence of iron oxide phases for Fe concentrations as high as 10% seems surprising, since the solubility of dopants in metal oxides is usually limited to 1–2% before phase segregation occurs. We attribute the apparent stability of 10% Fe-doped anatase TiO_2 nanoparticles to two factors. The most important one is the very similar ionic radii of the Ti^{4+} and Fe^{3+} ions: 0.61 Å and 0.65 Å, respectively. Secondly, the Coulomb attraction between the negatively charged Fe'_{Ti} and positively charged $V_O^{\bullet\bullet}$ decreases the total (negative) lattice energy. This enhances the stability of the nanoparticle and postpones phase segregation. Of course, phase segregation will eventually occur at concentrations beyond 10%. The actual solubility limit for Fe in anatase TiO_2 nanoparticles is, however, not well known and beyond the scope of this study.

The role of the particle size in these considerations is unclear. Recent studies show that the dopant concentration in nanoparticles can either be much lower than in bulk systems due the so-called "self-purification" effect,[16] or 1–4 orders of magnitude higher due to kinetic trapping of substitutional dopants during colloidal growth at relatively low temperatures.[33,34] Attempts have been made to develop a unifying model that explains both effects in terms of kinetically limited ad- and desorption of dopants during solution-based nanoparticle growth,[35] but it is difficult to reconcile such an interpretation to our observation that the Fe dopants *only* enter the TiO_2 nanoparticles while annealing at elevated temperatures (773 K). Invoking the trapped dopant model is clearly not appropriate under such conditions. It should be noted that a high-temperature post-synthesis treatment is not always necessary for other systems. For example, Fe dopant concentrations in ZnO in excess of 10% can be obtained by flame spray pyrolysis,[36] and electronic structure calculations show that the Fe actually stabilizes the ZnO nanoparticles by reducing the total energy of the particle.[37] One important difference between our system and the more covalently-bonded semiconductor nanocrystals described in the studies mentioned above is that our dopants are ionically instead of electronically compensated – compare Eq. (2) and (3). It is possible that the defect formation energy in such ionic systems decreases instead of increases with decreasing particle size due to, for example, defect association.[11] This would result in an *inverse* self-purification effect that could explain the high dopant solubility. Clearly, more detailed studies are needed to determine the physical origin of the high dopant solubility.

To probe the local structure surrounding the Ti^{4+} ions, Ti K-edge X-ray Absorption Near Edge Structure (XANES) spectra have been measured. The XANES spectra of pure TiO_2 and 5% Fe/TiO_2 are shown in Figure 7a for comparison. The three low-intensity pre-edge peaks (A_1, A_2, A_3) observed for all samples can be assigned to the transition from the 1s core level of Ti to three different kinds of molecular orbitals ($1t_{1g}$, $2t_{2g}$ and $3e_g$), and are characteristic of the octahedral coordination of Ti in the TiO_2 lattice.[38,39] The presence of tetrahedrally coordinated Ti would be evidenced by a single peak in between the A_1 and A_2 peaks.[40] Compared to pure TiO_2, a modest but clear increase of the shoulder peak intensity between A_1 and A_2 (marked T_{tet}) is indeed observed for Fe/TiO_2. This suggests that the large concentration of oxygen vacancies in Fe-doped TiO_2 may lead to the formation of tetrahedrally coordinated Ti^{4+} species.

Comparison of the anatase XANES spectrum to previously reported spectra is somewhat complicated by the inconsistent assignment of the pre-edge peaks in the

literature. In several studies on nano- or cluster-sized anatase the T_{tet}, A_2 and A_3 peaks in Figure 7a are labeled as A_2, A_3 and B, respectively.[41-44] However, since the T_{tet} peak is consistently absent in studies on bulk anatase,[44-46] it is unlikely to correspond to an A_2 transition. Others have associated this peak with a decrease in the Ti^{4+} coordination number,[39,47] which is in line with our interpretation in terms of tetrahedrally coordinated Ti^{4+}.

Before examining the Ti coordination in more detail, we briefly discuss the valence state of the Ti and Fe ions. For materials containing Ti^{4+}, the onset of the Ti K-edge – defined by the first maximum of the first derivative for the main edge-jump – is located at

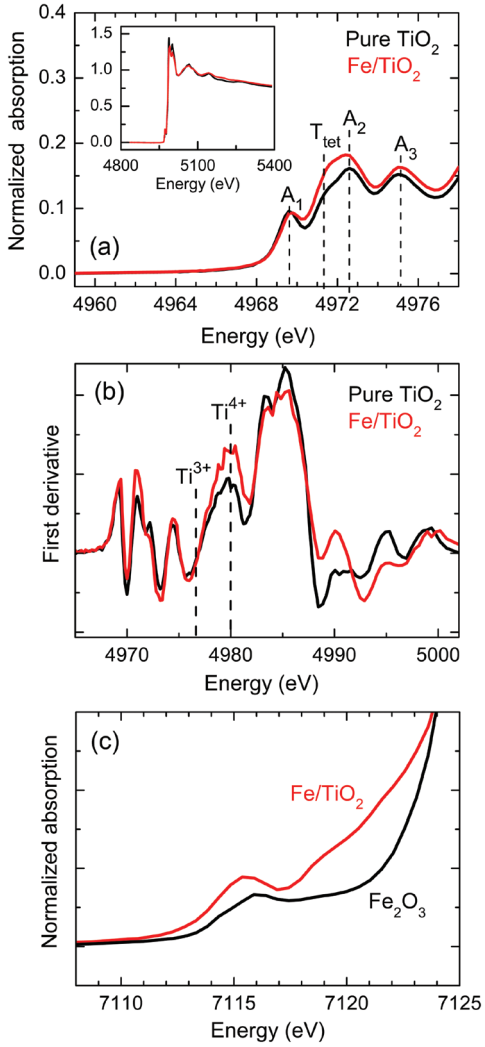

Figure 7: Ti K-edge XANES spectra (a) and its first derivative (b) for 5% Fe/TiO_2 and pure TiO_2 after annealing in air, and (c) Fe K-edge XANES spectra of 5% Fe/TiO_2 and commercial α-Fe_2O_3.

4980 eV (Figure 7b). When Ti^{4+} is reduced to Ti^{3+}, this peak is known to gradually shift to ~3 eV lower energies.[48,49] Since no such shift is observed upon Fe doping, we conclude that titanium ions remain in the 4+ valence state. This is indeed consistent with the ionic compensation mechanism of Eq. (2), which shows that Fe can be incorporated into the TiO_2 lattice without creating any free electrons. The Fe K-edge XANES spectrum of Fe-doped TiO_2 is shown in Figure 7c. A single pre-edge peak is observed, similar to that of commercial α-Fe_2O_3 reference powder. Comparison of these spectra to those reported by Vračar et al.[50] for $SrFe_xTi_{1-x}O_{3-\delta}$ (STF) shows that our Fe/TiO_2 spectra are similar to reduced STF, in which Fe is known to be in the +3 state. Specifically, the main peak of our Fe/TiO_2 sample lies in between the main α-Fe_2O_3 peak at 7116 eV and its lower-energy shoulder. If Fe^{4+} would be present, the main peak would be at slightly higher energies, as illustrated by Figure 3 in the paper by Vračar et al.[50] This confirms our earlier conclusion from the XPS data that Fe is present in the +3 oxidation state in these TiO_2 nanoparticles.

Further confirmation of the presence of tetrahedrally coordinated Ti^{4+} is required at this point, since 5-fold coordinated Ti^{4+} also produces a significant pre-edge feature.[39,47,51] Following the approach by Liu et al.,[49] we use the Ti-O bond length to distinguish between these possibilities. The interatomic distances of pure TiO_2 and Fe/TiO_2 are compared through the Fourier transformed Ti K-edge EXAFS data, shown in Figure 8. The Ti-O bond length of pure TiO_2 (anatase) is 1.93 Å, close to the value of 1.937 Å for most Ti-O bond lengths in the ideal anatase structure (a smaller fraction of the Ti-O bonds in the ideal structure have a length of 1.966 Å). For the Fe-doped samples, the Ti-O bond length shrinks to 1.81 Å. This is nearly identical to the Ti-O distance of 1.82 Å found for the TiO_4 tetrahedra in Ti-Si mixed oxides.[51] Although the small T_{tet} peak area indicates that only a modest fraction of the Ti^{4+} ions are tetrahedrally coordinated – presumably at the surface – such a small value of the *average* Ti-O bond length provides compelling evidence for the presence of these species in Fe-doped TiO_2 nanoparticles.

The results discussed above clearly show that doping of anatase TiO_2 nanoparticles

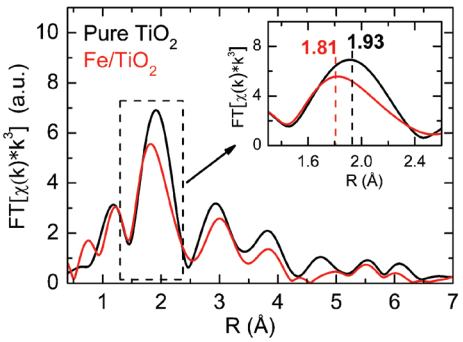

Figure 8: Magnitude part of Fourier transformed k^3-weighted $\chi(k)$ of the Ti K-edge EXAFS spectra for pure TiO_2 and Fe/TiO_2 (after phase correction).

with Fe results in i) the formation of a large number of oxygen vacancies (XRD, TEM, Raman), and ii) the presence of tetrahedrally coordinated Ti^{4+} species (XANES, EXAFS). These observations can be visualized as shown in Scheme 1, in which partial removal and rearrangement of the oxygen ions in TiO_6 octahedra (presumably at or near the surface of the nanoparticles) results in the formation of TiO_4 tetrahedra.

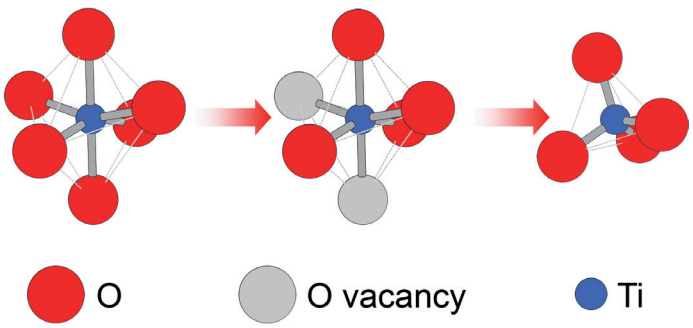

Scheme 1: Transformation from octrahedrally to tetrahedrally coordinated Ti^{4+} in TiO_2 when high concentrations of oxygen vacancies are present.

2.4 Conclusions

A series of Fe-doped anatase TiO_2 nanoparticles have been prepared with the aim of changing the local coordination geometry of Ti at the surface of these particles. For Fe/TiO_2 nanopowders dried at 373 K, Fe remains on the surface of the TiO_2 nanoparticles. After annealing in air at 773 K, the Fe ions are found to diffuse into the bulk of the TiO_2 nanoparticles, where they remain in the 3+ valence state as acceptor-type substituents for Ti^{4+}. The Fe dopants are charge-compensated by oxygen vacancies, and the concentration of these vacancies increases linearly with Fe content up to an Fe concentration of 10%. No evidence was found for the segregation of binary iron oxide phases. This unusually high dopant solubility is attributed to two factors: i) the nearly identical ionic radii of Ti^{4+} (0.61 Å) and Fe^{3+} (0.65 Å), and ii) the energetically favorable Coulomb attraction between the negatively charged Fe'_{Ti} and the positively charged $V_O^{\bullet\bullet}$. EXAFS and XANES analysis of the samples with a high oxygen vacancy concentration reveal the presence of a small amount of tetrahedrally coordinated Ti. These TiO_4 clusters are presumably present at the surface, where the lattice symmetry

constaints are more relaxed. The ability to tune the coordination geometry of Ti^{4+} by creating oxygen vacancies offers exciting opportunities to change the selectivity of these catalysts, while the stable presence of surface oxygen vacancies may lead to increased activities for many catalytic and photo-catalytic reactions.

Acknowledgements

We thank Dr. S. Nikitenko for assistance with the XAFS experiments at the DUBBLE BM26A beamline of the European Synchrotron Radiation Facility (ESRF, Grenoble, France). The Netherlands Organization for Scientific Research (NWO) is acknowledged for funding the XAFS experiments. Financial support for this project is provided by the Shell-TU Delft “Sustainable Mobility” program.

References

[1] Hoffmann, M. R.; Martin, S. T., Choi, W.; Bahnemann, D. W. *Chem. Rev.* **1995**, *95*, 69.

[2] Yang, C. C.; Yu, Y. H.; Van der Linden, B.; Wu, J. C. S.; Mul, G. *J. Am. Chem. Soc.* **2010**, *132*, 8398.

[3] Fujishima, A.; Honda, K. *Nature* **1972**, *238*, 37.

[4] Chen, X.; Liu, L.; Yu, P. Y.; Mao, S. S. *Science* **2011**, *33*, 746.

[5] Liu, H.; Ma, H. T.; Li, X. Z.; Li, W. Z.; Wu, M.; Bao, X. H. *Chemosphere* **2003**, *50*, 39.

[6] Fujishima, A.; Rao, T. N.; Tryk, D. A. *J. Photochem. Photobiol. C* **2000**, *1*, 1.

[7] Nguyen, T.; Wu, J. C. S. *Sol. Energy Mater. Sol. Cells* **2008**, *92*, 864.

[8] Yamashita, H.; Ichihashi, Y.; Zhang, S. G.; Matsumura, Y.; Souma, Y.; Tatsumi, T.; Anpo, M. *Appl. Surf. Sci.* **1997**, *121*, 305.

[9] Anpo, M.; Takeuchi, M.; Ikeue, K.; Dohshi, S. *Curr. Opin. Solid State Mater. Sci.* **2002**, *6*, 381.

[10] Carp, O.; Huisman, C. L.; Reller, A. *Prog. Solid. State. Chem.* **2004**, *32*, 33.

[11] Chiang, Y.-M.; Birnie, D. P.; Kingery, W. D. *Physical Ceramics*, Wiley, New York, **1997**.

[12] Bikondoa, O.; Pang, C. L.; Ithnin, R.; Muryn, C. A.; Onishi, H.; Thornton, G. *Nature Mater.* **2006**, *5*, 189.

[13] Zheng, Z.; Teo, J.; Chen, X., Liu, H.; Yuan, Y.; Waclawik, E. R.; Zhong, Z.; Zhu, H. *Chem. Eur. J.* **2010**, *16,* 1202.

[14] Boon, A. Q. M.; Looij, F.; Geus, J. W. *J. Mol. Catal.* **1992**, *75*, 277.

[15] O'Regan, B.; Grätzel, M. *Nature* **1991**, *353*, 737.

[16] Dalpian, G. M.; Chelikowsky, J. R. *Phys. Rev. Lett.* **2006**, *96*, 226802.

[17] Wu, Q.; Mul, G.; Van de Krol, R. *Energy Environ. Sci.* **2011**, *4*, 2140.

[18] Overbury, S. H.; Schwartz, V.; Mullins, D. R.; Yan, W.; Dai, S. *J. Catal.* **2006**, *241*, 56.

[19] Koningsberger, D. C.; Mojet, B. L.; Van Dorssen, G. E.; Ramaker, D. E. *Top. Catal.* **2000**, *10*, 143.

[20] Li, X., Yue, P., Kutal C., *New J. Chem.* **2003**, *27*, 1264.

[21] Ambrus, Z.; Balázs, N.; Alapi, T.; Wittmann, G.; Sipos, P.; Dombi, A.; Mogyorósi, K. *Appl. Catal. B* **2008**, *81*, 27.

[22] Zhang, J.; Chen, X.; Shen, Y.; Li, Y.; Hu, Z.; Chu, J. *Phys. Chem. Chem. Phys.* **2011**, *13*, 13096.

[23] Wang, C.; Wang, K.; Perng, T. *Appl. Phys. Lett.* **2010**, *96*, 143102.

[24] Choi, W.; Termin, A.; Hoffmann, M. R. *J. Phys. Chem.* **1994**, *98*, 13669.

[25] Zhu, J.; Zheng, W.; He, B.; Zhang, J.; Anpo, M. *J. Mol. Catal. A* **2004**, *216*, 35.

[26] Ghorai, T. K.; Biswas, S. K.; Pramanik, P. *Appl. Surf. Sci.* **2008**, *254*, 7498.

[27] Arana, J.; Díaz, O. G.; Rodríguez, J. M. D.; Melián, J. A. H.; Cabo, C. G.; Pena, J. P.; Hidalgo, M. C.; Navío-Santos, J. A. *J. Mol. Catal. A* **2003**, *197*, 157.

[28] Shannon, R. D. *Acta Crystallogr. A* **1976**, *32*, 751.

[29] Enache, C. S.; Schoonman, J.; Van de krol, R. *J. Electroceram.*, **2004**, *13*, 177.

[30] Smyth, D.M. *The defect chemistry of metal oxides* Oxford University Press, New York, 2000.

[31] Choi, H. C.; Jung, Y. M.; Kim, S. B. *Vib. Spectrosc.* **2005**, *37*, 33.

[32] Parker, J. C.; Siegel, R. W. *Appl. Phys. Lett.* **1990**, *57*, 943.

[33] Somaskandan, K.; Tsoi, G. M.; Wenger, L. E.; Brock, S. L. *Chem. Mater.* **2005**, *17*, 1190.

[34] Stowell, C. A.; Wiacek, R. J.; Saunders, A. E.; Korgel, B. A. *Nano. Lett.* **2003**, *3*, 1441.

[35] Du, M. H.; Erwin, S. C.; Efros, A. L. *Nano. Lett.* **2008**, *8*, 2878.

[36] George, S.; Pokhrel, S.; Xia, T.; Gilbert, B.; Ji, Z.; Schowalter, M.; Rosenauer, A.; Damoiseaux, R.; Bradley, K. A.; Mädler, L.; Nel, A. E. *ACS Nano* **2010**, *4*, 15.

[37] Xiao, J.; Kuc, A.; Pokhrel, S.; Schowalter, M.; Parlapalli, S.; Rosenauer, A.; Frauenheim, T.; Mädler, L.; Pettersson, L. G. M.; Heine, T. *Small* **2011**, *20*, 2879.

[38] Yamashita, H.; Ichihashi, Y.; Anpo, M. *J. Phys. Chem.* **1996**, *100*, 16041.

[39] Chen, L. X.; Rajh, T.; Jäger, W.; Nedeljkovic, J.; Thurnauer, M. C. *J. Synchrotron Rad.,* **1999**, *6*, 445.

[40] Ikeue, K.; Ikeda, S.; Watanabe, A.; Ohtani, B. *Phys. Chem. Chem. Phys.* **2004**, *6*, 2523.

[41] Angelomé, P. C.; Andrini, L.; Calvo, M. E.; Requejo, F. G.; Bilmes, S. A.; Soler-Illia, G. J. A. A. *J. Phys. Chem. C* **2007**, *111*, 10886.

[42] Wu, Z. Y.; Ouvrard, G.; Gressier, P. *Phys. Rev. B* **1997**, 55, 10382.

[43] Brydson, R.; Sauer, H.; Engel, W.; Thomas, J. M.; Zeitler, E.; Kosugi, N.; Kuroda, H. *J. Phys. Condens. Mat.* **1989**, *1*, 797.

[44] Notestein, J. M.; Andrini, L. R.; Kalchenko, V. I.; Requejo, F. G.; Katz, A.; Iglesia, E. *J. Am. Chem. Soc.* **2007**, *129*, 1122.

[45] Grunes, L. A. *Phys. Rev. B* **1983**, *27*, 2111.

[46] Ruiz-López, M. F.; Munoz-Páez, A. *J. Phys. Condens. Mat.* **1991**, *3*, 8981.

[47] Fernández-García, M.; Martínez-Arias, A.; Hanson, J. C.; Rodriguez, J. A. *Chem. Rev.* **2004**, *104*, 4063.

[48] Graetz, J.; Reilly, J. J.; Johnson, J. *Appl. Phys. Lett.* **2004**, *85*, 3.

[49] Wagemaker, M.; Lützenkirchen-Hecht, D.; Keil, P.; Van Well, A. A.; Frahm, R. *Physica B* **2003**, *336*, 118.

[50] Vračar, M.; Kuzmin, A.; Merkle, R.; Purans, J.; Kotomin, E. A.; Maier, J.; Mathon, O. *Phys. Rev. B* **2007**, *76*, 174107.

[51] Liu, Z.; Davis, J. *J. Phys. Chem.* **1994**, *98*, 1253.

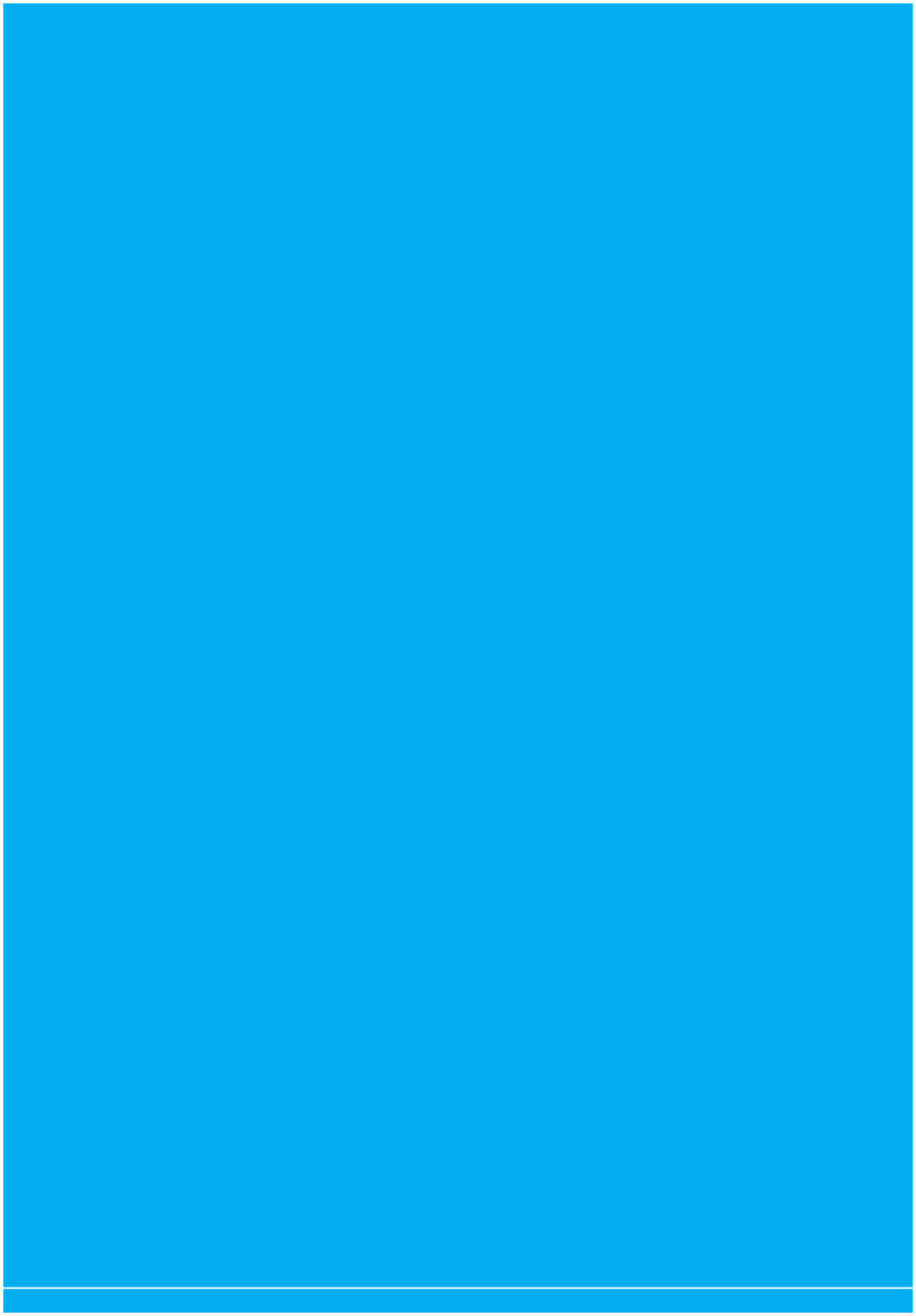

Chapter 3

Efficient NO adsorption and release at Fe^{3+} sites in Fe/TiO_2 nanoparticles

Abstract

The adsorption and release of nitrogen oxide (NO) molecules at the surface of Fe-doped TiO_2 nanoparticles, made by a template-free sol-gel process, have been studied. Fe^{3+} ions are found to be highly effective NO adsorption sites in Fe/TiO_2. Up to ~89 μmol/g of the adsorbed NO can be released by exposure to trace amounts of H_2O, which exceeds the water-induced release capacity of other NO storage materials by at least a factor of 2. The surprising efficiency of water as a trigger molecule for NO release is due to its large dipole moment, which causes a much stronger coordination to the Fe^{3+} species than is the case for NO. In addition, a new IR band at 1840 cm^{-1} has been found for Fe-doped TiO_2 nanoparticles exposed to NO gas. This band is assigned to the stretch vibration of an NO species coordinatively bonded to an Fe^{3+} site. In contrast to Fe^{2+}-NO vibrations in e.g. zeolites, Fe^{3+}-NO vibrations are seldom observed, and this is the first time that convincing evidence is reported for the presence of Fe^{3+}-NO in Fe/TiO_2. The implications of these findings for the application of Fe-doped TiO_2 as a novel NO storage and release material are briefly discussed.

3.1 Introduction

Many research efforts have been devoted to the abatement of NO_x (a mixture of NO and NO_2),[1] since a high concentration of NO_x in air causes damage to lung tissue and contributes to the formation of acid rain.[2] Increasingly strict emission legislation requires the development of effective techniques for removing NO_x in air.[3] Several approaches have been pursued, including NO_x storage and reduction catalysis (NSR) and selective catalytic reduction (SCR).[4] Photocatalytic decomposition of NO_x with TiO_2-based photocatalysts appears to be one of the most promising alternative approaches, allowing NO_x conversion at room temperature.[5]

In this paper we focus our attention on the very first step of any (photo)catalytic process: the (dark) adsorption of NO at the catalyst's surface. Room-temperature adsorption of NO at oxidized TiO_2 surfaces is known to be weak,[6] and the observation that just 0.1 mW/cm^2 of UV illumination is already sufficient to photocatalytically remove ppm levels of NO_x[7] suggests that adsorption or desorption of NO_x may be the rate-limiting step in the overall process. To improve and elucidate the adsorption of NO at TiO_2 catalyst surfaces, we have studied and compared the NO adsorption behavior at Fe-doped and undoped TiO_2 nanoparticles under dark conditions. Fe is chosen as a dopant because Fe^{2+} ions are known to be highly effective NO adsorption sites in e.g. zeolites.[8] We find that a large amount of NO can be adsorbed at Fe/TiO_2 via the formation of Fe^{3+}-NO complexes. However, since the bonding interaction between Fe^{3+} and NO is relatively weak, small amounts of more strongly adsorbing water molecules can effectively block the adsorption of NO. While this is not beneficial for a photocatalyst that will be operated under outdoor (humid) conditions, the ability to release adsorbed NO by using water as a 'trigger species' offers interesting possibilities to use Fe/TiO_2 nanoparticles as a novel reversible room-temperature NO storage material.

3.2 Experimental

Pure titanium dioxide (TiO_2) and 10 % Fe/TiO_2 nanoparticles are synthesized by a simple, template-free sol-gel method. For preparing 10% Fe/TiO_2, 8.311 g of $Fe(NO_3)_3.9H_2O$ (+99%) is fully dissolved in 375 ml ultrapure water (Milli-Q, 18.2 M .cm) and mixed with 2.6 ml HNO_3 (65% in H_2O) resulting in the formation of clear yellow solution as the first step. For preparing pure TiO_2, 375 ml ultrapure water is mixed with 2.6 ml HNO_3 without any $Fe(NO_3)_3.9H_2O$ as the first step. The nitric acid serves to stabilize the sol by decreasing the pH of the solution. Secondly, 62.5 ml titanium isopropoxide (TTIP) is dropwise added to the clear solution under vigorous stirring. It takes a few minutes for all the TTIP to be added to the solution, after which stirring is continued for 2 hours. This results in an opaque suspension that contains TiO_2 and propanol as the main reaction products. The suspension is then kept at 333 K while evaporating the propanol by using a rotary evaporator. After that the suspension is stirred for 4 hours at 333 K, and a homogenous colloidal solution is produced. The colloidal solution is first dried at 373 K, then annealed at 773 K to obtain powders for NO adsorption measurements.

X-ray diffraction (XRD, Bruker, D8 Advance) with Cu-K_α radiation is performed for crystal structure and particle size analysis. The crystal morphology is examined by high resolution transmission electron microscopy (TEM) using a FEI TECNAI TF20 electron microscope equipped with a FEG electron source and an EDX Energy Dispersive X-ray system for elemental analysis. The samples for the TEM-EDX measurments are prepared by placing a few droplets of a suspension of ground Fe-doped TiO_2 powder in ethanol on a Quantifoil® carbon polymer supported copper grid, following with drying at ambient conditions.

The valence states of Fe ions in TiO_2 are analyzed by high resolution X-ray photoelectron spectroscopy (XPS, Thermo Escalab 250) with a monochromatic Al K_α X-ray source. All binding energies are calibrated by the C 1s peak (284.6 eV) arising from adventitious carbon.

In-situ Diffuse Reflectance Infrared Fourier Transformed spectroscopy coupled with Mass Spectrometery (DRIFT-MS) is used for measuring NO species adsorbed on the surface of pure TiO_2 and Fe-doped TiO_2. The samples are mounted into a temperature-controlled reactor chamber, the output of which is coupled to a mass spectrometer (ThermostarTM GSD 301T from Pfeiffer Vacuum). A continuous flow of He with a relatively high concentration of NO (167 ppm, 30 ml/min) is used to ensure efficient adsorption of the target species. All DRIFT spectra represent the average of 64 consecutive scans with a resolution of 4 cm^{-1} at 303 K, referenced to a KBr background.

3.3 Results and discussion

The undoped and Fe-doped TiO_2 nanoparticles mainly consist of the anatase phase of TiO_2, as shown by the X-ray diffraction spectra in Fig. 1A. A small amount of rutile is also present, as evidenced by the main rutile peak at 27.4°. No Fe_2O_3 or other Fe-related crystal phases are observed, even for a 10% Fe concentration. The crystal sizes and peak positions are determined by fitting the main anatase (101) peak at 25.4°

using a pseudo-Voigt function (Fig. 1B). The results show a peak shift from 25.36 to 25.44 degrees, indicating that the incorporation of Fe in the TiO_2 lattice decreases the d_{101} interplanar lattice spacing. This is contrary to what is expected, since the ionic radius of Fe^{3+} (65 pm) is slightly larger than that of Ti^{4+} (61 pm). A likely explanation is that positively-charged oxygen vacancies ($V_O^{\bullet\bullet}$) are formed in order to compensate the negatively-charged Fe substituents. The corresponding ionic compensation equation can be written using standard Kröger-Vink notation (reaction (8), chapter 1).[17]

The Coulomb attraction between the negatively charged $Fe_{Ti}^{'}$ and positively charged $V_O^{\bullet\bullet}$ may result in the formation of $(V_O^{\bullet\bullet}\text{-}\,Fe_{Ti}^{'})^X$ defect associates, especially at high Fe concentrations (10%). The combined effect of a vacancy and a slightly larger substituent explains the observed reduction of the interplanar spacing of TiO_2.

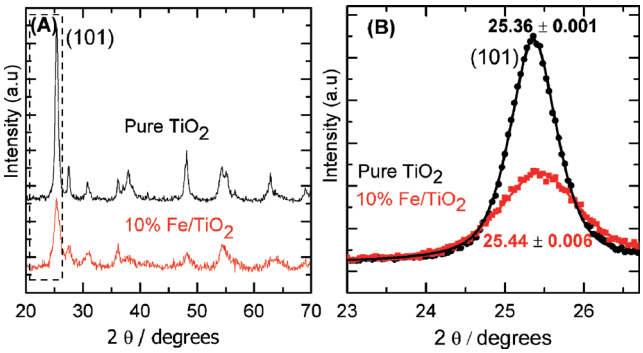

Figure 1: (A) XRD patterns of pure TiO_2 and 10% Fe-doped TiO_2. (B) XRD peak fitting of the anatase (101) peak using a pseudo-Voigt function for pure TiO_2 and Fe/TiO_2.

In addition to the peak shift, Fig. 1B shows significant peak broadening for the Fe-doped samples. Using the Scherrer equation, Fe doping is found to reduce the crystal size from 12 nm (pure TiO_2) to 6 nm for Fe-doped TiO_2. We tentatively attribute this to Fe^{3+} ions being homogeneously dispersed at the surface of the TiO_2 particles during their formation, thereby inhibiting their growth.

In order to further identify the morphologies and Fe doping in TiO_2, a combination of high resolution TEM and EDX is carried out. Fig. 2A shows the particle size to be ~6 nm for Fe-doped TiO_2, in good agreement with the XRD calculations. To determine the presence and dispersion of Fe, the EDX electron beam was focused on different areas (I, II, and III) of the TEM image (Fig. 2B). The presence of almost the same Ti : Fe intensity ratio for different areas in the TEM image suggests that the Fe is homogeneously dispersed over the TiO_2 nanoparticles. Moreover, quantification of the EDX peaks gives the expected Ti : Fe ratio of 10 : 1.

DRIFT measurements on the undoped and Fe-doped TiO_2 particles do not show any pronounced new IR absorption bands upon exposure to 167 ppm NO/He (Fig. 3).

This is consistent with previous studies, in which only minor amounts ($\Delta A \sim 0.02$) of nitrates were found on undoped TiO_2 at wavenumbers below 1600 cm^{-1}.[9] For Fe/TiO_2, the absence of NO-related bands can be rationalized by the fact that Fe dopants in TiO_2 are most likely present in the +3 state (see below), and Fe^{3+}-NO complexes are usually not observed or very weak.[8] Moreover, the presence of adsorbed water, as evidenced by IR bands at 2500-3750 cm^{-1}, 1620 cm^{-1} and 1642 cm^{-1},[9,10] may block the adsorption of NO species.

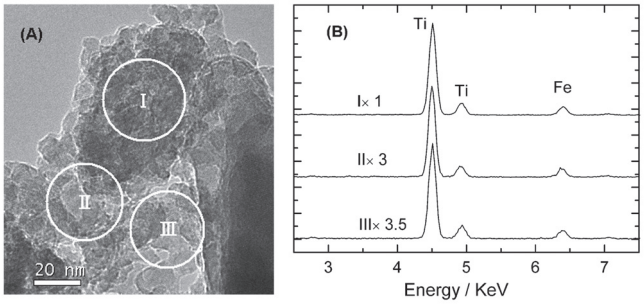

Figure 2: (A) High magnification TEM image of 10% Fe-doped TiO_2; (B) EDX spectra of 10% Fe-doped TiO_2 focusing on the area I, II and III of the TEM image.

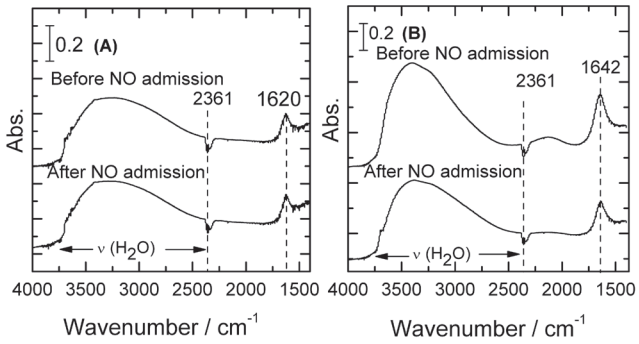

Figure 3: (A) DRIFT spectra of NO adsorption over undoped TiO_2. (B) DRIFT spectra of NO adsorption over 10% Fe-doped TiO_2. The band at ~2360 cm^{-1} corresponds to well known asymmetric stretch vibration of gas phase CO_2.[11]

To remove the adsorbed H_2O, both TiO_2 and Fe/TiO_2 have been pre-treated in-situ in a pure He atmosphere at 723 K for 20 min. Only a small H_2O signal remains between 2500-3700 cm^{-1}, as shown in Fig. 4. Upon exposure to NO, two new bands at 1840 cm^{-1} and 1578 cm^{-1} appear for Fe/TiO_2 (Fig. 4B). In contrast, no new bands are observed when exposing undoped TiO_2 to NO (Fig. 4A). The band at 1578 cm^{-1} has been assigned

to a bidentate nitrate group on the TiO_2 surface by Hadjiivanov et al.[12] The reason why this band is only observed for Fe-doped TiO_2 is attributed to the ~4 times larger specific surface area compared to undoped TiO_2 (6 nm vs. 12 nm particles as shown from the XRD peak widths).

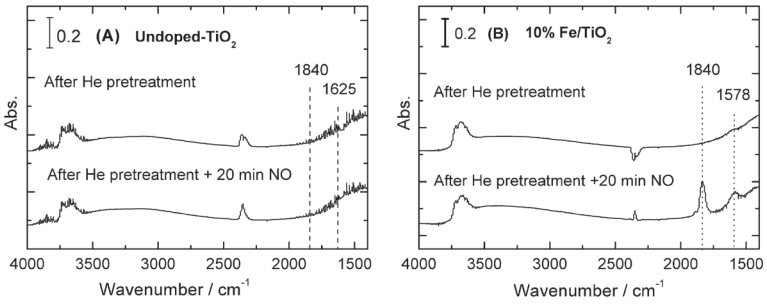

Figure 4: (A) DRIFT spectra of undoped TiO_2 after in-situ pretreatment in pure He at 723 K (top curve) followed by 20 min. exposure to 167 ppm NO in He (bottom curve). (B) Similar spectra for 10% Fe-doped TiO_2.

Although NO adsorption over different oxides containing Fe^{2+} and Fe^{3+} ions has been intensively studied by the IR technique[8] the band at 1840 cm^{-1} has not been specifically assigned in the literature before. Miyata et al. reported IR bands at 1845-1853 cm^{-1}, but they tentatively attributed these bands to NO adsorbed at Fe^{2+} species in ternary phases, such as $FeAl_2O_4$ or $FeTiO_3$.[13] Based on the low-temperature synthesis method we employed here, and the XRD data shown in Fig. 1A, the presence of such phases can be ruled out in our case. The concensus is that IR bands in this region are due to N=O stretch vibrations of coordinatively-bonded mono-nitrosyls.[14] Since we did not observe this band for undoped TiO_2 (even for $\Delta A \sim 0.02$), it must be due to either Fe^{2+}-(NO) or Fe^{3+}-(NO) species in Fe/TiO_2.

The presence of Fe^{2+}-(NO) species is unlikely, since its main absorption band is at 1824 cm^{-1}.[13] This is confirmed by XPS analysis of our as-synthesized Fe/TiO_2, shown in Fig. 5. The peak at 711.2 eV demonstrates the presence of Fe^{3+}, while the absence of a peak at 709.3 eV reveals that Fe^{2+} is not present.[15,16] To further rule out the presence of Fe^{2+} species, the sample was also pre-treated in a 20% O_2/He mixture to convert all Fe^{2+} to Fe^{3+}.[18] As shown in Fig. 6A, this again results in an absorption band at 1840 cm^{-1} upon exposure to NO, which strongly supports the assignment of this band to an Fe^{3+}-(NO) complex.

To explain the higher frequency of the NO stretch vibration in Fe^{3+}-NO compared to ν(NO) in Fe^{2+}-NO (1824 cm^{-1}), a closer look at the nature of the Fe-NO bond is necessary. The electron configuration of NO is $(\sigma_s)^2(\sigma_s^*)^2(\pi_{x,y})^4(\sigma_z)^2(\pi_{x,y}^*)^1$.[19] As outlined by Hadjiivanov, the partial transfer of an electron in the σ_z bonding orbital of NO is accompanied by back-donation of a metal 3d electron to the π^* antibonding orbital.[10] This de-stabilizes

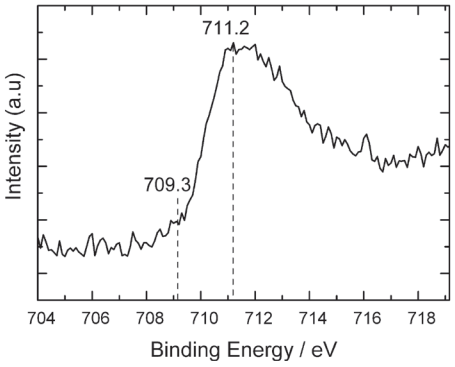

Figure 5: XPS Fe-2p spectra of 10% Fe-doped TiO_2.

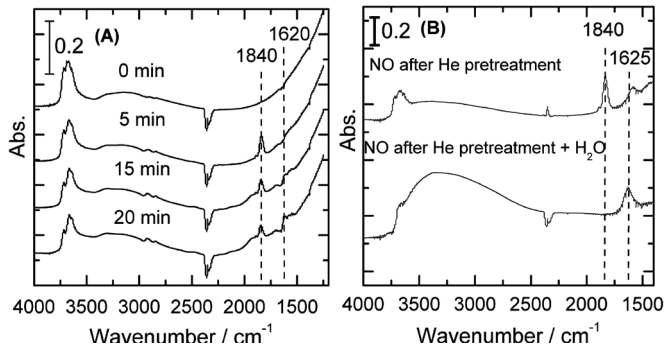

Figure 6: (A) Admission of NO for 10% Fe/TiO_2 after in-situ annealing in 20% O_2 / He to 723 K. (B) Influence of water vapour on adsorbed NO for 10% Fe-doped TiO_2.

the N-O bond, which explains why ν(NO) in coordinatively-bonded NO is lower than that of NO molecules in the gas phase (1876 cm^{-1}).[20] A more simple ionic bond model that involves donation of the unpaired electron in the anti-bonding π* orbital would increase the bond order of NO from 2.5 to 3 and result in a spectral signature at higher frequencies; this is not observed. Since Fe^{3+} has fewer d electrons than Fe^{2+}, π back-donation is less significant, resulting in a stronger N-O bond for the Fe^{3+}-NO complex. We believe that this explains the higher frequency of the NO stretch vibration (1840 cm^{-1}) compared to that observed in Fe^{2+}-NO species (1824 cm^{-1}). An alternative description can be given in terms of Fe^{3+} presenting a more polar environment than Fe^{2+}. It therefore exerts a greater pull on the π* electron in NO, which increases the NO bond order and its vibration frequency.[21]

The coordination of the adsorbed NO molecule to the Fe^{3+} species at the surface is illustrated in Scheme 1 for the (101) surface of anatase TiO_2. Although other surface orientations will certainly be present in these Fe/TiO_2 nanopowders, the (101) surface

has the lowest energy[22] and is therefore taken as a representative case. As can be seen in Scheme 1, the Fe^{3+} species at the (101) surface are generally five-fold coordinated by oxygen, and can achieve a full six-fold coordination upon adsorption of NO. Although the Fe-N-O bond angle has not been studied in Fe/TiO_2 catalysts, studies on 6-fold coordinated Fe species in nitrosylmetalloporphyrins[23] suggest a linear bond angle for Fe^{3+}-NO based on the electron counting formalism described by Enemark and Feltham.[24]

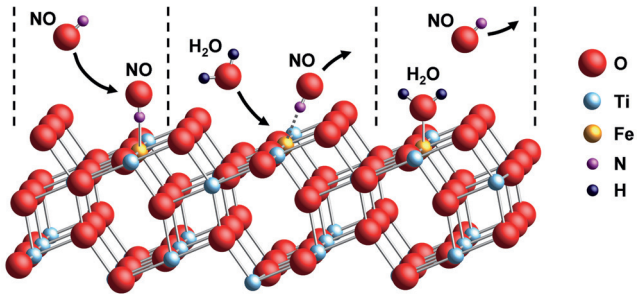

Scheme 1: Adsorption model of NO and H_2O on the (101) surface of Fe-doped anatase TiO_2.

An especially important observation from Fig. 6A is that the intensity of the band at 1840 cm^{-1} decreases with continued exposure to NO. At the same time, the bands at 1620 cm^{-1} and 3500-2500 cm^{-1} increase. These have been assigned to adsorbed H_2O on the TiO_2 surface,[13] which is confirmed by a control experiment in which water was deliberately added to the gas supply (Fig. 6B). The adsorbed H_2O comes from residual water in the He/O_2 supply, and cannot be entirely avoided. The reduced intensity of the band at 1840 cm^{-1} suggests that H_2O adsorption is preferred over NO adsorption for Fe/TiO_2. This is consistent with the fact that H_2O has a stronger dipole moment than NO, and is therefore expected to be more strongly coordinated to Fe^{3+} species. The stronger dipole moment of H_2O also leads to a stronger adsorption on undoped TiO_2 surfaces (ΔH_{ads} ~69 kJ/mole for H_2O adsorption, vs. 48 kJ/mole for NO adsorption[10,25]). The fact that even a very small amount of water (few ppm) is already sufficient to remove the Fe^{3+}-NO species explains why these species have not been identified in previous studies.[26] NO species coordinated to Fe^{2+} appear to be less easily removed by water and are therefore more often observed.[14] This is indeed consistent with our interpretation in terms of a higher degree of π back-bonding, which results in a stronger bond between Fe^{2+} and NO (at the expense of the N-O bond strength).

Direct evidence to support the blocking effect of NO adsorption by H_2O is provided by in-situ mass spectrometry (Fig. 7). First, the material was saturated with NO using a flow of 167 ppm NO in 1 bar He at T=303 K. Then, at t=0, the saturated Fe/TiO_2 was exposed to water. As shown in Fig. 7, this results in the immediate desorption of NO gas. No H_2O is detected at the reactor outlet at this stage, indicating that all water molecules are being adsorbed at the catalyst surface. This is confirmed by a modest

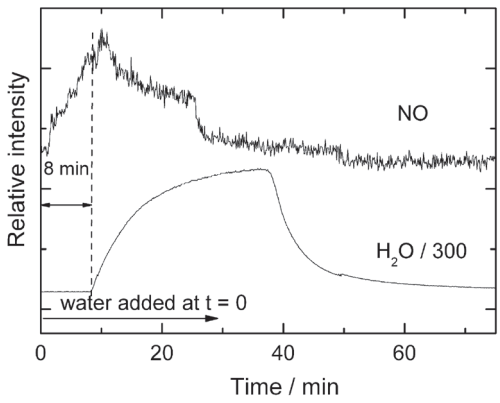

Figure 7: The influence of H_2O vapor to NO adsorption for Fe-doped TiO_2.

but clear increase of the 1620 cm^{-1} band in the DRIFT spectra between 0 - 20 min in Fig. 6A. After 8 minutes, the sample surface is saturated with H_2O and the water signal at the reactor outlet increases. At this point all NO has been replaced with water, as evidenced by a decrease in the NO signal. This proves that the presence of water not only prevents the adsorption of NO, it also leads to desorption of previously-adsorbed NO species.

The NO release capacity in Fig. 7 can be determined from a calibration of the MS spectra. The calibration is performed using a flow of 167 ppm NO/He without having a sample in the reactor (Fig. 8). The area of the NO pulse is equated to the total number of NO molecules passing through the reactor between t = 30 and t = 58 min.
Using this calibration, the integrated area of the NO signal between t = 0 and t = 50 min. in Fig. 7 (using the horizontal part of the right-hand side of the curve as a baseline)

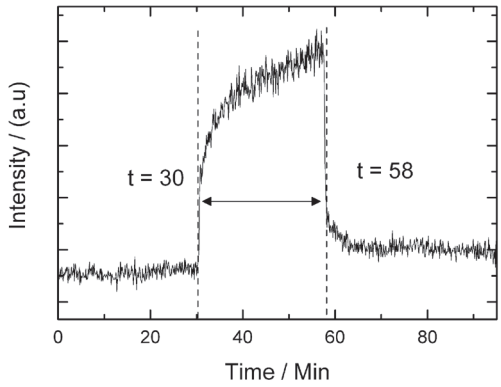

Figure 8: MS spectra of continuously flowing 167 ppm NO/He for 28 minutes.

is found to correspond to (4.47 ± 0.2)×10^{-6} mol NO. With 0.05 g of sample being used for the in-situ DRIFT-MS measurements, the NO release capacity at 303 K is found to be (89 ± 4) µmol/g. This is ~2-3 times higher than the room-temperature NO_x storage capacity of BaO/Al_2O_3-based materials that are widely used for NSR catalysis, and comparable to the NO uptake capacity of these materials at 300-400°C.[27,28] State-of-the-art NO storage materials based on metal organic frameworks (MOFs) can store up to 3 mmol/g at room temperature, but at much higher pressures (1 bar NO).[29] Moreover, these materials release only a few µmol/g of NO upon exposure to water.[29] This shows that Fe^{3+} sites at Fe/TiO_2 nanoparticles are very effective adsorption sites for NO, and that water is an efficient trigger molecule to release NO adsorbed at Fe/TiO_2.

3.4 Conclusions

In conclusion, we have found that Fe^{3+} species at the surface of Fe/TiO_2 nanoparticles act as effective adsorption sites for NO molecules, with an uptake/release capacity as high as 89 µmol NO per gram of catalyst. A new IR band at 1840 cm^{-1} was found and attributed to the NO stretch vibration in a Fe^{3+}-NO complex. Compared to Fe^{2+}-NO, the more polar environment near the Fe^{3+} reduces the degree of π back-bonding, which leads to a weakening of the Fe^{3+}-NO bond as evidenced by the easy desorption of NO in the presence of trace amounts of water. H_2O therefore effectively 'blocks' NO adsorption at Fe^{3+}, which explains why reports on Fe^{3+}-NO are far less common than those on Fe^{2+}-NO in the (photo)catalysis literature. While the easy displacement of NO by water is clearly undesired in practical photocatalysts, nanoparticulate Fe/TiO_2 is an interesting novel NO storage material for dry environments, or for applications where controlled release of NO – triggered by a water pulse – is desired.

Acknowledgements

The authors gratefully acknowledge the kind help from B. van der Linden and C.C. Yang of the Catalysis Engineering group. Financial support for this work is provided by the Shell-TU Delft "Sustainable Mobility" programme.

References

[1] S. Devahasdin, C. Fan, K. Li and D.H. Chen, *J. Phtochem. Photobiol. A*, 2003, **156**, 161.

[2] J. A. Rodriguez, T. Jirsak, G. Liu, J. Hrbek, J. Dvorak and A. Maiti, *J. Am. Chem. Soc.*, 2001, **123**, 9597.

[3] K. C. Taylor, *Catal. Rev. Sci. Eng.*, 1993, **35**, 457.

[4] S. Roy, M. S. Hgde and G. Madras, *Appl. Energy*, 2009, **86**, 2283.

[5] Y. Ohko, Y. Nakamura, N. Negishi, S. Matsuzawa and K. Takeuchi, *J. Photochem. Photobiol. A,* 2009, **205**, 28.

[6] D. C. Sorescu, C. N. Rusu and J. T. Yates, *J. Phys. Chem. B*, 2000, **104**, 4408.

[7] M. Kaneko and I. Okura (Eds.), Photocatalysis - Science and Technology, Springer, 2002, pp.149.

[8] G. Mul, M. W. Zandbergen, F. Kapteijn, J. A. Moulijn and J. Pérez-Ramíez, *Catal. Lett.,* 2004, **93**, 113.

[9] J. C. S. Wu and Y. T. Cheng, *J. Catal.*, 2006, **237**, 393.

[10] M. Takeuchi, G. Martra, S. Coluccia and M. Anpo, *J. Phys. Chem. C,* 2007, **111**, 9811.

[11] Z. H. Cheng, A. Yasukawa, K. Kandori and T. Ishikawa, *Langmuir*, 1998, **14**, 6681.

[12] K. Hadjiivanov and H. Knözinger, *Phys. Chem. Chem. Phys.,* 2000, **2**, 2803.

[13] H. Miyata, Y. Nakagawa, S. Miyagawa and Y. Kubokawa, *J. Chem. Soc. Faraday Trans.,* 1998, **84**, 2129.

[14] K. I. Hadjiivanov, *Catal. Rev. Sci. Eng.,* 2000, **42**, 71.

[15] Y. Zhang, Y. Shen, F. Gu, M. Wu, Y. Xie and J. Zhang, *Appl. Surf. Sci.,* 2009, **256**, 85.

[16] J. Arana, O. G. Díaz, J. M. D. Rodríguez, J. A. H. Melián, C. G. Cabo, J. P. Pena, M. C. Hidalgo and J. A. Navío-Santos, *J. Mol. Catal. A,* 2003, **197**, 157.

[17] Y.-M. Chiang, D. P. Birnie, W. D. Kingery, Physical Ceramics, Wiley, New York, 1997.

[18] G. Talut, H. Reuther, J. Grenzer and S. Zhou, *Hyperfine Interact*, 2009, **191**, 95.

[19] H. B. Gray, Chemical Bonds: An introduction to atomic and molecular structure, 2nd ed., University Science Books, 1994.

[20] K. P. Huber and G. Herzberg, Molecular spectra and molecular structure, Vol. 4, Van Nostrand: Princeton, NJ, 1979.

[21] P. Moënne-Locooz, *Nat. Prod. Rep.,* 2007, **24**, 610.

[22] U. Diebold, N, Ruzycki, G. S. Herman and A. Selloni, *Catal. Today*, 2003, **85**, 93.

[23] W. R. Scheidt and M. K. Ellison, *Acc. Chem. Res.,* 1999, **32**, 350.

[24] J. H. Enemark and R. D. Feltham, *Coord. Chem. Rev.,* 1974, **13**, 339.

[25] N. Bredemeyer, S. Buhr and D. Hesse, *Chem. Eng. Technol.,* 2000, **23**, 527.

[26] D. L. King and J. B. Peri, *J. Catal.,* 1983, **79**, 164.

[27] E. Fridell, H. Persson, B. Westerberg, L. Olsson and M. Skoglundh, *Catal. Lett.,* 2000, **66**, 71.

[28] X. Li, J. Chen, P. Lin, M. Meng, Y. Fu, J. Tu and Q. Li, *Catal. Commun.*, 2004, **5**, 25.

[29] B. Xiao, P. S. Wheatley, X. Zhao, A. J. Fletcher, S. Fox, A. G. Rossi, I. L. Megson, S. Bordiga, L. Regli, K. M. Thomas and R. E. Morris, *J. Am. Chem. Soc.*, 2007, **129**, 1203.

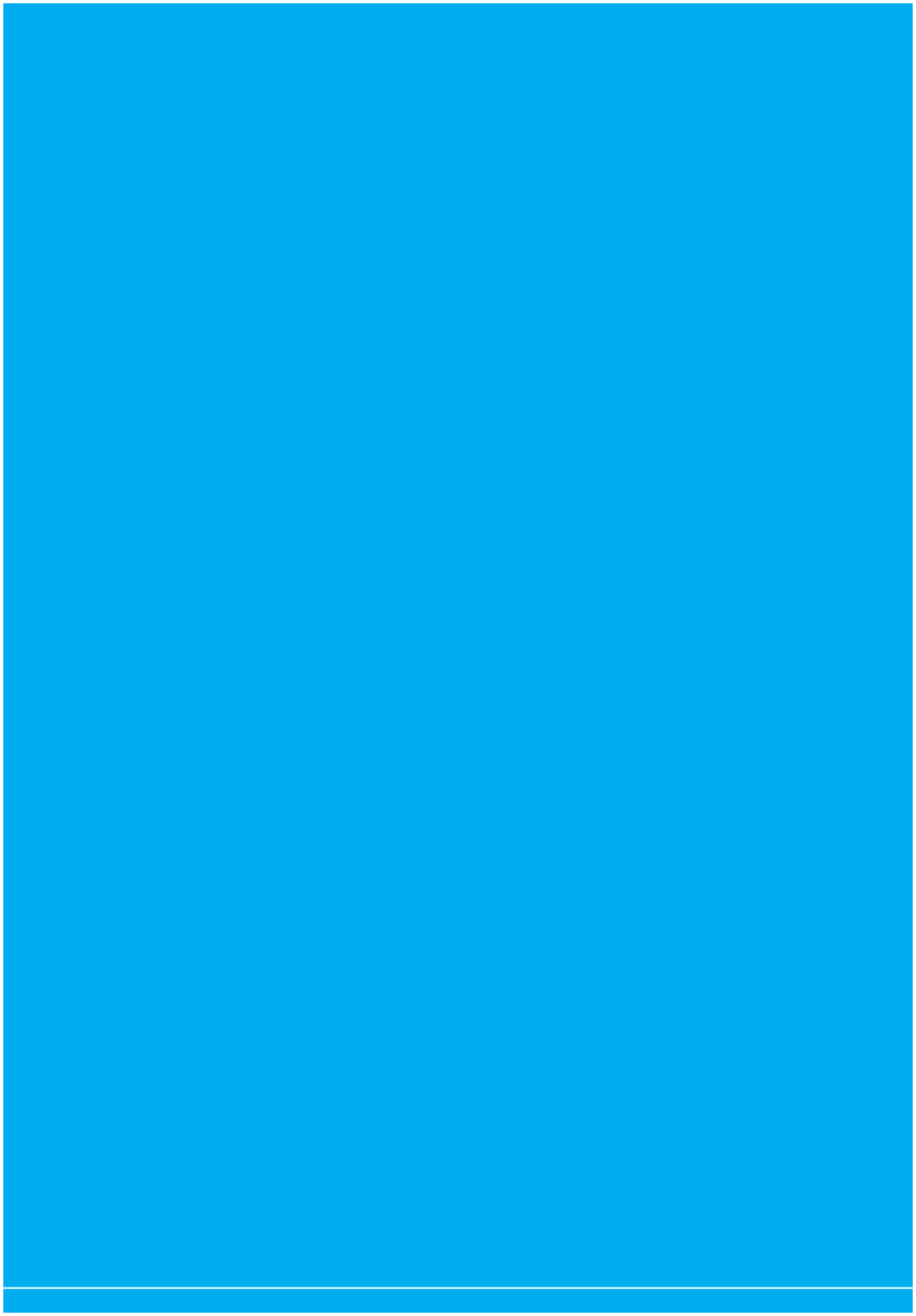

Chapter 4

Selective photoreduction of nitric oxide to nitrogen by nanostructured TiO_2 photocatalysts: the role of oxygen vacancies and iron dopant

Abstract

Conventional TiO_2-based photocatalysts oxidize NO_x to nitrate species, which do not spontaneously desorb and therefore de-activate the catalyst. We show that the selectivity of this reaction can be changed by creating a large concentration of oxygen vacancies in TiO_2 nanoparticles through thermal reduction in a reducing atmosphere. This results in the photo*reduction* of nitric oxide (NO) to N_2 and O_2, species which spontaneously desorb at room temperature. The activity of the photoreduction reaction can be greatly enhanced by doping the TiO_2 nanoparticles with Fe^{3+}, an acceptor-type dopant that stabilizes the oxygen vacancies. Moreover, the photo-induced reduction of Fe^{3+} to Fe^{2+} provides a recombination pathway that almost completely suppresses the formation of NO_2 and thus enhances the selectivity of the reaction for N_2 formation. Gas chromatography confirms that N_2 and O_2 are formed in a stoichiometric ratio, and the activity for NO decomposition is found to be limited by the concentration of oxygen vacancies. A series of internally consistent reaction equations is proposed that describes all experimentally observed features of the photocatalytic process. The observed influence of oxygen vacancies on the activity and selectivity of photo-induced reactions may lead to new routes towards the design of highly selective photocatalysts.

4.1 Introduction

Most of the world's energy consumption is based on the oxidation of fossil fuels in air. Examples are internal combustion engines in cars and turbines for power generation plants. These processes produce massive amounts of greenhouse gases, such as CO_2 and NO_x. NO_x (a mixture of NO and NO_2)[1] is formed when atmospheric nitrogen and oxygen react as a result of the high temperatures that are reached during fuel combustion.[2,3] Over the past few decades, atmospheric NO_x concentrations have greatly increased because of the growing number of automobiles and growing industrial activities.[4] This is reason for concern, since the emission of NO_x causes damage to human lung tissue and contributes to the formation of acid rain.[5] TiO_2, one of the best-known semiconductor photocatalysts, can decompose NO_x at room temperature and ambient pressure and has been widely studied for this purpose.[6-9] When TiO_2 is irradiated with photon energies exceeding its band gap of ~ 3.2 eV,[10] electrons are excited from the valence band (VB) to the conduction band (CB), resulting in the formation of electron–hole (e^-–h^+) pairs. A certain fraction of these charge carriers are able to reach the surface of the TiO_2, and are captured by surface adsorbed species on Ti sites to form superoxide anions and hydroxyl radicals.[11,12] The free radicals are very active and can react with NO to form nitrates.[13] The main problem of this approach, however, is that these nitrates can not spontaneously desorb. These species therefore de-activate the photocatalyst's surface, reducing the material's ability to remove NO_x from air. To avoid de-activation, the nitrates need to be washed away by rain.[14] The resulting nitric acid is corrosive and could pollute the soil when the concentration becomes too high. The removal of NO_x from air without de-activation and secondary pollution is therefore an urgent and demanding challenge.

One of the most promising ways to resolve this problem is to change the selectivity of the photocatalytic reaction so that NO_x is converted to N_2 and O_2. No de-activation would occur for this photo-reduction reaction since nitrogen and oxygen readily desorb from the surface.[15] As reported by Anpo et al.,[16] the selectivity towards NO photo-reduction can be greatly improved by reducing the coordination number of Ti^{4+} from its usual value of 6 (TiO_6 octahedra) to 4 (TiO_4 tetrahedra). This has been successfully achieved by depositing isolated TiO_4 clusters inside the cavities of zeolite-Y with ion beam implantation.[16,17] However, the large scale application of zeolites with ion beam implantation techniques is economically unattractive.

In this paper, we propose a new strategy to change the photocatalytic selectivity of TiO_2 based on the creation of a large and stable concentration of oxygen vacancies. We will show that indeed results in the photoreduction of NO to N_2 and O_2, and that the photo-oxidation reaction can be largely suppressed. A series of reaction mechanisms that explain these observations will be given.

4.2 Experimental section

Synthesis of Fe-doped TiO_2 thin films. A simple, template-free sol-gel method was employed for synthesizing pure TiO_2 and Fe-doped TiO_2 (Fe/TiO_2) colloidal solutions.[18] Briefly, titanium isopropoxide (TTIP, Acros, +98%) was dropwise added to ultrapure water, slightly acidified with nitric acid, under vigorous stirring. For the preparation of Fe-doped TiO_2 samples, a certain amount of $Fe(NO_3)_3 \times 9H_2O$ was dissolved into the aqueous solution before adding the TTIP. After hydrolysis of TTIP in the aqueous solution, an opaque suspension was obtained, which contains TiO_2 and propanol as the main reaction products. A homogeneous colloidal solution was produced after evaporating the propanol at 333 K in a rotary evaporator. Fe-doped TiO_2 powders were synthesized with different Fe concentrations ranging from 0% (undoped) to 1% Fe (atomic Fe/Ti ratio). Both TiO_2 and Fe/TiO_2 mesoporous films were fabricated by tape casting 300 µl sample solutions onto blank glass substrates (Schott Borofloat 33, 10×5 cm^2). The solutions were made by mixing 2 ml of the colloid (density: 0.130 g/ml) with 180 µl 10% Triton X-100 in H_2O and 0.02 g polyethylene glycol. After tape casting, the films (area: 10 × 3.8 cm^2) were dried in air to evaporate the water and fired at 723 K in air to remove any remaining organic components. The same method, but without the tape casting step, was used to convert part of the Fe/TiO_2 colloidal solutions into powders.

Structural characterization. The crystal structures of Fe-doped TiO_2 and pure TiO_2 nanoparticles were analyzed by X-ray diffraction (XRD, Bruker D8 Advance) using Co-Kα radiation (λ = 0.178897 nm). The specific surface areas of the powder samples were determined by BET adsorption measurements on a Quantachrome Autosorb-6B instrument at 77 K in liquid nitrogen. Prior to these measurements, the samples were pretreated in vacuum at 623 K for 16 hours. The Raman spectra were recorded by a Renishaw Raman imaging microscope (system 2000). A 514.5 nm Ar^+ laser line with a power output of 20 mW was used for excitation. A Leica DMLM optical microscope with a Leica PL floutar L500/5 objective lens was used to focus the beam on the sample. The 520 cm^{-1} peak of a Si wafer served as a wavelength reference for the Raman spectra.

Activity measurements. The photocatalytic activity of the samples was evaluated in a continuous flow setup (Figure 1) equipped with an on-line chemiluminescence-based NO_x analyzer (Teledyne Instruments, Model 200E) with a measurement range of 0-2 ppm. The samples are placed in a 10 cm wide reactor trough, 5 mm below a fused silica optical window, consistent with international standard NEN-ISO 22197-1:2007. A continuous 1 L/min flow of ~1000 ppb NO in air, passed over the sample surface, which was irradiated by a UV light source (75 W facial tanner, Philips HB172) with an intensity of ~2 mW/cm^2. To confirm the photo-reduction ability for Fe-doped TiO_2, 1000 ppb NO in pure N_2 or pure He (Linde Gas Belgium NV) were also used as target pollutants under the same experimental conditions. The NO and NO_x (=NO+NO_2) concentrations were continuously recorded every 10 seconds, while the NO_2 concentration is automatically calculated by the analyzer from the concentration difference between NO_x and NO.

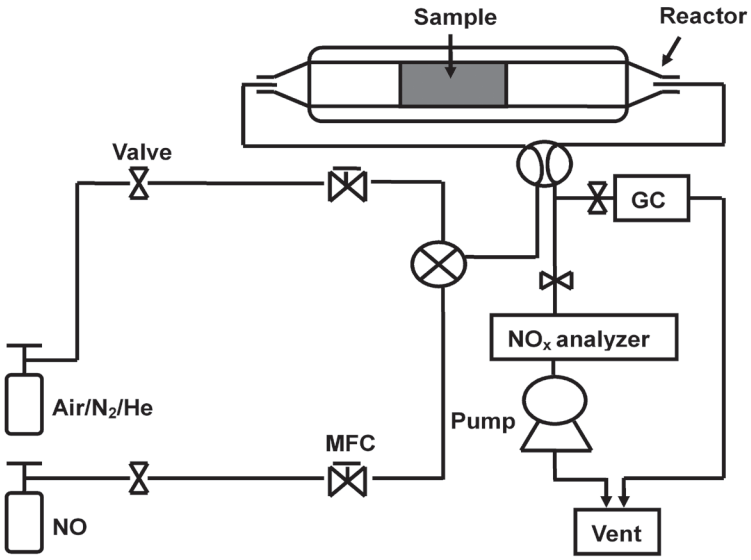

Figure 1: Schematic diagram of the continuous-flow NO_x photocatalytic setup. Air, pure nitrogen or helium was used as a carrier gas.

The N_2 and O_2 concentrations were measured by on-line gas chromatography. The gas chromatograph (Shimadzu, GC-2014) was equipped with a Pulsed Discharge Detector (PDD) operating at 493 K. The photocatalytic products were separated by a combination of Porapak Q and GsBP-PLOT molsieve columns using pure helium (99.9999%) as carrier gas. In order to exceed the detection limit of the GC, a flow of 100 ppm NO in He was used as the target pollutant for GC measurements.

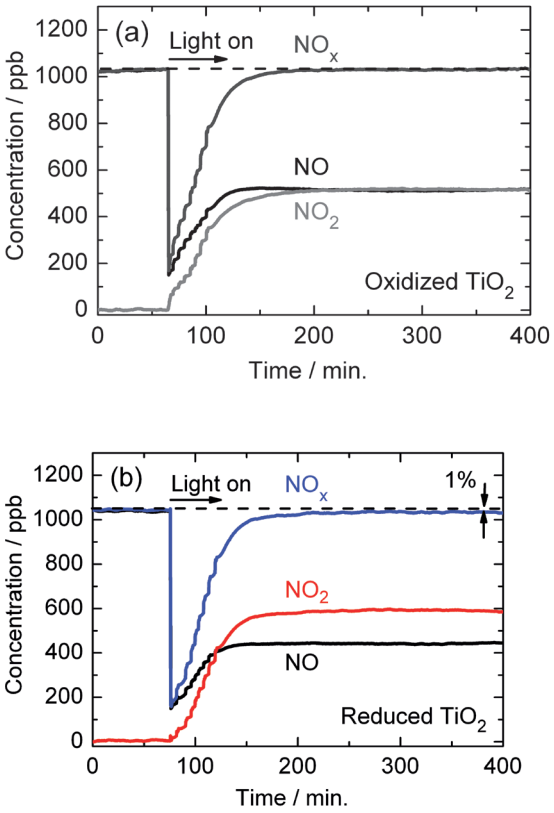

Figure 2: Photocatalytic degradation of NO in air for (a) oxidized and (b) reduced TiO_2 under UV light irradiation. The 1% of lost NO_x in b) is attributed to the photo-reduction of NO to something other than NO or NO2.

4.3 Results and discussion

To investigate the influence of oxygen vacancies on the decomposition of NO over undoped TiO_2, the photocatalytic activity for stoichiometric TiO_2 (as-prepared TiO_2 that is fully oxidized by a heat treatment at 723 K in air) and reduced TiO_2 (heat treatment at 723 K in a 2% H_2/Ar atmosphere) are compared. The results are shown in Figure 2, and we briefly describe the overall features here before presenting more detailed reaction schemes later in this paper. The photocatalytic reactions are initiated by illuminating the sample with UV light after 1 hour equilibration in a ~ 1 ppm NO atmosphere in the dark. For oxidized TiO_2, the NO concentration immediately decreases by ~ 800 ppb upon illumination (Figure 2a). This is due to the reaction of gas-phase NO species

with adsorbed superoxide anions (O_2^-), resulting in the formation of nitrate groups. The superoxide anions are formed by the reduction of adsorbed O_2 by photoexcited electrons. Since the nitrate groups do not spontaneously desorb, the surface slowly saturates and the NO concentration at the reactor outlet increases again.[14,19] Integration of the NO_x peak area below the 1040 ppb baseline in Figure 2a yields a total number of 0.69 x 10^{18} nitrate adsorbates, which corresponds to ~ 5% of the total number of surface sites (~ 1.3 × 10^{19} cm^{-2}, based on 0.019 g of TiO_2, a BET surface area of 71 m^2/g and a surface site density of 1 × 10^{15} cm^{-2} for 5-fold coordinated Ti^{4+} at the lowest-energy {101} surface[20]). At the same time, 50% of the NO is photo-oxidized to NO_2 at the illuminated TiO_2 surface via reaction of NO with photo-generated hydroxyl radicals. This undesired reaction (the toxicity of NO_2 exceeds that of NO) also occurs in air, but under ambient conditions the process is very slow. Clearly, illuminated TiO_2 strongly catalyzes this reaction.[20] After ~ 200 min., the surface is fully saturated with nitrate groups and no net change in the NO_x concentration occurs anymore.

Reduced TiO_2 shows a slightly higher activity for the photo-oxidation of NO to NO_2 than oxidized TiO_2 under otherwise identical conditions (Figure 2b). We attribute this to the presence of oxygen vacancies that are formed during the reduction treatment.[21] (reaction (7), Chapter 1). In-plane vacancies such as these, or step- or kink-sites are well known to be able to enhance the catalytic activity for certain reactions by providing energetically favorable ad- or desorption sites.[23-26]

A less pronounced but arguably more important observation from the data in Figure 2b is that after the surface is saturated with NO_3^- groups, the sum of the NO and NO_2 concentrations is no longer equal to the initial NO concentration of 1040 ppb. About 1% of the NO_x (10 ppb) has disappeared and must have been converted to another species. Since NO_3^- and NO_2 are the only stable oxidation products after NO conversion, we attribute the 1% of 'lost' NO_x to the formation of a reduction product, such as N_2O or N_2.

Although the 1% of lost NO_x can be accurately and very reproducibly measured, the amount is rather small. We attribute this to the fact that reaction (1) is reversible, which causes part of the reduced TiO_2 to be re-oxidized while exposed to air. Before exploring further evidence for the photo-reduction reaction and possible mechanisms that cause it, we first need to stabilize the oxygen vacancies in reduced TiO_2. This can be achieved by doping the TiO_2 nanoparticles with Fe, a process that we recently studied in detail.[27] The Fe^{3+} substitutes for Ti^{4+} ions in the lattice, and the effective negative charge of this acceptor-type dopant is compensated by the positively-charged oxygen vacancies (reaction (8), Chapter 1). Evidence for the formation of oxygen vacancies upon Fe doping is provided by a combination of XRD and Raman measurements (Figure 3). The XRD patterns show that the d_{101} lattice spacing decreases linearly with increasing Fe concentration (Figure 3a), which proves that Fe ions are indeed incorporated as dopants in the TiO_2 lattice. The fact that the lattice spacing decreases, even though Fe^{3+} is slightly larger than Ti^{4+},[28] is due to the formation of oxygen vacancies.[27] Further evidence for the presence of oxygen vacancies is given by Raman spectroscopy. As indicated in Figure 3b, the Raman peak position of the anatase E_g mode shows a linear shift with increasing Fe concentration. Such a shift was first observed for reduced (undoped) anatase TiO_2 by Parker et al.,[29,30] who were able to relate the size of the shift to the oxygen stoichiometry. Parker's results are plotted in Figure 3b (dashed line) on

the same x-axis scale, using the assumption that one oxygen vacancy is formed for every two Fe ions – see Eq. (2). The slopes of the data points and the dashed line are identical. Together with the XRD data, this confirms that the Fe dopants are indeed fully charge-compensated by oxygen vacancies.[27]

The degradation of NO over Fe-doped TiO_2 is shown in Figure 4a. The initial stage of the reaction after turning on the light is similar to that observed for undoped TiO_2: a fast decrease of the NO concentration (adsorption at photo-generated superoxide sites) followed by a slower increase of the NO signal as the surface becomes saturated with NO_3^- groups (de-activation). However, the amount NO_x that is presumably 'lost' to photo-reduction has now increased to 3%. This is an increase of a factor of 3 compared to undoped reduced TiO_2. We attribute this large increase to the higher concentration of

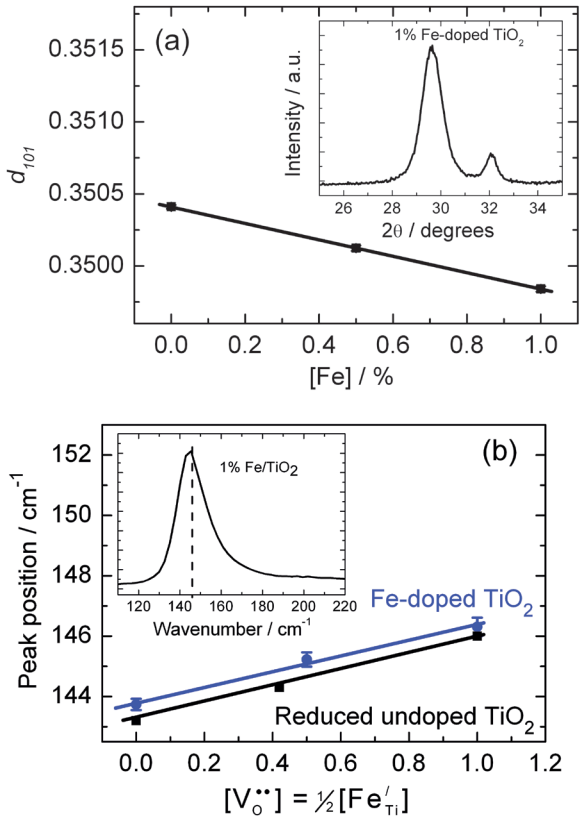

Figure 3: (a) Shift of the anatase (101) peak as a function of Fe concentration in Fe/TiO_2 nanoparticles. The XRD pattern in the inset shows that anatase (main peak) is the dominant phase, with only a small amount of rutile (peak at 32°). (b) Position of the anatase E_g Raman peak (inset) as a function of Fe concentration for Fe/TiO_2 (this study) and as a function of oxygen stoichiometry for undoped TiO_2 (Parker et al.[29]).

oxygen vacancies, which are now stabilized by the presence of charge-compensating Fe acceptors.

A second important observation in Figure 4a is that the formation of NO_2 is almost completely suppressed after 300 min. After reaching steady-state conditions, only 3% of the NO is continuously converted to NO_2. This is much less than the 50 – 60% observed for undoped TiO_2 (Figure 2). Apparently, Fe doping strongly suppresses the *activity* for NO_2 formation, but also increases the *selectivity* towards photoreduction from 0 to 50% (3% reduction + 3% oxidation).

To further prove the ability of 1% Fe-doped TiO_2 to photo-reduce NO, pure N_2 (99.999%) was used instead of air as the carrier gas for the NO pollutant. Figure 4b shows that even in the absence of oxygen, 4.5% of the NO_x continuously disappears after reaching steady state conditions. This is again consistent with what would be expected for an overall photo-reduction reaction.

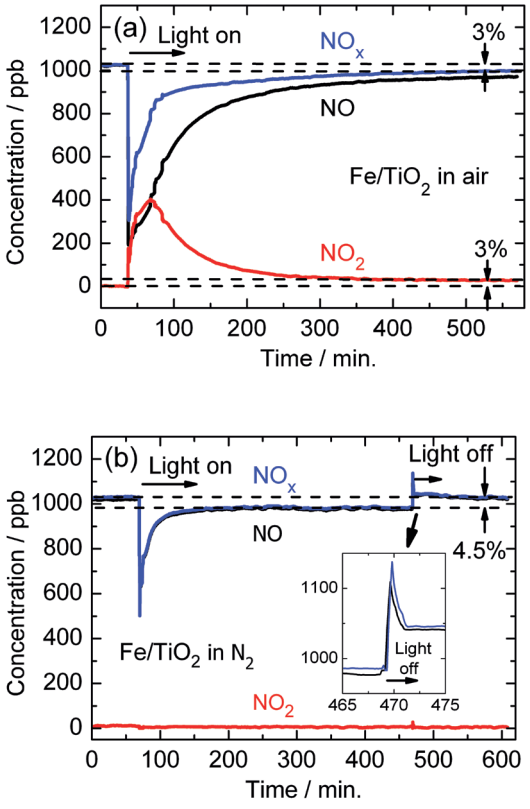

Figure 4: Photocatalytic degradation of NO over 1% Fe/TiO_2 (a) in air and (b) in pure N_2.

It should be noted that even in an N_2 atmosphere, the NO concentration briefly decreases during the first 50 seconds after the light is turned on (Figure 4b). As outlined above, this is due to the reaction of NO with adsorbed O_2^- species, resulting in the formation of NO_3^-. The O_2^- species are formed while the sample is exposed to air and ambient light prior to the experiment, and do not spontaneously desorb after replacing the air in the reactor chamber with N_2. Further inspection of Figure 4b shows that no NO_2 is formed during the initial and steady-state phases of the photoreaction. This indicates that the selectivity for photo-reduction is 100% for 1% Fe-doped TiO_2 in the absence of oxygen.

A final observation from Figure 4b is the immediate desorption of a small amount of NO after turning off the UV light. This indicates the presence of a small amount of unreacted, adsorbed NO at the TiO_2 surface. From integration of the desorption peak, the amount of desorbed NO corresponds to ~0.04% of the total number of TiO_2 surface sites.[31] This is a much smaller fraction than the number of adsorbed nitrate species mentioned before, which suggests that NO quickly reacts to NO_3^- after being adsorbed.

To support our assumption that the 'lost' NO in Figure 4 is photo-catalytically reduced, gas chromatography measurements were carried out to identify the chemical nature of the reaction product(s). This indeed revealed the presence of N_2 and O_2, while no other species (such as N_2O) were detected. The absence of N_2O can be explained by the absence of lateral interactions between adsorbed NO species at these low NO concentrations.[32] As shown in Figure 5, the concentrations of N_2 and O_2 gradually increase until steady-state conditions are reached after ~80 min. Both gases evolve in a stoichiometric ratio, which is consistent with the absence of N_2O formation. It should be noted that the sum of the N_2 and O_2 concentrations is ~1% of the initial NO concentration, i.e., 4.5 times less than the fraction of NO converted in Figure 4b. We attribute this to the 100 times larger total concentration of NO used for the GC experiment. Such a large concentration may saturate the total number of available reaction sites at the surface, explaining the lower fractional conversion. A control experiment with undoped TiO_2, also shown in Figure 5, did not show any N_2 or O_2 evolution. This clearly shows that Fe doping of TiO_2 changes its photo-catalytic selectivity for NO degradation from oxidation to reduction.

Based on all these observations, we propose the following series of reactions to describe the various processes that occur:

1. Photo-oxidation of NO to NO_2 and NO_3^-

The reaction of photo-induced electrons and holes with surface adsorbed oxygen and hydroxyl groups (~ 1.8 mmol/g for anatase,[33] which are known to be present on oxide surfaces that are exposed to air) results in the formation of superoxide anions and hydroxyl radicals:[11,12]

$$h\nu \xrightarrow{TiO_2} e^- + h^+ \quad (3)$$

$$Ti(O_2)_{ads} + e^- \xrightarrow{k_1} Ti(O_2^-)_{ads} \quad (4)$$

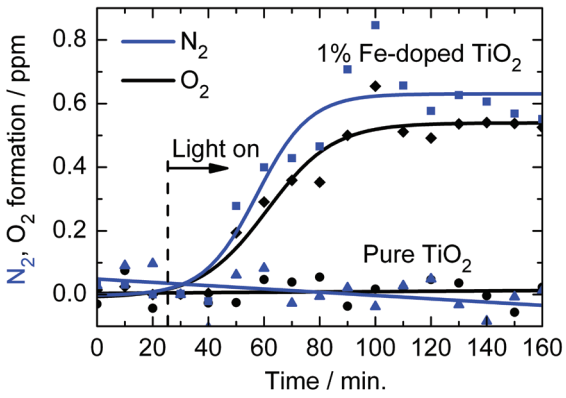

Figure 5: Photocatalytic conversion of NO to N_2 and O_2 over 1% Fe-doped TiO_2. The sample was irradiated with UV light, and the target pollutant was 100 ppm NO in He.

$$Ti-OH^- + h^+ \rightarrow Ti-OH^\bullet \quad (5)$$

The superoxide anion can directly oxidize nitric oxide to a nitrate adsorbate:

$$Ti(O_2^-)_{ads} + NO(g) \rightarrow Ti(NO_3^-)_{ads} \quad (6)$$

At the same time, photo-oxidation of NO by hydroxyl radicals leads to the formation of NO_2:

$$Ti-OH^\bullet + NO \rightarrow Ti-H + NO_2(g) \quad (7)$$

While the Ti–H bond seems unusual, DFT calculations suggest that it can indeed exist at the (001), (100) and (101) surfaces of anatase (the hydrogen binds to under-coordinated Ti atoms, resulting in a Ti–H bond length of ~1.75 Å and a slightly outward relaxation of the Ti atoms).[33] At the initial stage of the reaction (before reaching steady-state), the net overall reaction can thus be summarized as

$$Ti(O_2)_{ads} + Ti-OH^- + h\nu + 2NO(g) \rightarrow Ti(NO_3^-)_{ads} + Ti-H + NO_2(g) \quad (8)$$

The sum reaction (8) indicates that NO_2 and NO_3^- are simultaneously produced, consistent with the data shown in Figure 2a.

Since the adsorbed nitrate groups do not spontaneously desorb, reactions (6) and (4) will stop after a while and the catalyst slowly de-activates. Since NO_2 formation via photo-generated holes—reactions (5) and (7)—persists after de-activation, there must be an alternative reaction path for the photo-generated electrons under steady-state conditions. A likely pathway is the following:[12,34]

$$Ti-H+O_2(g)+e^- \xrightarrow{k_2} Ti-OOH^- \quad (9)$$

$$Ti-OOH^- + Ti-H \rightarrow Ti-OH^- + Ti-OH^\bullet \quad (10)$$

$$Ti-OH^\bullet + e^- \rightarrow Ti-OH^- \quad (11)$$

Under steady-state conditions, reactions (3), (5), (7) and (9-11) all occur simultaneously and can be summed up to give:

$$2NO(g)+O_2(g)+2h\nu \xrightarrow{TiO_2} 2NO_2(g) \quad (12)$$

2. Suppression of NO_2 formation

The presence of Fe^{3+} markedly changes the reaction mechanism for NO_2 formation, as illustrated by Figure 4a. During the initial stage of illumination, NO_2 is again formed via the mechanism described by reaction (8). However, instead of re-generating Ti–H sites via reactions (9-11) after de-activation, the photo-generated electrons can now reduce Fe^{3+}:

$$Fe^{3+} + e^- \xrightarrow{k_3} Fe^{2+} \quad (13)$$

Fe^{2+} is a well known adsorption site for nitric oxide, leading to the formation of mono- or di-nitrosyl species, [35,36]

$$Fe^{2+} + nNO(g) \rightarrow Fe^{2+}(NO)_{n,ads} \quad (14)$$

where *n* equals 1 or 2, respectively. This species can be oxidized again via adjacent hydroxyl radicals, or by direct capture of photo-generated holes:

$$Fe^{2+}(NO)_{n,ads} + Ti-OH^\bullet \rightarrow Fe^{3+}(NO)_{n,ads} + Ti-OH^- \quad (15a)$$

$$Fe^{2+}(NO)_{n,ads} + h^+ \rightarrow Fe^{3+}(NO)_{n,ads} \quad (15b)$$

The oxidation of Fe^{2+} to Fe^{3+} reduces the degree of π back-bonding, which weakens the Fe^{3+}–NO bond and results in desorption:[18]

$$Fe^{3+}(NO)_{n,ads} \rightarrow Fe^{3+} + nNO(g) \quad (16)$$

The sum of reactions (3), (5), (13-14), (15a) and (16) represents a NO-mediated recombination mechanism that explains why so little NO_2 is formed over Fe-doped TiO_2 after reaching steady-state conditions.

The formation of $Fe^{2+}(NO)_n$ species via reaction (14) is supported by the immediate release of NO to the gas phase (reaction (16)) when turning off the UV light, as shown in Figure 4b. Note that this observation also rules out reaction (15b), since no holes are available in the dark. Reaction (15a) therefore seems a more likely pathway for re-oxidation of Fe^{2+}.

3. Photo-reduction

The formation of N_2 and O_2 (Figure 5) can occur via at least two different routes. One possibility is that a small amount of tetrahedrally coordinated Ti is formed in the Fe-doped TiO_2 samples. This species has been reported as the active site for catalytic decomposition of NO into N_2 and O_2 at Ti-modified zeolites by Anpo and co-workers.[17,36] Since most Ti ions at the TiO_2 surface are 5-fold coordinated, a single oxygen vacancy created at or near the surface could indeed lead to a 4-fold coordinated Ti^{4+} center. However, the Ti-O bond length would still be similar to the 1.93 Å found in bulk TiO_2, whereas the tetrahedrally coordinated TiO_4 centers that are reported to photoreduce NO to N_2 have a significantly smaller bond length (~1.78 Å).[37] Such a strong reduction in bond length would require very high oxygen vacancy concentrations, much higher than those present in our 1% Fe-doped TiO_2.[27] Based on these arguments, the possibility that the formation of N_2 and O_2 is due to tetrahedrally coordinated Ti^{4+} seems unlikely.

A more plausible explanation is that oxygen vacancies act as catalytic centers that capture the oxygen-end of the NO molecules:

$$V_{O(surf)}^{\bullet\bullet} + 2e^- + NO(g) \rightarrow O_{surf} - N \qquad (17)$$

Since the captured NO molecules have no net charge, mobile oxygen vacancies[38] are able to diffuse close to the captured molecule and capture another NO molecule on a neighbouring site. Alternatively, the $O_{surf} - N$ species themselves may be sufficiently mobile—for example via a surface vacancy diffusion mechanism—to meet each other. They can then react to form N_2:

$$2O_{surf} - N \rightarrow 2O_{surf} + N_2(g) \qquad (18)$$

Since N_2 has a higher thermodynamic stability than NO ($\Delta G_f^0(NO)$ = +87.6 kJ/mol), reaction (18) will be exothermic. The released energy helps to release the trapped oxygen atoms from the lattice sites, resulting in the formation of O_2:

$$2O_{surf} \rightarrow 2V_O^{\times} + O_2(g) \qquad (19)$$

The photo-generated holes (h^+) can then re-oxidize the neutral oxygen vacancies to their normal 2+ state:

$$V_O^{\times} + 2h^+ \rightarrow V_O^{\bullet\bullet} \qquad (20)$$

Summing up reactions (3) and (17-20) gives the overall photo-reduction reaction:

$$2NO(g) + 4hv \xrightarrow{2V_O^{\bullet\bullet}} N_2(g) + O_2(g) \quad (21)$$

Repeating the experiment of Figure 4b for a longer time showed no change in the fraction of NO that is lost to photo-reduction – a value of 4.5% was found even after 1050 min. This corresponds to turn-over number of ~ 2 nitric oxide molecules per oxygen vacancy site, which confirms that this defect acts as a catalytic center.

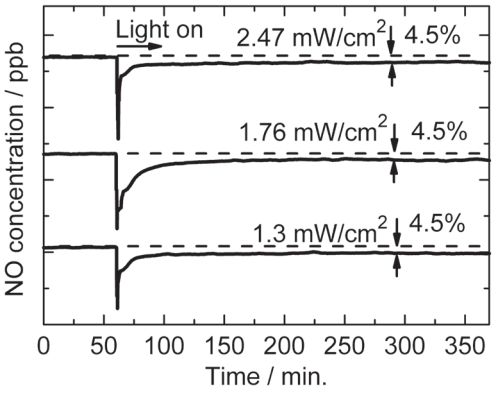

Figure 6: Influence of UV light intensity on the photocatalytic activity for NO degradation of 1% Fe-doped TiO_2 in pure N_2.

Before any further attempts can be made to improve the photocatalytic activity of the material, it is important to identify the rate-limiting factor of the overall photo-reduction process. Possible external factors include the illumination intensity and the concentration of oxygen vacancies. The influence of the UV light intensity on NO decomposition for 1% Fe-doped TiO_2 is shown in Figure 6. Clearly, the photon flux is not a limiting factor in this range of light intensities.

The influence of oxygen vacancies on the photocatalytic activity is investigated by repeating the experiment of Figure 4b with half the concentration of oxygen vacancies (0.5% instead of 1% Fe, all other conditions are the same). As shown in Figure 7, the NO conversion efficiency is 3%, significantly less than the 4.5% in Figure 4b. This shows that the concentration of oxygen vacancies indeed limits the photocatalytic activity for NO reduction. Further improvements of this system may therefore be possible by increasing the concentration of Fe. We recently showed that Fe dopant concentrations of up to 10% in TiO_2 nanoparticles are possible before segregation of iron oxide occurs.[27]

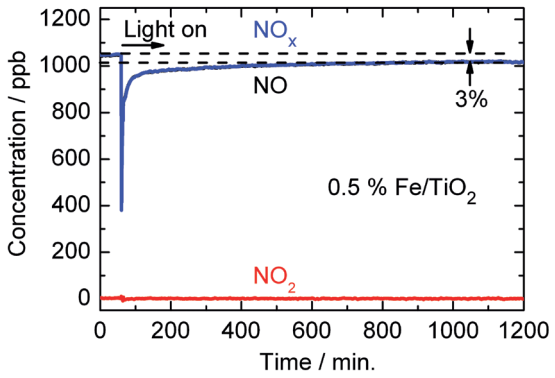

Figure 7: Photocatalytic decomposition of NO for 0.5% Fe/TiO_2 in pure N_2.

4.4 Conclusions

We have found that oxygen vacancies in nano-sized TiO_2 serve as active centers for the photocatalytic reduction of nitric oxide into N_2 and O_2. By doping the material with Fe, the mechanism of the reaction can be influenced in two distinct ways: i) Fe^{3+} is an acceptor-type dopant that stabilizes the oxygen vacancies through charge-compensation, thereby increasing the *activity* of the photoreduction reaction, and ii) Fe^{3+} can be photo-reduced to Fe^{2+}, providing a recombination pathway that suppresses the formation of NO_2 and thus enhances the *selectivity* of the reaction for N_2 formation. While the conversion efficiency is still modest, the Fe/TiO_2 photocatalyst does not show any signs of de-activation. In contrast to the standard $DeNO_x$ catalysts based on TiO_2, the conversion is not blocked by nitrate species that have to be washed away periodically. The material is also easier and cheaper to synthesize than NO photo-reduction catalysts based on modified zeolites.

Further improvement of the photocatalytic activity seems simply a matter of increasing the dopant concentration. For Fe, dopant concentrations of up to 10% have been reported, which leaves ample room for further optimization. Alternatively, other acceptor-type dopants can be explored. Based on the proposed reaction mechanisms, it is important to choose dopants that can be reduced to the 2+ oxidation state in order to avoid the oxidation of NO to NO_2. Cr, Co or Ni are therefore more suitable choices than e.g. Al or Ga. Further explorations along these lines may lead to a new generation of highly selective photocatalysts.

Acknowledgements

The authors gratefully acknowledge Prof. D. Bahnemann (Leibnitz Universität Hannover, Germany) for advice and J. Middelkoop for practical help with setting up the NO_x analysis system. We thank B. Boshuizen for designing a Labview program to read the NO_x analyzer.

References

[1] Devahasdin, S.; Fan, C.; Li, K.; Chen, D. H. *J. Photochem. Photobiol. A* **2003**, *156*, 161-170.

[2] Roy, S.; Baiker, A. *Chem. Rev.* **2009**, *109*, 4054-4091.

[3] Wu, J. C. S.; Cheng, Y. *J. Catal.* **2006**, *237*, 393-404.

[4] Taylor, K. C. *Catal. Rev. Sci. Eng.* **1993**, *35*, 457-481.

[5] Rodriguez, J. A.; Jirsak, T.; Liu, G., Hrbek, J.; Dvorak, J.; Maiti, A. *J. Am. Chem. Soc.* **2001**, *123*, 9597-9605.

[6] Maggos, T.; Bartzis, J.G.; Liakou, M.; Gobin, C. *J. Hazard. Mater.* **2007**, *146*, 668-673.

[7] Negishi, N.; Takeuchi, K.; Ibusuki, T. *J. Mater. Sci.* **1998**, *33*, 5789-5794.

[8] Lin, Y. M.; Tseng, Y. H.; Huang, J. H.; Chao, C. C.; Chen. C. C.; Wang, I. *Environ. Sci. Technol.* **2006**, *40*, 1616-1621.

[9] Anpo, M. *Pure Appl. Chem.* **2000**, *72*, 1265-1270.

[10] Wang, J.; Tafen, D. N.; Lewis, J. P.; Hong, Z.; Manivannan, A.; Zhi, M.; Li, M.; Wu, N. *J. Am. Chem. Soc.* **2009**, *131*, 12290-12297.

[11] Du, Y.; Rabani, J. *J. Phys. Chem. B* **2003**, *107*, 11970-11978.

[12] Hoffmann, M. R.; Martin, S. T. ; Choi, W. ; Bahnemann, D. W. *Chem. Rev.* **1995**, *95*, 69-96.

[13] Dalton, J. S.; Janes, P. A.; Jones, N. G.; Nicholson, J. A.; Hallam, K. R. ; Allen, G. C. *Environ. Pollut.* **2002**, *120*, 415-422.

[14] Wang, H.; Wu, Z.; Zhao, W.; Guan, B. *Chemosphere*, **2007**, *66*, 185-190.

[15] Anpo, M.; Zhang, S. G.; Mishima, H.; Matsuoka, M.; Yamashita, H. *Catal. Today* **1997**, *39*, 159-168.

[16] Anpo, M.; Takeuchi, M.; Ikeue, K.; Dohshi, S. *Curr. Opin. Solid State Mater. Sci.* **2002**, *6*, 381-388.

[17] Yamashita, H.; Ichihashi, Y.; Zhang, S.G.; Matsumura, Y.; Souma, Y.; Tatsumi, T.; Anpo, M. *Appl. Surf. Sci.* **1997**, *121*, 305-309.

[18] Wu, Q.; Mul, G.; Van de Krol, R. *Energy Environ. Sci.* **2011**, *4*, 2140-2144.

[19] Komazaki, Y.; Shimizu, H.; Tananka, S. *Atmos. Environ.* **1999**, *33*, 4363-4371.

[20] Henningsson, A.; Andersson, M. P.; Uvdal, P.; Siegbahn, H.; Sandell A. *Chem. Phys. Lett.* **2002**, *360*, 85-90.

[21] Liu, H.; Ma, H. T.; Li, X. Z.; Li, W. Z.; Wu, M.; Bao, X. H. *Chemosphere* **2003**, *50*, 39-46.

[22] Chiang, Y. M.; Birnie, D. P.; Kingery, W. D. Physical Ceramics, Wiley, New York, 1997.

[23] Gong, X. Q.; Selloni, A.; Batzill, M.; Diebold, U. *Nature Mater.* **2006**, *5*, 665-670.

[24] Beck, T. J.; Klust, A.; Batzill, M., Diebold, U.; Valentin, C. D.; Selloni, A. *Phys. Rev. Lett.* **2004**, *93*, 0361041-0361044

[25] Thompson, T. L.; Yates, J. T. *Chem. Rev.* **2006**, *106*, 4428-4453.

[26] Henderson, M. A.; Epling, W. S.; Perkins, C. L.; Peden, C. H. F. *J. Phys. Chem. B* **1999**, *103*, 5328-5337.

[27] Wu, Q.; Zheng, Q.; Van de Krol, R. *J. Phys. Chem. C* **2012**, *116*, 7219-7226.

[28] Shannon, R. D. *Acta Crystallogr. A* **1976**, *32*, 751-767.

[29] Parker, J. C.; Siegel, R. W. *Appl. Phys. Lett.* **1990**, *57*, 943-945.

[30] Parker, J. C.; Siegel, R. W. *J. Mater. Res.* **1990**, *5*, 1246-1252.

[31] The number of desorbed NO molecules was determined by integrating the NO_x curve from t = 469 min. to t = 471.5 min. in Fig. 4b. The final concentration of 1040 ppb was used as a baseline. This corresponds to 5.2 x 10^{15} NO molecules. Based on the weight of the sample (0.019 g) and a BET surface area of 71 m^2/g, this corresponds to ~ 0.04 % of the total amount of the sample's surface sites.

[32] Diebold, U. *Surf. Sci. Rep.* **2003**, *48*, 53-229.

[33] Carneiro, J. T.; Almeida, A. R.; Moulijn, J. A.; Mul, G. Phys. Chem. Chem. Phys. 2010, 12, 2744-2750.

[34] Barnard, A. S.; Zapol, P. *Phys. Rev. B* **2004**, *70*, 235403.

[35] Zhang, Z.; Wang, C.; Zakaria, R.; Ying, J. Y. *J. Phys. Chem. B* **1998**, *102*, 10871-10878.

[36] Mul, G.; Pérez-Ramírez, J.; Kapteijn, F.; Moulijn, J. A. *Catal. Lett.* **2002**, *3*, 129-138.

[37] King, D. L.; Peri, J. B. *J. Catal.* **1983**, *79*, 164-175.

[38] Hu, Y.; Martra, G.; Zhang, J.; Higashimoto, S.; Coluccia, S.; Anpo, M. *J. Phys. Chem. B* **2006**, *110*, 1680-1685.

[39] Yamashita, H.; Ichihashi, Y.; Anpo, M.; Hashimoto, M.; Louis, C.; Che, M. *J. Phys. Chem.* **1996**, *100*, 16041-16044.

[40] Schaub, R.; Wahlström, E.; Rønnau, A.; Lægsgaard, E.; Stensgaard, I.; Besenbacher, F. *Science* **2003**, *299*, 377-379.

Chapter 5

A dopant-mediated recombination mechanism in Fe-doped TiO_2 nanoparticles for the photocatalytic decomposition of nitric oxide

Abstract

The photon-assisted adsorption and catalytic decomposition of nitric oxide (NO) over undoped and Fe-doped TiO_2 nanoparticles have been investigated by in-situ Diffuse Reflectance Infrared Fourier Transformed (DRIFT) spectroscopy, in-situ X-ray Photoelectron Spectroscopy (XPS) and on-line NO_x analysis. The DRIFT spectra and on-line NO_x analysis reveal that the usual photo-oxidation of NO to NO_2 is strongly suppressed by the Fe dopant. This is found to be caused by the photo-reduction of Fe^{3+} to Fe^{2+}, which is an effective adsorption site for nitric oxide species. The DRIFT spectra indeed reveal a new band at 1805 cm^{-1}, which is assigned to the N=O stretch vibration in a $Fe^{2+}(NO)_2$ complex. Instead of producing NO_2, photo-generated hydroxyl radicals oxidize the Fe^{2+} back to Fe^{3+}. This causes the NO to desorb again, effectively closing an NO-mediated recombination loop. These results support the recently proposed reaction mechanisms for the photocatalytic decomposition of NO over undoped and Fe-doped TiO_2 (*J. Am. Chem. Soc.*, doi:10.1021/ja302246b, see Chapter 4 in this thesis), and provide new insights for the development of highly selective photocatalysts based on doped metal oxides.

5.1 Introduction

Nitric oxide (NO_x) is one of the most harmful environmental pollutants in air. It causes damage to the lung tissue of human beings, and contributes to the formation of acid rain and depletion of the ozone layer.[1] The emission of NO_x, a mixture of NO and NO_2,[2] is mainly produced by the chemical reaction of N_2 and O_2 during the high-temperature combustion of fossil fuels in air.[3,4] Although NO_x emissions have slightly decreased since the late 1990s, concerns are that they will greatly increase again due to the growing number of automobiles in developing countries. Many technologies have been devoted to the removal of NO_x, including NO_x storage and reduction catalysis (NSR), selective catalytic reduction (SCR) and photocatalysis.[5,6] The photocatalysis route is arguably the most attractive one, since it can remove NO_x in dilute form from air at room temperature. TiO_2, one of the most popular photocatalysts, is particularly efficient at decomposing NO_x.[7]

The photocatalytic activity of TiO_2 originates from the presence of photo-generated electrons (e^-) in the conduction band and holes (h^+) in the valence band under irradiation with UV light.[8] However, these excited electrons and holes are not stable and can quickly recombine, releasing their energy in the form of heat.[9] To ensure that a sufficiently large fraction of the carriers can reach the surface before recombining, TiO_2 is generally studied in nanostructured form. Once the electrons and holes arrive at the surface, they react with adsorbed oxygen to form superoxide anions and hydroxyl radicals, respectively.[10,11] These species further react with adsorbed NO_x to form surface nitrates.[12,13] These nitrates do not spontaneously desorb and de-activate the catalyst until they are washed away by rain. To avoid this de-activation, several efforts have been made to change the selectivity of the photocatalytic reaction so that NO_x is photo-reduced to N_2 and O_2, both of which easily desorb from the surface. Anpo et

al. showed that highly dispersed tetrahedrally-coordinated 'TiO_2' clusters in zeolites can indeed photo-reduce NO_x into N_2 and O_2.[14] The reaction mechanism, however, remains unclear.[15] More recently, we have reported an alternative, more economical NO photoreduction catalyst in the form of nanostructured Fe-doped TiO_2.[16] We elucidated the adsorption of NO species at the Fe/TiO_2 surface,[17] and proposed a mechanism that explains how the photo-reduction of the Fe^{3+} dopant changes the selectivity of the NO decomposition reaction. In this paper, we will show direct experimental evidence that further supports this reaction mechanism.

5.2 Experimental

Undoped (pure) titanium dioxide (TiO_2) and 1% Fe-doped TiO_2 nanoparticles were synthesized by a simple, template-free sol-gel method.[17] For preparing 1% Fe/TiO_2, 0.8311 g of $Fe(NO_3)_3.9H_2O$ (+99%, Acros) was fully dissolved in 375 ml ultrapure water (Milli-Q, 18.2 MΩ.cm) and mixed with 2.6 ml HNO_3 (65% in H_2O) resulting in the formation of clear yellow solution. The TiO_2 nanoparticles were formed by dropwise addition of 62.5 ml of titanium tetra-isopropoxide (TTIP, Acros, 98%) to this solution under vigorous stirring. A part of colloidal solution was dried at 373 K to form a powder, and further annealed at 773 K in air to improve the crystallinity and to ensure that the Fe ions are incorporated as substitutional dopants in the TiO_2 lattice.[17] The remaining colloidal solutions were tape-casted onto a blank glass substrate (Schott Borofloat 33) to form a thin mesoporous film. Undoped TiO_2 nanopowders were prepared in a similar manner by omitting the $Fe(NO_3)_3$ precursor.

The crystal structures of the Fe-doped TiO_2 nanoparticles were determined by X-ray diffraction (XRD, Bruker, D8 Advance) with Cu-Kα radiation. UV–vis spectra of the samples were recorded on a Perkin-Elmer Lambda 900 spectrometer with an integrating sphere assembly. A $BaSO_4$ standard was used as a reference sample for baseline correction. Particle morphologies are studied by high resolution transmission electron microscopy (TEM) using a FEI TECNAI TF20 electron microscope equipped with a field emission gun (FEG) and an energy dispersive X-ray (EDX) system for elemental analysis. The sample powders for TEM-EDX measurements were dispersed in an ethanol solution and a few drops of the suspension were placed onto a Quantifoil® carbon polymer-supported copper grid, following by drying at ambient conditions.

The valence state of the Fe dopants was analyzed by X-ray photoelectron spectroscopy (XPS, Thermo Escalab 250) with a monochromatic Al Kα X-ray source. A quartz window on the UHV chamber allowed UV irradiation of the the sample surface during the XPS measurement (LC8 spot light source, Hamamatsu). The 1s peak of adventitious carbon at 284.6 eV was used as an internal reference for calibrating the XPS binding energy.

In-situ diffuse reflectance infrared fourier transformed spectroscopy (DRIFT, Thermo Nicolet Nexus with a MCT/A detector) was used for monitoring the presence of adsorbed NO, N_2O and NO_2 species on the nanopowder surface. The temperature-controlled chamber was equipped with two CaF_2 windows for the IR measurements, and a quartz window that allowed in-situ excitation of the sample. A 150 W Xe lamp

with a 370 nm bandpass filter (Newport type 10BPF10-370) served as a UV excitation source. A continuous flow of He with relatively high concentrations of either NO, NO_2 or N_2O (167 ppm, 30 ml/min) was used to ensure efficient adsorption of the target species. All DRIFT spectra represent the average of 64 consecutive scans with a resolution of 2 cm^{-1} at 303 K, and are referenced to the sample background.

The NO_x present in the gas phase during the photocatalytic process is directly detected by an on-line chemiluminescence-based NO_x analyzer (Teledyne Instruments, Model: 200E) with a sensitivity range of 0 – 2 ppm. The analyzer measures the concentrations of NO and NO_x (=NO+NO_2), and calculates the NO_2 concentration from the difference between these values. A continuous flow of NO/He gas (~ 1 ppm, 1 L/min) was used as initial target pollutant. The mesoporous thin film samples (10 cm × 5 cm) were placed into a rectangular PMMA reactor (40 cm × 10 cm × 5 cm), in accordance with NEN-ISO 22197-1:2007. A facial tanner (75 W, Philips HB172) was used as a UV light source, providing a UV intensity of 1.76 mW/cm^2 at the sample surface. The intensity of UV light source was measured by a Lutron UVA light meter (model: UVA-365).

5.3 Results and discussion

UV-Vis diffuse reflection spectra have been recorded to investigate how the Fe dopant is incorporated into the samples. The results are shown in Figure 1. The steep increase of the absorption at ~400 nm is due to the indirect band gap of pure anatase TiO_2.[20] Compared with pure TiO_2, Fe-doped TiO_2 shows a small red shift of the absorption onset towards the visible region. This is attributed to the charge-transfer transition between the *d*-electrons of Fe and the conduction band of the TiO_2,[21] which indicates that Fe is present as a substitutional dopant inside the TiO_2 nanoparticles.[18]

The particle morphologies and Fe distribution in the samples are investigated by TEM and EDX measurements, respectively. The TEM image in Fig. 2a reveals a particle size of ~10 nm for 1% Fe-doped TiO_2. Close inspection of a higher resolution TEM image (Fig. 2b) reveals fringes separated by 0.35 nm. This indicates the presence of the anatase form of TiO_2 (d_{101} = 0.35 nm), which is further confirmed by the main anatase (101) peak in the XRD pattern (Fig. 2c). Compared to pure TiO_2, a small but significant peak shift of the anatase (101) towards higher 2-theta angles is found for Fe-doped TiO_2, which indicates a small decrease in the (101) lattice spacing. This is attributed to the formation of oxygen vacancies that charge-compensate the Fe acceptor-type dopants.[18] In addition, a small rutile peak is also found for both pure TiO_2 and Fe-doped TiO_2. The anatase-to-rutile peak intensity ratio decreases with increasing Fe concentration (Fig. 2c), which is in accordance with reports that cation doping favors the anatase-to-rutile phase transformation.[22]

In order to determine the Fe distribution in the nanoparticles, the EDX beam was focused at the edge and at the center of a particle, indicated as regions 1 and 2 in Figure 2b, respectively. The EDX signals from these regions are shown in Fig. 2d. Two obvious Ti peaks (4.49 keV, 4.93 keV) and a small Fe peak at ~6.37 keV are present.

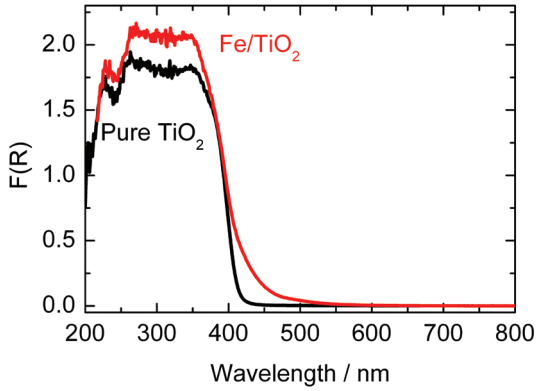

Figure 1: UV-Vis diffuse reflection spectra of pure TiO_2 and 1% Fe/ TiO_2 nanoparticles. F(R) is the Kubelka-Munk function, which is defined as $F(R) = (1-R)^2/2R$ with R being the measured reflection ($R = R_{sample}/R_{standard}$).[19]

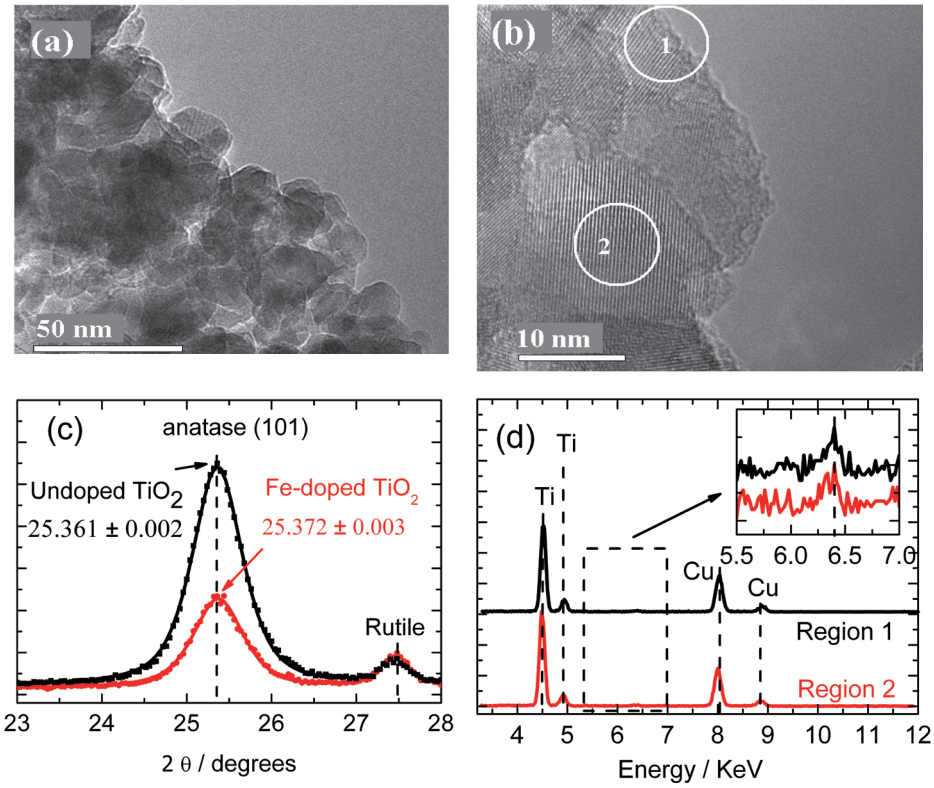

Figure 2: (a) TEM image of 1% Fe-doped TiO_2; (b) High resolution TEM image of 1% Fe-doped TiO_2; (c) XRD patterns of undoped TiO_2 and 1% Fe-doped TiO_2, fitted with pesudo-Voigt function; (d) EDX spectra of 1% Fe-doped TiO_2 focused on regions 1 and 2 shown in b). The Cu peaks originate from the support grid.

Integration of the peak areas indicates nearly the same Fe : Ti ratios for region 1 (0.9 ± 0.3 %) and region 2 (1.2 ± 0.4 %). This suggests that no significant accumulation of Fe at the surface of the particle occurs.

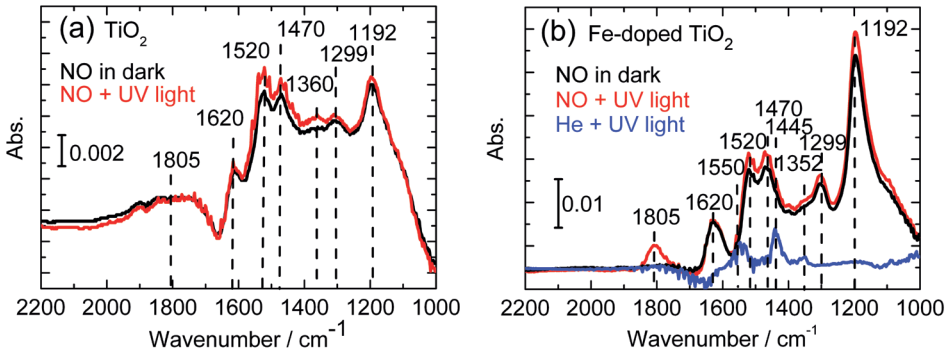

Figure 3: (a) DRIFT spectra of undoped TiO_2 in the presence of 167 ppm NO in the dark and under UV irradiation; (b) Similar spectra and blank test (UV light irradiation in pure He) for 1% Fe-doped TiO_2. The bands at 1352 cm^{-1}, 1445 cm^{-1} and 1550 cm^{-1} in the absence of NO are assigned to adventitious hydrocarbon oxides, bidentate carbonate and adsorbed O_2,[29-31] respectively.

To gain more insight into the photocatalytic reaction mechanism, DRIFT spectra of undoped TiO_2 and Fe-doped TiO_2 were measured in the presence of NO to investigate the presence of adsorbed intermediates. Before UV irradiation (in the dark), the DRIFT spectrum of undoped TiO_2 in the presence of NO shows a series of clear IR absorption bands (Fig. 3a). These bands are attributed to adsorbed H_2O (1620 cm^{-1}), monodentate nitrate ($-NO_3^-$, 1520 cm^{-1}), monodentate nitrito ($-ONO^-$, 1470 cm^{-1}), nitrite ($-NO_2^-$, 1299 cm^{-1}), and bidentate nitrate (1192 cm^{-1}) groups.[4,23,24] After turning on the UV light, the intensities at 1520 cm^{-1} and 1470 cm^{-1}, and to lesser extent those at 1299 cm^{-1} and 1192 cm^{-1}, show a modest increase. This indicates the photocatalytic oxidation of NO to nitric groups under UV irradiation. In addition, illumination results in a new small band at 1360 cm^{-1}, which is attributed to adsorbed NO_2 on the anatase surface.[25] This indicates the photocatalytic oxidation of NO to NO_2 in the presence of surface-adsorbed O_2.[26,27] NO_2 quickly desorbs from the TiO_2 surface, and its short residence time explains the relatively small signal of the 1360 cm^{-1} band. The increased intensities of the bands at 1520 cm^{-1} (NO_3^-) and 1360 cm^{-1} (NO_2) upon illumination are consistent with the reaction mechanism that proposed in chapter 4 (reactions 3-7).[16]

Since NO_3^- can not spontaneously desorb, reactions (2) and (4) will stop after the surface becomes saturated with NO_3^-. However, the band at 1360 cm^{-1} remains present, even after saturation, indicating continued production of NO_2 via reactions (3) and (5). This means that there must be an alternative reaction pathway for the photo-generated

electrons. A likely pathway is the reduction of protonated Ti^{4+} sites, resulting in the formation of surface hydroxyls via hydrogenperoxo species (reactions (9-11) in chapter 4).

For Fe-doped TiO_2 under UV irradiation, a small increase of the IR intensities at 1520 cm^{-1}, 1470 cm^{-1}, 1299 cm^{-1}, and a larger increase at 1192 cm^{-1} are observed (Fig. 3b). The ratio at which these bands increase suggests that the formation of bidentate nitrate groups (1192 cm^{-1}) is preferred over that of monodentate nitric groups in Fe-doped TiO_2. We attribute this to the larger concentration of oxygen vacancies in the Fe-doped samples,[18] which leaves more room at adjacent Ti^{4+} ions for a bidentate coordination. Another difference compared to the spectra for undoped TiO_2 is the absence of the band at 1360 cm^{-1}. This indicates that NO_2 formation is suppressed by Fe doping. A more detailed explanation for this will be given later (*vide infra*).

The most obvious spectral change for the Fe-doped TiO_2 in Fig. 3b is the appearance of a pronounced band at 1805 cm^{-1} under UV illumination. This band is not present for undoped TiO_2 under the same experimental conditions, nor is it present for Fe/TiO_2 in the absence of NO (Fig. 3b, blue curve). This suggests it is due to a photo-converted NO species adsorbed at a Fe surface site. Although NO-related photocatalytic reaction products for various oxides containing Fe^{2+} and Fe^{3+} ions have been intensely studied by IR spectroscopy,[29] the band at 1805 cm^{-1} has not yet been assigned in the literature.

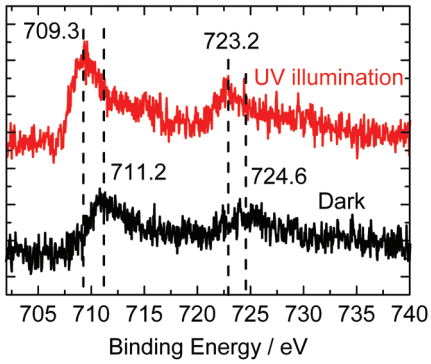

Figure 4: In-situ Fe-2p XPS spectra of 1% Fe-doped TiO_2 in the dark and under UV irradiation.

To further investigate the origin of the band at 1805 cm^{-1}, we first clarify the valence state of the Fe ions at the surface of the sample by comparing the XPS spectra in the dark and under UV irradiation. As shown in Fig. 4, the dark spectrum of Fe-doped TiO_2 show peaks at 711.2 eV and 724.6 eV, which correspond to the Fe $2p_{3/2}$ and Fe $2p_{1/2}$ binding energies of Fe^{3+}, respectively.[33] Under UV irradiation the peaks at 711.2 eV and 724.6 eV shift to 709.3 eV and 723.2 eV, respectively, which indicates the presence of Fe^{2+}.[34,35] These results show that most—if not all—of the Fe^{3+} ions are reduced to Fe^{2+} by the photo-generated electrons as indicated in reaction (13) in chapter 4.[36]

This reaction only starts after the surface is saturated with NO_3^- species. This is because the electrons first prefer to reduce O_2 since the O_2/O_2^- energy level is below that of Fe^{3+}/Fe^{2+}.[37,38] After saturation, reactions (2) and (4) can no longer occur, and reduction of Fe^{3+} to Fe^{2+} can take place instead. The consumption of the photo-generated electrons by Fe^{3+} would also inhibit reaction (7) and suppress the formation of NO_2. This explains why the band at 1360 cm^{-1} is not observed for Fe-doped TiO_2 in Fig. 3b.

Direct evidence that the presence of Fe indeed suppresses the formation of NO_2 is shown in Fig. 5. After turning on the UV light, the NO concentration briefly decreases due to the formation of surface nitrates. When the surface is saturated with NO_3^-, the NO concentration at the reactor outlet increases again. As discussed in detail in a previous paper,[16] the NO concentration does not go back to its initial value, since ~5% is continuously converted into N_2 and O_2. More importantly, no NO_2 formation occurs, whereas similar experiments for undoped TiO_2 show that 50% of the NO is photo-oxidized to NO_2.[16]

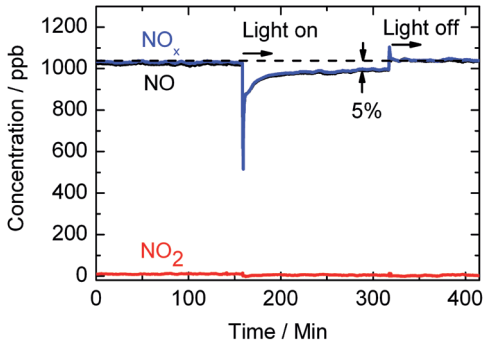

Figure 5: Photocatalytic degradation of NO over 1% Fe/TiO_2 in pure He atmosphere.

The Fe^{2+} that is formed is a well known and efficient adsorption site for NO.[39] Therefore, the band at 1805 cm^{-1} in Fig. 3b may be due to an NO reaction product coordinated to Fe^{2+}. Possible NO reaction products, other than the nitrate, nitrito and nitrite species identified above, are neutral nitrosyl (NO), NO_2 and N_2O species. To investigate these possibilities, DRIFT spectra were recorded with gaseous NO_2 and N_2O as the target species, in the dark and under UV illumination. No peak at 1805 cm^{-1} was observed for any of these measurements, which shows that the IR band at 1805 cm^{-1} cannot be attributed to adsorbed NO_2 or N_2O.

This leaves the possibility that the band at 1805 cm^{-1} is due to a nitrosyl species. The vibrational frequency indeed falls within the range of 1966 – 1710 cm^{-1} that is associated with various forms of adsorbed NO.[24] For ternary Fe-containing oxides, Miyata et al. reported Fe^{2+}-NO bands in the range of 1826-1853 cm^{-1} (Table 1). A somewhat lower frequency of 1810 cm^{-1} was found for the Fe^{2+}-$(NO)_2$ di-nitrosyl species in Fe/SiO_2.[40]

Table 1: Observed N–O stretching modes of NO_x species coordinated to various Fe surface sites.

Wavenumber (cm^{-1})	Assignment	Catalysts	Reference
2250	Fe^{2+}-(N_2O)	Fe-ZSM-5	42
1824	Fe^{2+}-(NO)	$FeAl_2O_4$	43
1845-53	Fe^{2+}-(NO)	$FeTiO_3$	43
1810	Fe^{2+}-$(NO)_2$	Fe/SiO_2	38
1805	Fe^{2+}-$(NO)_2$	Fe-doped TiO_2	this paper
1840	Fe^{3+}-(NO)	Fe-doped TiO_2	17
1625	$Fe^{2+}(NO_2)$	Fe-ZSM-5	44
1575	$Fe^{n+}(NO_3)$	Fe-ZSM-5	44
1914, 1900	Ti^{4+}-$(NO)_n$	TiO_2	45

The coordination of two nitrosyl species to a single Fe^{2+} ion would require slightly more free space around this ion. In our case, this space can be provided by the presence of oxygen vacancies that charge-compensate the Fe dopant. Taking all these considerations into account, we assign the band at 1805 cm^{-1} to a dinitrosyl species coordinated to Fe^{2+}. The formation of this species can be described by reactions (1), (11) and (12):

$$Fe^{2+} + 2NO \rightarrow Fe^{2+}(NO)_{2,ads} \quad (12)$$

It should be noted that the frequency of the N=O stretch vibration in $Fe^{2+}(NO)_2$ is significantly lower than that of gaseous NO (1876 cm^{-1}).[41] This is due to back-donation of the Fe^{2+} *d*-electrons to the π^* antibonding orbitals of the NO molecules.[14] This back-donation weakens the N–O bond, resulting in a lower vibration frequency. Another consequence of back-donation is that it stabilizes the interaction between Fe^{2+} and NO, which explains why dinitrosyls are commonly observed on transition metal ions rich in *d*-electrons.[46]

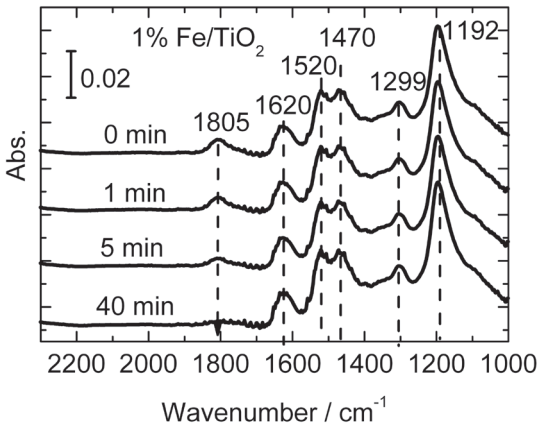

Figure 6: DRIFT spectra of 1% Fe-doped TiO_2 in a 167 ppm NO/He atmosphere. The band at 1805 cm^{-1} completely disappears within a few minutes after turning off the UV light.

To better understand the nature of the adsorbed dinitrosyl species, a series of DRIFT spectra are recorded immediately after turning off the UV light. As shown in Fig. 6, the band at 1805 cm^{-1} completely disappears after 40 minutes, while other nitric bands (e.g. 1520 cm^{-1}, 1470 cm^{-1}, 1299 cm^{-1} and 1192 cm^{-1}) remain the same. This shows that the NO species adsorbed at the Fe^{2+} sites ($Fe^{2+}(NO)_{2,ads}$) spontaneously desorb. This is attributed to the re-oxidation of Fe^{2+} to Fe^{3+} by an adjacent hydroxyl radical that was previously formed through reaction (3):[16]

$$Fe^{2+}(NO)_2 + Ti-OH^{\bullet} \rightarrow Fe^{3+}(NO)_{2,ads} + Ti-OH^{-} \quad (13)$$

The re-oxidation of Fe^{2+} to Fe^{3+} reduces the amount of π back bonding.[17] This decreases the stability of Fe–NO bond and explains why NO spontaneously desorbs after turning off the UV light:

$$Fe^{3+}(NO)_{2,ads} \rightarrow Fe^{3+} + 2NO(g) \quad (14)$$

The sum of reactions (1), (3), and (11-14) represents a NO-mediated recombination mechanism that explains why so little NO2 is formed at the surface of Fe-doped TiO_2 nanoparticles. The difference between the reaction mechanisms for undoped and Fe-doped TiO_2 is illustrated in Scheme 1.

Direct evidence for NO desorption is provided by the on-line NO_x analysis (Fig. 5), at the point where the UV illumination is turned off. An expanded view of this part is shown in Fig. 7. After turning off the UV light, a small amount of released NO is detected by the NO_x analyzer, as evidenced by the peak at t = 317 min. Integration of this peak shows that the number of desorbed NO molecules corresponds to ~2% of the total number of Fe sites at the surface.[47] We tentatively attribute this rather small value to

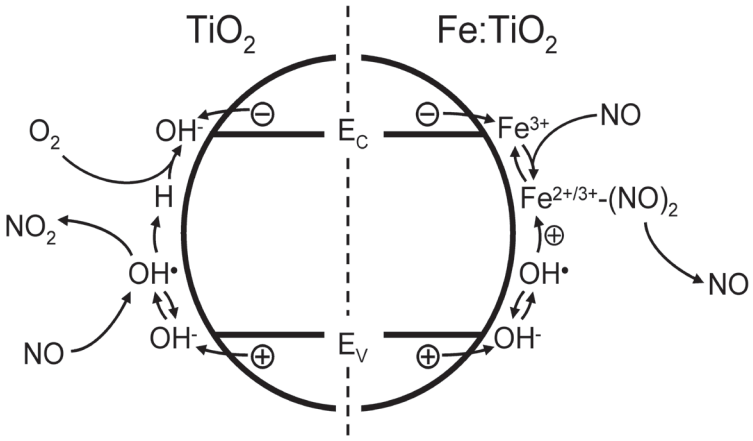

Scheme 1: Suppression of NO_2 formation at the surface of Fe-doped TiO_2 nanoparticles.

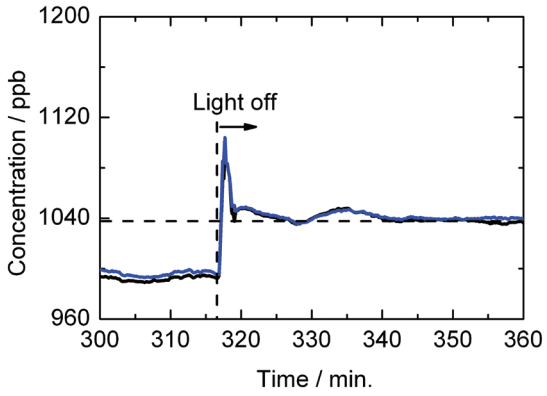

Figure 7: NO release for 1% Fe-doped TiO_2 after the UV irradiation is turned off.

the presence of trace amounts of water. We previously showed that H_2O binds more strongly to surface Fe species than NO, so it may block a large part of the available Fe surface sites.[17]

5.4 Conclusions

In conclusion, the presence of an Fe dopant in TiO_2 nanoparticles provides a recombination pathway that suppresses the formation of NO_2 during the photocatalytic decomposition of nitric oxide. XPS evidence shows that Fe^{3+} is photo-reduced to Fe^{2+} under UV illumination. The formation of Fe^{2+} is accompanied by a new IR band at 1805 cm^{-1}, which is assigned to the N=O stretch vibration in a Fe^{2+}-$(NO)_2$ complex. This Fe^{2+} is re-oxidized to Fe^{3+} by the photo-generated holes via an adjacent hydroxyl radical group (Ti-$OH^{\bullet}$), which triggers the release of the NO species. This work demonstrates that dopants can be used to suppress undesired reactions at metal oxide surfaces, offering a convenient and effective way to develop highly selective photocatalysts.

Acknowledgements

The authors gratefully acknowledge the kind help from B. van der Linden of the Catalysis Engineering group in Delft University of Technology and G. Mul from University of Twente. Financial support for this work is provided by the Shell-TU Delft “Sustainable Mobility” programme.

References

[1] J. A. Rodriguez, T. Jirsak, G. Liu, J. Hrbek, J. Dvorak and A. Maiti, *J. Am. Chem. Soc.*, 2001, **123**, 9597.

[2] S. Devahasdin, C. Fan, K. Li and D.H. Chen, *J. Phtochem. Photobiol. A*, 2003, **156**, 161.

[3] M. Kitano, M. Matsuoka, M. Ueshima, and M. Anpo, *Appl. Catal. A*, 2007, **325**, 1.

[4] J. C. S. Wu and Y. T. Cheng, *J. Catal.,* 2006, **237**, 393.

[5] W. Shan, F. Liu, H. He, X. Shi and C. Zhang, *Chem. Commun.*, 2011, **47**, 8046.

[6] S. Devahasdin, C. Fan, K. Li, D. H. Chen, *J. Photochem. Photobiol. A*, 2003, **156**, 161.

[7] Y. Ohko, Y. Nakamura, N. Negishi, S. Matsuzawa and K. Takeuchi, *J. Photochem. Photobiol. A,* 2009, **205**, 28.

[8] Z. Zhang, C. C. Wang, R. Zakaria and J. Y. Ying, *J. Phys. Chem. B*, 1998, **102**, 10871.

[9] X. H. Wang, J.-G. Li, H. Kamiyama, M. Katada, N. Ohashi, Y. Moriyoshi, and T. Ishigaki, *J. Am. Chem. Soc.,* 2005, **127**, 10982.

[10] J. M. Coronado, A. J. Maira, J. C. Conesa, K. L. Yeung, V. Augugliaro and J. Soria, *Langmuir*, 2001, **17**, 5368.

[11] M. R. Hoffmann, S. T. Martin, W. Choi and D. W. Bahnemann, *Chem. Rev.,* 1995, **95**, 69.

[12] T. H. Lim, S. M. Jeong, S. D. Kim and J. Gyenis, *J. Photochem. Photobiol. A: Chem.,* 2000, **134**, 209.

[13] S. Laufs, G. Burgeth, W. Duttlinger, R. Kurtenbach, M. Maban, C. Thomas, P. Wiesen and J. Kleffmann, *Atmos. Environ.*, 2010, **44**, 2341.

[14] J. Zhang, Y. Hu, M. Matsuoka, H. Yamashita, M. Minagawa, H. Hidaka and M. Anpo, *J. Phys. Chem. B*, 2001, **105**, 8395.

[15] J. Yang, C. Chen, H. Ji, W. Ma and J. Zhao, *J. Phys. Chem. B*, 2005, **109**, 21900.

[16] Q. Wu and R. van de Krol, *J. Am. Chem. Soc.,* doi:10.1021/ja302246b (in press)

[17] Q. Wu, G. Mul and R. van de Krol, *Energy Environ. Sci.*, 2011, **4**, 2140.

[18] Q. Wu, Q. Zheng and R. van de Krol, *J. Phys. Chem. C,* 2012, **116**, 7219.

[19] *C. Anderson and A. J. Bard, J. Phys. Chem. B*, 1997, 101, 2611.

[20] X. Li, P. Yue and C. Kutal, *New J. Chem.* 2003, **27**, 1264.

[21] J. Zhu, F. Chen, J. Zhang, H. Chen and M, Anpo, *J. Photochem. Photobiol. A,* 2006, **180**, 196.

[22] *C. S. Enache, J. Schoonman and R. van de Krol, Appl. Surf. Sci.*, 2006, 252, 6342.

[23] K. Hadjiivanov and H. Knözinger, *Phys. Chem. Chem. Phys.,* 2000, **2**, 2803.

[24] K. Hadjiivanov, V. Bushev, M. Kantcheva and D. Klissurski, *Langmuir*, 1994, **10,** 464.

[25] T. J. Dines, C. H. Rochester and A. M. Ward, *J. Chem. Soc. Faraday Trans.*, 1991, **87**, 643.

[26] *J. C. Yu, J. Lin, D. Lo and S. K. Lam, Langmuir*, 2000, **16**, 7304.

[27] J. S. Dalton, P. A. Janes, N. G. Jones, J. A. Nicholson, K. R. Hallam and G. C. Allen, *Environ. Pollut.,* 2002, **120**, 415.

[28] A. S. Bamard, P. Zapol, *Phys. Rev. B,* 2004, **70**, 235403.

[29] M. Rivallan, G. Ricchiardi, S. Bordiga and A. Zecchina, *J. Catal,.* 2009, **264**, 104.

[30] S. S. Malwadkar, R. S. Gholap, S. V. Awate, P. V. Korake, M. G. Chaskar, N. M. Gupta, *J. Photochem. Photobiol. A,* 2009, **203**, 24.

[31] I. X. Green and J. T. Yates, *J. Phys. Chem. C*, 2010, **114**, 11924.

[32] W. Su, J. Zhang, Z. Feng, T. Chen, P. Ying and C. Li, *J. Phys. Chem. C*, 2008, **112**, 7710.

[33] Y. Zhang, Y. Shen, F. Gu, M. Wu, Y. Xie and J. Zhang, *Appl. Surf. Sci.,* 2009, **256**, 85.

[34] J. K. Arana, O. G. Díaz, J. M. D. Rodríguez, J. A. H. Melián, C. G. Cabo, J. P. Pena, M. C. Hidalgo and J. A. Navío-Santos, *J. Mol. Catal. A,* 2003, **197**, 157.

[35] M. Descostes, F. Mercier, N. Thromat, C. Beaucaire and M. Gautier-Soyer, *Appl. Surf. Sci.,* 2000, **165**, 288.

[36] W. Hung, Y. Chen, H. Chu and T. Tseng, *Appl. Surf. Sci.,* 2008, **255**, 2205.

[37] W. Choi, A. Termin and M. R. Hoffmann, *J. Phys. Chem.*, 1994, **98**, 13669.

[38] A. Fujishima, T. N. Rao, D. A. Tryk, *J. Photochem. Photobiol. C: Photochem. Rev.*, 2000, **1**, 1.

[39] G. Mul, J. Pérez-Ramírez, F. Kapteijn and J. A. Moulijn, *Catal. Lett.*, 2002, **80**, 129.

[40] S. Yuen, Y. Chen, J. E. Kubsh and J. A. Dumeslc, *J. Phys. Chem.,* 1982, **86**, 3022.

[41] K. P. Huber and G. Herzberg, *Molecular spectra and molecular structure,* vol. 4, Van Nostrand, Princeton, NJ, 1979.

[42] A. Wacław, K. Nowińska, W. Schwieger and A. Zielińska, *Catal. Today*, 2004, **90**, 21.

[43] H. Miyata, Y. Nakagawa, S. Miyagawa and Y. Kubokawa, *J. Chem. Soc. Faraday Trans.,* 1998, **84**, 2129.

[44] G. D. Pirngruber and J. A. Z. Pieterse, *J. Catal.,* 2006, **237**, 237.

[45] G. Ramis, G. Busca and V. Lorenzelli, *Appl. Catal.*, 1990, **64**, 243.

[46] K. I. Hadjiivanov, *Catal. Rev. Sci. Eng.,* 2000, **42**, 71.

[47] The total number of desorbed NO molecules was calculated by integrating NO_x curve (from t = 317.2 min. to t = 340.7 min.) in Fig. 7. The final concentration of 1040 ppb was used as a baseline. With 0.019 g of thin film sample, a BET surface area of 71 m^2/g, and a Fe:Ti ratio of 1%, this corresponds to ~2% of the total number of Fe surface sites.

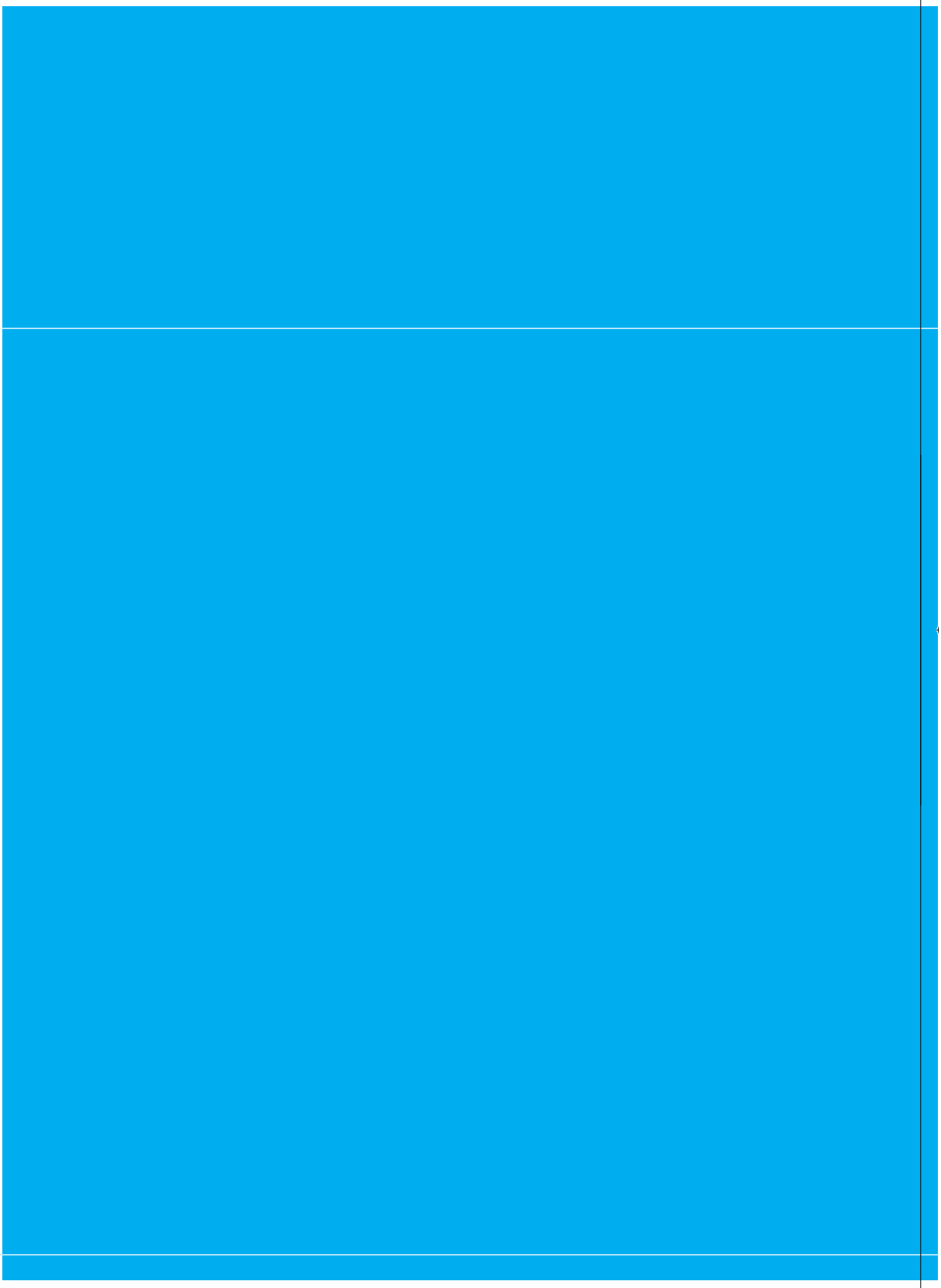

Summary and outlook

Summary and Outlook

Conventional TiO_2 based photocatalysts oxidize NO_x to nitrates which do not automatically desorb and have to be washed away from the catalyst surface. To avoid this, the research described in this thesis aims to design new photocatalysts that can photo-*reduce* NO into N_2 and O_2. Previous efforts in the literature have shown that catalysts prepared by depositing isolated titanium oxide clusters (TiO_4, tetrahedra) inside the cavities of zeolite-Y using ion beam implantation technology show high activity for N_2 and O_2 formation. However, large scale application of zeolites using ion beam technology is economically unattractive. We aim to create a large number of oxygen vacancies in TiO_2 to 'artificially' create TiO_4 species. The basic principles of photocatalysis and the overall approach taken in this thesis have been described in Chapter 1. The following chapters describe how a series of Fe-doped TiO_2 nanoparticles were prepared and systematically investigated for creating and stabilizing oxygen vacancies for changing NO photocatalytic selectivity from oxidation to reduction.

The synthesis and characterization of Fe-doped TiO_2 nanoparticles with different Fe concentrations have been described in Chapter 2. A simple, template free sol-gel method was used for synthesizing pure TiO_2 and Fe-doped TiO_2 nanoparticles. For as-synthesized samples after drying at 373 K, most iron is located at the surface. However, after firing at 773 K, the iron diffuses into the bulk of the TiO_2 up to 10% Fe doping. No evidence for phase segregation was found For the XRD patterns, the anatase (101) peak position shifts towards smaller *d* values with increasing Fe concentration. The observed shift is linear with the amount of Fe. This is in accordance with Vegard's law and this indicates the incorporation of Fe into TiO_2 lattice. However, the decrease in lattice constant is contrary to what one might initially expect, since the radius of Fe^{3+} ions (0.65 Å) is slightly larger than Ti^{4+} radius (0.61 Å) for six-fold coordinated ions. The attribution of decreased *d* lattice spacing to Fe^{4+} with relative small radius can be ruled out from Fe K-edge XANES spectra. Instead, the decrease in lattice spacing was attributed to a high concentration of oxygen vacancies. These oxygen vacancies are formed in order to compensate the effective negative charge of the Fe acceptor dopant. The presence of oxygen vacancies are further confirmed by Raman spectra. A similar linear shift at the strongest anatase (E_g mode) is observed by comparing Fe-doped TiO_2 with reduced TiO_{2-x} from Parker et al. This confirms that oxygen vacancies are indeed present in our material.

The surprising high solubility of Fe is mainly due to nearly the same radius of Ti^{4+} and Fe^{3+}, and energetically favorable Coulomb attraction between the negatively charged Fe acceptor and the positively charged oxygen vacancies. Intriguingly, XANES measurements indicate that the coordination geometry of Ti is changed from octahedral to tetrahedral at high oxygen vacancy concentrations. The tetrahedrally coordinated TiO_4 clusters are presumably present at the surface, where the lattice symmetry constaints are more relaxed. The phenomenon that coordination geometry can be changed by creating large number of oxygen vacancies provides a new way for designing highly selective photocatalyst.

The first step of photocatalysis, NO adsorption and release at Fe^{3+} sites in Fe/TiO_2 nanoparticles, is studied by in-situ Diffuse Reflection Infrared Fourier Transformed

spectroscopy coupled with Mass Spectrometry (DRIFT, Chapter 3). In this chapter, Fe^{3+} ions are found to be highly effective NO adsorption sites after in-situ heat treatment. With replacement of trace amount of H_2O, ~ 89 µmol/g NO can be released from the surface of 10% Fe-doped TiO_2. This can be explained by a much larger dipole moment of H_2O than that of NO. In addition, the phenomenon that adsorbed H_2O can effectively block NO adsorption explains why Fe^{3+}-NO species are often not observed. In addition, a new IR band at 1840 cm^{-1} is assigned to the stretch vibration of N-O bond over Fe^{3+} site. This is the first clear evidence for the presence of Fe^{3+}-NO on Fe-doped TiO_2 nanoparticles. While easy replacement of NO by H_2O molecules is clearly undesirable for practical use of photocatalysts, the controllable NO adsorption and release offer potential application of Fe-doped TiO_2 as a new NO storage and release material.

In order to identify the contribution of oxygen vacancies to catalytic selectivity, photocatalytic measurements of pure TiO_2 after annealing in air (unreduced TiO_2) and in a 2% H_2/Ar atmosphere (reduced TiO_2) are compared. The photocatalytic activities are now evaluated by a combination of NO_x analyzer and gas chromatography (GC). With UV light irradiation, 1% NO photo-reduction was detected after reaching catalytic equilibrium, while no photo-reduction can be found for unreduced TiO_2. This indicates that oxygen vacancies may contribute to photo-reduction selectivity. To further prove the role of oxygen vacancies, Fe doped TiO_2 with different oxygen vacancy concentrations are further evaluated for NO decomposition. For 1% Fe-doped TiO_2, 3% NO photo-reduction are found in air after achieving the photocatalytic equilibrium. The reduction activity is three times improvement over reduced TiO_2 at the same experimental conditions. Furthermore, 4.5% NO photo-reduction are found in pure N_2 atmosphere. This is higher efficiency than that in air atmosphere. This strongly support our interpretation of photo-reduction ability from Fe-doped TiO_2. In this case, the formation of gas phase NO_2 is now completely suppressed. This is consistent with our observation from in-situ DRIFT spectra. In addition, more oxygen vacancies would indeed lead to more photo-reduction activity. This is supported by our observation that 0.5% Fe-doped TiO_2 can only photo-reduced 3% NO in pure N_2.

The direct evidence for NO photo-reduction is provide by GC measurements. For 1% Fe-doped TiO_2, almost the same amount of N_2 and O_2 are produced after reaching catalytic equilibrium. This excludes the possibility of N_2O formation. Whereas, pure TiO_2 shows no formation of N_2 and O_2 at the same experimental conditions.

Two possible explanations are provided for the formation of N_2 and O_2 in chapter 4. One of the possible explanations is that a small amount of tetrahedrally coordinated Ti-oxides are formed. However, the formation of tetrahedrally coordinated Ti would require two oxygen vacancies to be present on the same Ti sites. As positively charged oxygen vacancies would repel with each other and very low concentrated oxygen vacancies are present up on 1% Fe doping, the formation of tetrahedrally coordinated Ti is not very likely.

A more likely explanation is that oxygen vacancies may act as catalytic centers for trapping O atom of NO molecules, thus, lowering the bond energy of NO. The trapped nitric molecules have no net charges. This allows mobile oxygen vacancies to come close together for trapping the other NO molecules. This could favor the formation of more thermodynamically stable N_2 and release energy during bond re-organization. The

released energy may easily knock out the trapped oxygen nearby. Therefore, gas phase O_2 is produced. Although the mechanism of photocatalytic reduction is still not yet exactly clear, the contribution of oxygen vacancies to NO photo-reduction selectivity provides a promising way for designing new and highly selective photocatalysts.

To confirm the reaction mechanism from Chapter 4, the photon-assisted NO adsorption-desorption and reaction species on the surface of the samples are investigated in Chapter 5. The combination of DRIFT spectra and on-line NO_x analyzer confirms that Fe dopant can actually suppress the formation of NO_2 during photocatalytic process. The suppression of NO_2 formation is caused from reduction of Fe^{3+} to Fe^{2+} by photo-generated electrons. In addition, the photon-assisted NO adsorption shows a new IR band at 1805 cm^{-1}, which is attributed to N=O stretch vibration in a Fe^{2+}-$(NO)_2$ complex. However, NO desorbs after turning off UV light. This is directly observable from NO_x analyzer. The explanation is that photo-generated hydroxyl radicals oxidize the Fe^{2+} back to Fe^{3+}, which is confirmed from XPS spectra. The re-oxidation would trigger the release of NO due to weak bonding of NO over Fe^{3+}. These results support the NO adsorption-desorption and photocatalytic mechanism in chapter 3 and chapter 4.

Outlook

The results presented in this thesis clearly indicate that oxygen vacancies contribute to transformation of photocatalytic selectivity from oxidation (mainly NO_2 and NO_3^- formation) to reduction (N_2 and O_2 formation). However, oxygen vacancies in pure TiO_2 are not stable. Therefore, Fe dopant is used for creating and stabilizing oxygen vacancies. However, the overall activity comparing to pure TiO_2 is still quite low. The explanation is that Fe doping also introduces deep charge recombination centre between the conduction band and valence band of TiO_2. The reduction activity may be further improved by doping with other elements (e.g. N, Cu, Zn). The other option is to combine with other semiconductors with proper band leve for making heterojunctions.

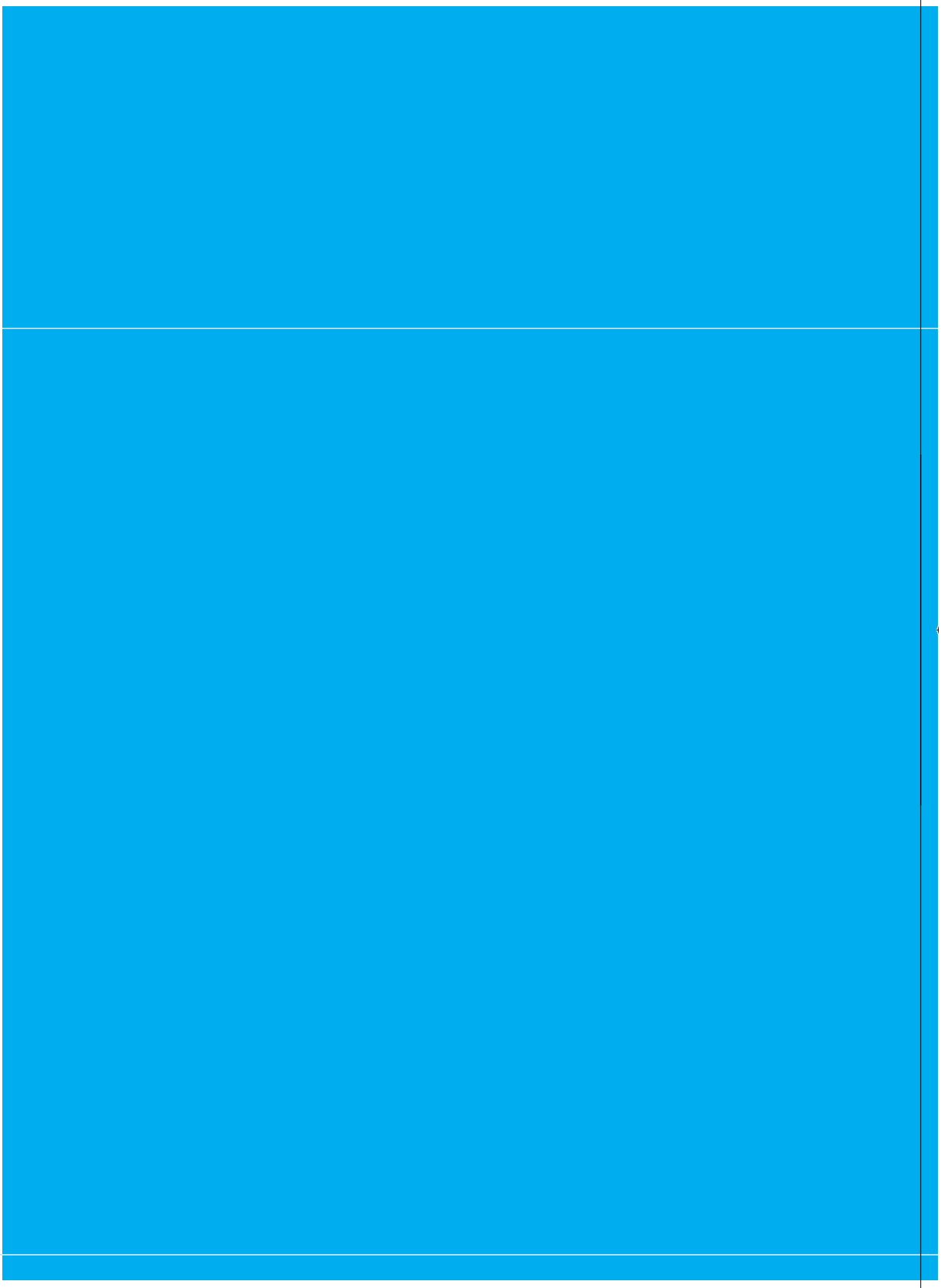

Samenvatting en toekomstperspectief

Samenvatting en toekomstperspectief

Conventionele, op titaandioxide (TiO_2) gebaseerde fotokatalysatoren oxideren NO_x tot nitraten. Deze nitraten desorberen slechts met behulp van wassen van het TiO_2 oppervlak. Het doel van dit proefschrift is een nieuwe fotokatalysator te ontwerpen welke NO kan foto*reduceren* tot N_2 en O_2. Dit proces zou de benodigde was-stap voorkomen aangezien N_2 en O_2 wel kunnen vrijkomen van het TiO_2 oppervlak. Eerdere pogingen uit de literatuur hebben laten zien dat katalysatoren die bestaan uit in de holtes van zeoliet-Y geïsoleerde TiO_4 clusters (tetraëdrisch gecoördineerd) een hoge activiteit voor de vorming van N_2 en O_2 vertonen. Deze clusters worden gemaakt met behulp van een ionenbundel implantatie methode. De toepassing van deze techniek op grote schaal is echter economisch onaantrekkelijk. In dit proefschrift wordt een alternatief uitgewerkt op basis van zuurstof-deficiënt TiO_2 waarmee een kunstmatig equivalent van de katalytisch actieve TiO_4-groepen kan worden gemaakt. De basis principes van de fotokatalyse en de globale aanpak genomen in dit proefschrift worden beschreven in hoofdstuk 1. De volgende hoofdstukken beschrijven hoe een serie van Fe-gedoteerde TiO_2-nanodeeltjes werd gemaakt om gestabiliseerde zuurstofvacatures te verkrijgen welke voor een selectiviteit richting de fotoreductie van NO zorgen in plaats van foto-oxidatie.

De synthese en karakterisering van Fe-gedoteerde TiO_2-nanodeeltjes met verschillende Fe-concentraties worden beschreven in hoofdstuk 2. Een simpele, sjabloon-vrije sol-gel methode is toegepast voor de synthese van zuivere en Fe-gedoteerde TiO_2-nanodeeltjes. Na drogen op 373 K van de gesynthetiseerde deeltjes blijkt het Fe zich vooral aan het oppervlak te bevinden. Na uitstoken op 773 K daarentegen diffundeert het Fe ook naar de binnenkant van de TiO_2 deeltjes waarbij een maximale concentratie van 10% Fe verkregen kan worden. Er zijn geen tekenen van fase-segregatie waargenomen. Met behulp van Röntgendiffractie patronen is een lineaire verschuiving te zien van de anatase (101) piekpositie naar kleinere *d*-waarden als functie van de Fe-concentratie. Dit komt overeen met de wet van Vegard en dit is een indicatie van de menging Fe in het TiO_2 rooster. Echter, de verkleining van de roosterconstante is het tegenovergestelde van wat *a priori* werd verwacht, aangezien de diameter van Fe^{3+}-ionen (0.65 Å) ietwat groter is dan die van Ti^{4+}-ionen (0.61 Å) met zesvoudige omringing. De mogelijke verklaring voor de kleinere roosterconstante dat ijzer zich als Fe^{4+} in het rooster bevindt hebben we met behulp van K-edge XANES spectra ontkracht. In plaats hiervan is de hoge concentratie van zuurstofvacatures die gevormd worden om de effectieve negatieve lading van de Fe-acceptoren te compenseren de reden voor de verkleinde *d*. De aanwezigheid van deze zuurstofvacatures is aangetoond met behulp van Raman spectra. Een vergelijkbare lineaire piekverschuiving van de sterkste anatase modus (E_g) is geobserveerd voor sterk gereduceerd TiO_2-x door Parker *et al*. Dit bevestigd de aanwezigheid van zuurstofvacatures in ons materiaal.

De verrassend hoge oplosbaarheid van Fe in TiO_2 wordt voornamelijk veroorzaakt door de vergelijkbare radii van Ti^{4+} en Fe^{3+} en de energetisch voordelige Coulomb aantrekking tussen de negatief geladen Fe-acceptor en de positief geladen zuurstofvacatures. Intrigerend genoeg laten XANES metingen zien dat de coördinatie van Ti verandert van octaëdrisch naar tetraëdrisch bij een hoge concentratie zuurstofvacatures. Van

de tetraëdrisch gecoördineerde TiO_4-clusters wordt aangenomen dat ze zich aan het oppervlak bevinden, waar de rooster symmetrie restricties gerelaxeerd zijn. Het fenomeen dat een grote hoeveelheid zuurstofvacatures de coördinatiegeometrie kan veranderen verschaft een nieuwe route voor het ontwerpen van zeer selectieve fotokatalysatoren.

De eerste stap van de hier bestudeerde fotokatalyse, NO adsorptie en desorptie aan Fe^{3+} ionen aan het oppervlak van de Fe/TiO_2 nanodeeltjes, is bestudeerd met behulp van *in situ* Diffuse Reflectie Infrarood Fourier getransformeerde spectroscopie (DRIFT). Hieruit blijkt dat Fe^{3+}-ionen zeer effectieve NO adsorptie locaties zijn na een *in situ* behandeling bij hoge temperatuur. Door blootstelling aan een kleine hoeveelheid H_2O komt zo'n 89 µmol NO per gram TiO_2 spontaan vrij van het oppervlak van 10% gedoteerd Fe/TiO_2. Dit kan verklaard worden door het veel grotere dipoolmoment van H_2O ten opzichte van dat van NO. Dat H_2O de adsorptie van NO kan blokkeren verklaart waarom NO op een Fe^{3+}-locatie over het algemeen niet wordt geobserveerd. Een nieuwe IR-band van de N-O-binding op Fe^{3+}-locaties is gevonden bij 1840 cm^{-1}. Dit is het eerste duidelijke bewijs voor de aanwezigheid van Fe^{3+}-NO op Fe-gedoteerde TiO_2 nanodeeltjes. Hoewel een makkelijke inwisseling van NO door H_2O moleculen niet gewenst bij toepassing van het materiaal als fotokatalysator, is de controleerbare NO adsorptie op deze sites wel een potentiele toepassing van Fe-gedoteerd TiO_2 als een nieuw NO-opslag materiaal.

Om de bijdrage van zuurstofvacatures aan de katalytische selectiviteit te onderzoeken vergelijken we fotokatalytische metingen aan ongedoteerd TiO_2 uitgestookt in lucht (stoichiometrisch TiO_2) en hetzelfde TiO_2 uitgestookt in 2% H2/Ar (gereduceerd TiO_2-x). De activiteiten zijn geëvalueerd met behulp van een combinatie van een NO_x analysator en gaschromatografie (GC). Het gereduceerd TiO_2 fotoreduceert 1% van het NO na het bereiken van katalytisch evenwicht, terwijl geen bewijs voor fotoreductie kan worden gevonden bij UV-belichting van stoichiometrisch TiO_2. Dit geeft aan dat zuurstof vacatures de selectiviteit voor de fotoreductiereactie beïnvloeden. Om deze rol van zuurstofvacatures verder aan te tonen, is de fotokatalytische activiteit van Fe-gedoteerd TiO_2 met verschillende concentraties zuurstofvacatures op eenzelfde manier geëvalueerd. Een 1% Fe-gedoteerd TiO_2 sample vertoont in lucht 3% NO fotoreductie na het bereiken van evenwicht. Deze reductieactiviteit is drie maal groter dan de activiteit van gereduceerd TiO_2 onder dezelfde experimentele condities. In een N_2 atmosfeer wordt een conversie van 4.5% voor NO reductie gevonden. Dit is een sterke aanwijzing dat fotoreductie van NO mogelijk is aan Fe-gedoteerd TiO_2. Ook wordt de NO2 formatie volledig onderdrukt, consistent met de *in situ* DRIFT resultaten. Tevens werd gevonden dat een hogere concentratie zuurstofvacatures leidt tot meer reductie van NO.

Direct bewijs voor de fotoreductie van NO wordt geleverd door de GC metingen. Na het bereiken van evenwicht produceert 1% Fe-gedoteerd TiO_2 gelijke hoeveelheden N_2 en O_2. De vorming van N_2O kan daardoor uitgesloten worden. Zuiver TiO_2 laat geen vorming van N_2 en O_2 zien onder gelijke experimentele condities.

Twee mogelijke verklaringen voor de vorming van N_2 en O_2 worden beschreven in hoofdstuk 4. De eerste is dat een kleine hoeveelheid tetraëdrisch gecoördineerde Ti-oxides worden gevormd. Dit vereist echter dat twee zuurstofvacatures zich tegelijkertijd naast één Ti atoom bevinden. Aangezien twee positief geladen zuurstofvacatures elkaar

zullen afstoten en er een lage absolute concentratie zuurstofvacatures aanwezig voor 1% Fe, is de vorming van deze tetraëdrische Ti-posities zeer onwaarschijnlijk.

De tweede, meer waarschijnlijke verklaring is dat het zuurstof atoom in NO de zuurstofvacature opvult tijdens adsorptie en dat de vacature zich als katalytisch actieve site gedraagd. De ingevangen nitraatmoleculen hebben geen netto lading, waardoor mobiele zuurstofvacatures direct naast een ingevangen NO molecuul zijn aan te treffen. Wanneer wederom een NO molecuul afvangen wordt in zo'n vacature, dan kunnen de stikstof atomen van de naast elkaar gelegen NO moleculen reageren tot N_2. De energie die daarbij vrijkomt kan helpen bij de vrijlating van de overgebleven zuurstofatomen, waarbij O_2 wordt geproduceerd. Hoewel het exacte mechanisme van fotoreductie nog onbekend is, kan de bijdrage van zuurstofvacatures aan de NO fotoreductie reactie worden toegepast om nieuwe, zeer selectieve fotokatalysatoren te ontwikkelen.

Om het bovenstaande reactiemechanisme te staven zijn de NO adsorptie-desorptie en reactanten op het oppervlak van de nanopoedersamples onder UV-belichting onderzocht in hoofdstuk 5. De combinatie van DRIFT spectroscopie en *on-line* NO_x analyse bevestigt dat Fe dotering de vorming van NO_2 daadwerkelijk onderdrukt. Dit wordt veroorzaakt door de reductie van Fe^{3+} naar Fe^{2+} door fotogegenereerde elektronen. Een nieuwe IR-band is waargenomen bij 1805 cm-1, welke kan worden toegekend aan de N=O strek-vibratie in een Fe^{2+}-$(NO)_2$ complex. NO desorbeert echter zodra de UV-belichting gestopt wordt. XPS spectra laten zien dat dit samenvalt met de her-oxidatie van Fe^{2+} naar Fe^{3+}, vermoedelijk door foto-gegenereerde hydroxyl radicalen. Deze reoxidatie triggert vervolgens de loslating van NO van het oppervlak door de zwakke bindingssterkte van NO met Fe^{3+}, hetgeen consistent is met de resultaten die zijn beschreven in hoofdstukken 3 en 4.

Vooruitzicht

De resultaten gepresenteerd in dit proefschrift tonen aan dat zuurstofvacatures een belangrijke rol spelen in de transformatie van fotokatalytische selectiviteit van oxidatie (formatie van voornamelijk NO_2 en NO_3^-) naar reductie (N_2 en O_2 formatie). Zuurstofvacatures zijn echter niet stabiel in TiO_2. Doteren met Fe zorgt voor de vorming en stabilisering van hoge concentraties zuurstofvacatures. Hoewel vele malen hoger dan dat van zuiver TiO_2, is de absolute activiteit van Fe-gedoteerd TiO_2 is echter nog steeds laag. De verklaring hiervoor is dat doteren met Fe ook ladingsrecombinatiecentra diep in de bandgap van TiO_2 creëert. De reductieactiviteit zou verder verbeterd kunnen worden door doteren met andere elementen (bijvoorbeeld N, Cu, Zn). Een andere optie is om het gedoteerd TiO_2 te combineren met halfgeleiders met de juiste bandenniveaus om zo een heterojunctie te maken.

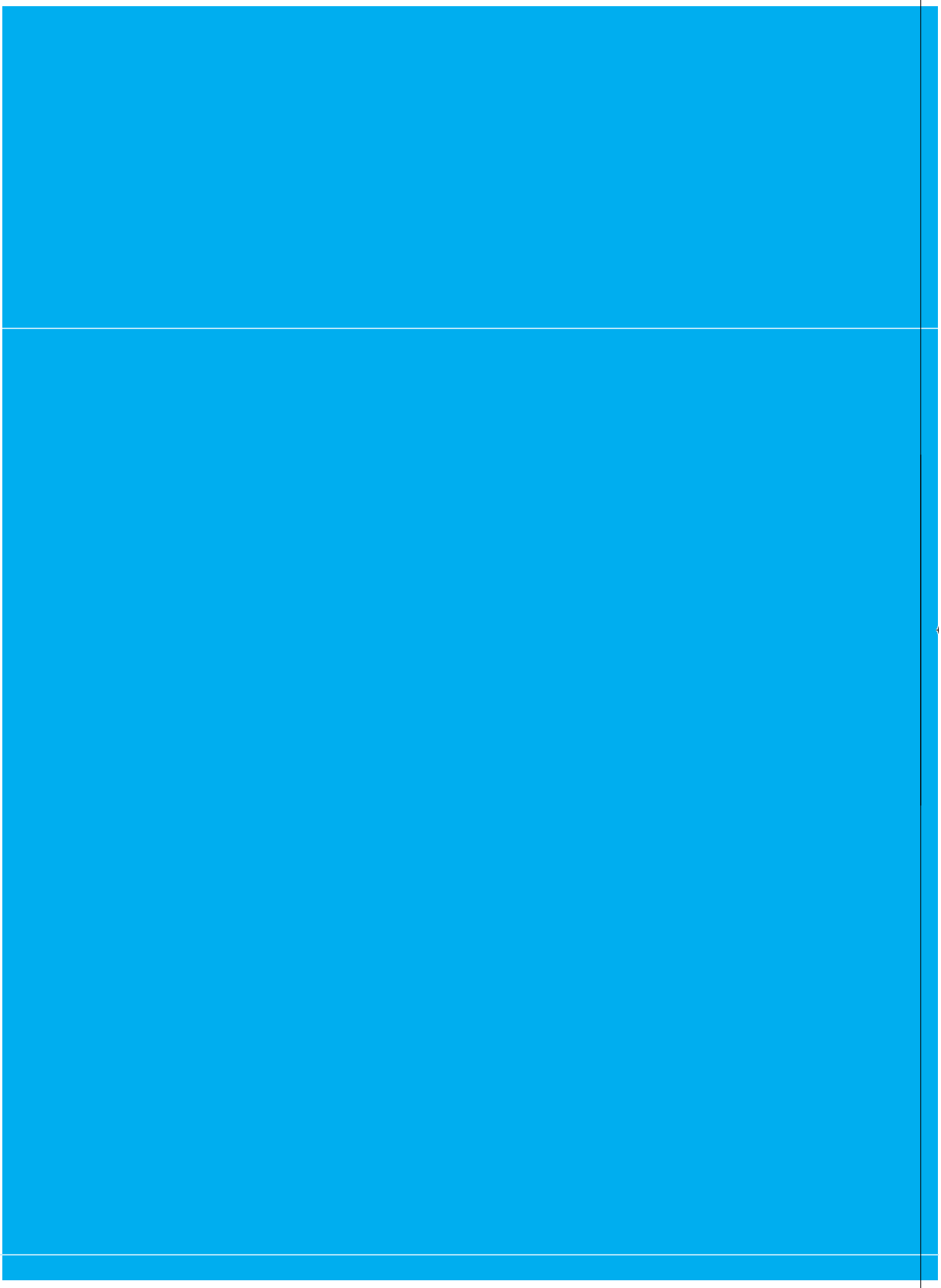

Acknowledgements

Time flies. I have spent four years in a beautiful university – TU Delft for Ph. D study. In which I have learned a lot of things from my supervisors, colleagues and friends, not only in research, but also in life. Especially, I want to thank the group that I stay most of the time – Materials for Energy Conversion and Storage.

I would like to sincerely thank my supervisor, Dr. Roel van de Krol. Because of him, I went to TU Delft for Ph. D study. Because of him, I got many new scientific insights that I never realized. Because of his strict requirements, I am confident that I will overcome more difficulties in the future.

I would like to give special thanks to Prof. Bernard Dam. He gave me a lot of valuable suggestions. He is a very kind man. He gave me space to think and to decide in the group.

I would also like to thank Yongqi Liang, one of my colleagues. As far as I can remember, he translates between my and Roel van de Krol during my Ph. D interview. With his kind help, I successfully become a Ph. D student. Moreover, I am very appreciated for his guidance during Ph. D study.

In addition, I would like to thank many other people in MECS group (e.g. Arjen Didden, Lennard Mooij, Yen Tran, Joost Middelkoop, Fatwa Abdi, Heleen van Rooijen). With their kind help, I can finish the Ph. D thesis smoothly.

Here, I would also like to thank some other people outside MECS group. Prof. Guido Mul. With his knowledge in IR, I got publication in Energy Environ. Sci., which is a very good journal. Chieh-Chao Yang, Qiang Zheng, Jianrong Li, Qingxiang Xu and Yunan Gao, We built up a small Chinese community, which we enjoy Chinese culture in the Netherlands.

Finally, I would like to thank my wife, Meimei Xie. Because of her, I am not alone in the Netherlands. Especially, she gave a special gift during my Ph. D, a new born baby.

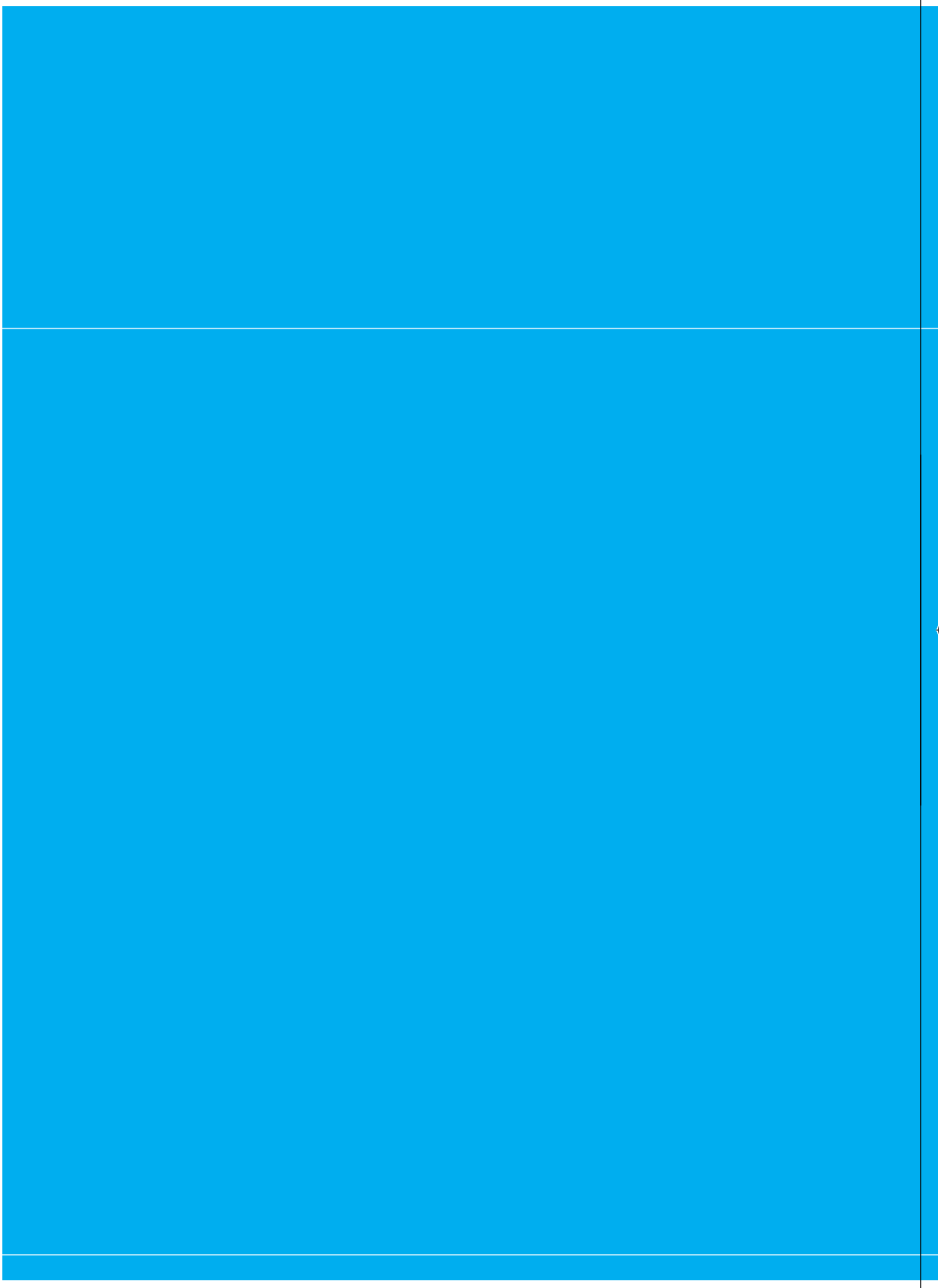

List of Publications

List of publications

1. Q. Wu, G. Mul and R. van de Krol, Efficient NO adsorption and release at Fe^{3+} sites in Fe/TiO_2 nanoparticles, *Energy Environ. Sci.*, 2011, **4**, 2140 (Chapter 3)
2. Q. Wu, Q. Zheng and R. van de Krol, Creating oxygen vacancies as a novel strategy to form tetrahedrally coordinated Ti^{4+} in Fe/TiO_2 nanoparticles, *J. Phys. Chem. C*, 2012, **116**, 7219. (Chapter 2)
3. Q. Wu and R. van de Krol, Selective photoreduction of nitric oxide to nitrogen by nanostructured TiO_2 photocatalysts: the role of oxygen vacancies and iron dopant, *J. Am. Chem. Soc.*, 2012, **134**, 9369 (Chapter 4)
4. Q. Wu, C. C. Yang and R. van de Krol, A dopant-mediated recombination mechanism in Fe-doped TiO_2 nanoparticles for the photocatalytic decomposition of nitric oxide (Chapter 5, submitted)

Oral presentations

1. Q. Wu and R. van de Krol, Modified TiO_2 photocatalysts for NO_x remediation, 18th International Conference on Photochemical Conversion and Storage of Solar Energy in Souel, South Korea, 2010.
2. Q. Wu, N. Teng, M. Zweemer and R. van de Krol, From photo-oxidation to photo-reduction: energy and environmental sustainability, International conference on TiO_2 Photocatalytic and Advanced Oxidation Technologies for the Treatment of Water, Air, Soil and Surfaces, Gdansk, Poland, 2011.
3. Q. Wu and R. van de Krol, Photo-reduction of NO_x with Fe-doped TiO_2 nanoparticles, Symposium GG: Titanium dioxide nanomaterials (Materials Research Society), USA, 2011.

Curriculum Vitae

Qingping Wu was born at Putian, P. R. China on 1st May, 1979. In 1999, he started study in Fuzhou University, China as an undergraduate student. In July, 2003, he got a B. Sc. in chemistry. After that, he continued the study in Fuzhou University as a master student. In 2006, he obtained M. Sc. in Physical Chemistry. Later, he started the first job in Lu'an group (company) for investigating industrial production of polysilicon. In September, 2007, he studied in Materials for Energy Conversion and Storage (MECS) group, TU Delft, The Netherlands as a Ph. D student. During his Ph. D studies, he published several papers in well known journals (e.g. *J. Am. Chem. Soc., Energy. Environ. Sci. and J. Phys. Chem. C*). He also presents his interesting results in several international conferences. The results of the Ph. D research that has been done are therefore analyzed in-depth in this thesis...